

FUNCTIONAL ORGANIZATION OF VISUAL CORTEX IN BUSH BABIES
AND OWL MONKEYS REVEALED BY OPTICAL
IMAGING OF INTRINSIC SIGNALS

By

Xiangmin Xu

Dissertation

Submitted to the Faculty of the
Graduate School of Vanderbilt University
in partial fulfillment of the requirements
for the degree of
DOCTOR OF PHILOSOPHY


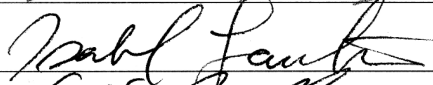
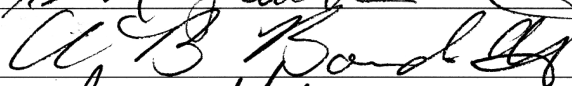
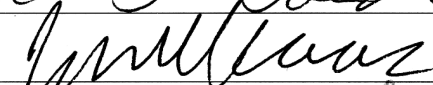
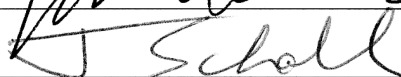
in

Psychology

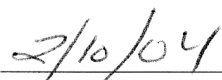
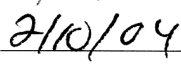
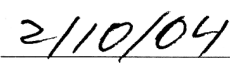
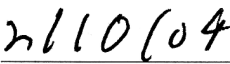
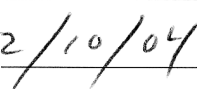
May, 2004

Nashville, Tennessee

Approved:

Date:

ACKNOWLEDGEMENTS

As I complete my studies at Vanderbilt, I would like to convey my gratitude and appreciation to all the people who have helped me during all my years here.

First, I would like to express my deep thanks to Vivien for being a caring and considerate mentor! Her excellent guidance and loving care has made my studies here rewarding and enjoyable. Her hard work and passionate interest in research have inspired me to do well in whatever I do, now and in the future.

I am also grateful to my other outstanding committee members, Jon Kaas, Jeff Schall, A.B. Bonds and Isabel Gauthier, for their advice and help during my studies.

Many thanks go to the Casagrande lab members, both the past and present ones. In particular I would like to thank Julie Mavity-Hudson for her excellent research support and her extra work on ‘tutoring’ me in English. The postdocs and students I have worked with in Vivien’s lab over these past years are Jamie Boyd, Amy Wiencken-Barger, Jennifer Ichida, Gyula Sary, Yuri Shostak, Zhuang Song, David Royal, Ilya Khaytin, Maria Couppis and Fatih Yazar. Special thanks also go to John Allison, who has always been kind to offer timely experimental help as well as wise and provoking thoughts.

I feel fortunate to have worked with Dan Shima, Jim Stefansic, Christine Collins, Peter Kaskan, Michael Gallucci and Alicia Thomas on various optical imaging projects. I would like to thank Bill Bosking and many other friends outside Vanderbilt for their help and encouragement. I also appreciate help from the animal care staff at Wilson Hall, especially Mary Feurtado.

I would like to thank all the undergraduate students directly working with me in the past years for their help and beneficial interactions, including Patrick Pratumrat, Matt Jones, Behin Barahimi, Tiffany Anderson, Fangbai Wu, Jennifer Treece, and many others.

In addition, I hope that the other faculty and students that I have interacted with in the Department of Psychology know how much they have helped me and how much I have learned from them and accept my thanks. They include Ford Ebner, Andrew Tomarken, Joe Lappin, Randolph Blake, Tim McNamaria, San-Hun Lee, Duje Tardin, David Lyon, Pei-chun Fang and Lu Li, among others.

I would like to express thanks to Peng Wang for her cheering me up, which made the writing process more bearable. I would like to acknowledge help from the office staff in the Departments of Psychology and Cell & Developmental Biology, including Pat Burns, Dan Stewart and Carol Johnson. I also need to thank many other persons who helped me at various stages and I have not mentioned here.

Finally, my greatest debt is to my Mom and Dad for their selfless love and support. They are the best. Their expectation and encouragement has always been my motivation to keep going!

This work was supported by grant EY01778 and cores EY08126 and HD15052.

TABLE OF CONTENTS

	Page
ACKNOWLEDGMENTS	ii
LIST OF TABLES	vii
LIST OF FIGURES	viii
Chapter	
I. INTRODUCTION	1
Functional architecture of visual cortex	1
Remaining questions	5
Thesis overview	8
II. OPTICAL IMAGING REVEALS THE VISUOTOPIC ORGANIZATION OF V1 AND MT IN BUSH BABIES	10
Introduction	10
Materials and methods	11
General preparation	11
Optical imaging and visual stimuli	12
Image analysis	14
CMF calculation	15
Histology and alignment	15
Results	16
Visuotopic organization of V1	16
Visuotopic organization of MT	24
Discussion	34
V1	35
MT	36
CMF and point image size	37
III. FUNCTIONAL ORGANIZATION OF VISUAL CORTEX IN THE OWL MONKEY	39
Introduction	39
Material and methods	40

	General preparation	40
	Visual stimuli and optical imaging	42
	Image analysis	43
	Electrophysiological verification	45
	Histology, alignment and data analysis	45
Results		47
	Defining visual areas	47
	The general organization of orientation preference in V1, V2 and V3	50
	Relationship between pinwheel centers and CO blobs in V1	58
	Relationship of orientation preference domains to the CO bands in V2 and V3	63
Discussion		65
	Orientation preference and CO blobs in V1	66
	The organization of orientation and CO compartments in V2	69
	The functional organization of V3	72
IV.	ORIENTATION AND DIRECTION PREFERENCE ORGANIZATION IN BUSH BABY MT	73
	Introduction	73
	Materials and Methods	73
	General preparation	74
	Optical imaging and visual stimuli	75
	Image analysis	76
	Histology and alignment	77
	Results	77
	Discussion	84
V.	IS ORIENTATION PREFERENCE IS ORGANIZED DIFFERENTLY AT DIFFERENT ECCENTRICITIES IN BUSH BABY V1	87
	Introduction	87
	Materials and Methods	89
	General preparation	89
	Optical imaging and visual stimuli	90
	Image analysis	91
	Measurement of iso-orientation domains	92
	Examination of the distribution of pinwheel centers over CO blobs/interblobs	93
	Results	94
	Orientation preference organization in central and peripheral V1	94

	Magnitude of orientation selectivity	94
	Iso-orientation domain sizes in central and peripheral V1	98
	Re-examination of the relationship between CO blobs and pinwheel centers	98
	Discussion	100
	Species differences in orientation preference organization	100
	Modular distribution and eccentricity	103
VI.	THE ORGANIZATION OF SPATIAL FREQUENCY PREFERENCE IN BUSH BABY V1	106
	Introduction	106
	Materials and Methods	107
	General preparation	107
	Optical imaging and visual stimuli	108
	Image analysis	109
	Comparison of CO maps and SF preference map	110
	Results	111
	General structure of SF maps	111
	Eccentricity dependent variation	115
	Relationship between the spatial frequency and orientation maps	115
	Relationship between spatial frequency preference and CO modules	118
	Discussion	122
	Cortical organization of SF preference	122
	Relationship between CO blobs and SF preference	124
VII.	CONCLUSIONS	127
	REFERENCES	132

LIST OF TABLES

Table	Page
1. The relationship between pinwheel centers and blobs	62
2. Relationship between V1 size, number of CO blobs and pinwheels	67
3. Comparison of iso-orientation domain sizes in central and peripheral V1	99

LIST OF FIGURES

Figure	Page
1. Optical imaging of topographically limited stimuli (Case 1).	17
2. Optical imaging of topographically limited stimuli (Case 2)	18
3. The V1/V2 border determined by the topographical mapping	20
4. Comparison between the cortical magnification factor (CMF) measured by optical imaging mapping and microelectrode recordings	23
5. High resolution of visuotopic mapping	25
6. Visualization of area MT in vivo by optical imaging of intrinsic signals	27
7. The retinotopic organization of MT and surrounding cortex revealed by stimuli restricted to part of the visual field	29
8. The retinotopic organization of MT revealed by drifting gratings in horizontal or vertical windows in different locations	30
9. The cortical magnification factor as a function of eccentricity in areas V1 and MT	33
10. Visuotopic organization of V1, V2 and V3	49
11. Orientation difference maps of V1 and V2	51
12. Functional maps of orientation preference in V1 and V2	54
13. Comparison of the organization of orientation preference in V1, V2 and V3	56
14. The relationship between pinwheels, CO blobs and interblobs in V1	59
15. The relationship between zones of high and low orientation selectivity and CO light and dark bands in V2	60
16. Comparisons between CO modules and orientation preference domains in owl monkey V3	61

17.	Activation patterns in MT using full screen drifting gratings of different orientations .	79
18.	Functional maps of orientation preference in MT	80
19.	The relation of orientation preference maps to direction of movement maps in MT	83
20.	Comparison of the maps of orientation preference in central and peripheral V1	96
21.	Time course plots of intrinsic signal magnitude at different eccentricities	97
22.	The distribution of orientation pinwheel centers in CO blobs and interblobs in central V1	101
23.	Single condition maps of combinations of orientation and spatial frequency (SF)	113
24.	Single condition maps of SFs	114
25.	A color-coded SF preference map.	116
26.	Eccentricity-dependent variation in spatial frequency representation	117
27.	The relationship between orientation preference and SF preference maps	119
28.	Comparison between the spatial frequency map and the CO map	121
29.	Histogram distributions of peak SFs over CO blobs and interblobs	123

CHAPTER I

INTRODUCTION

Vision is the primary sensory modality in primates including humans, and this is reflected in the complexity of the visual system and the extent of the cerebral cortex used for visual processing (Van Essen et al., 1990; Felleman & Van Essen, 1991; Casagrande and Kaas, 1994). It has been proposed that in primates there are more than 30 different visual areas, organized in two major separate visual processing streams within a hierarchical and parallel framework (Ungerleider and Mishkin, 1982; Desimone and Ungerleider, 1989; Van Essen et al., 1990; Felleman & Van Essen, 1991; Ungerleider and Haxby, 1994).

Within the context of the integrated visual system, this thesis focuses on aspects of the functional organization of early visual areas, including the organization of visuotopy, orientation preference and spatial frequency preference. The sections below provide a brief background to relevant issues concerning visual cortical organization as well as an introduction to key questions that are the focus of this thesis.

Functional architecture of visual cortex

In visual cortex, much work has gone into characterizing its modular organization in order to understand how cortical neurons are grouped to process different aspects of visual information (see LeVay and Nelson, 1991; Swindale, 1998; 2000). Early electrophysiological and anatomical studies by Hubel and Wiesel showed that in the

primary visual cortex (of cats and macaque monkeys), neurons with similar response properties (i.e., orientation specificity and ocular dominance) tended to be grouped in vertical columns, with each column oriented perpendicular to the surface of the cortex and spanning its full thickness (Hubel and Wiesel, 1962; 1968; 1977). A full complement of columns, of either type, left plus right eye or a complete 180° of orientation preference was defined as a hypercolumn, about 1- 2 mm in diameter. Hubel and Wiesel (1977) proposed that these different columns are organized with respect to each other such that they intersect at right angles within the topographical representation of the visual field. They suggested that orientation and ocular dominance maps might be organized in such a way as to optimize the uniform representation of all possible combinations of orientation and eye of origin at each retinal position (Hubel and Wiesel, 1977). Their model, also called an "ice-cube" model, has been influential in shaping thoughts about the functional architecture of the primary visual cortex (Hubel and Wiesel, 1977; Swindale, 1990; 1998). Later, with the proposal of cytochrome oxidase (CO) blobs as a specialized system devoted to the processing of color information in primates, the ice-cube model was extended to include blobs within each module (Livingstone and Hubel, 1984). The model's essence lies in the concept of a modular organization of visual cortex. In such a view, the cortex can be thought of as containing many small machines of more or less identical structure designed to handle different aspects of visual information at each topographic location. This concept also has been extended to extrastriate cortical areas such as well-studied visual area 2 (V2) (see Roe and Ts'o, 1997).

In more recent years, the concept of an ice-cube like modular architecture in the strict sense has been challenged. The relationships between CO blobs, ocular-dominance columns, and iso-orientation domains in macaque visual cortex have been re-examined with optical imaging of intrinsic signals. It has been found that in macaque V1, the centers of orientation pinwheels (where orientation preference changes in a radial fashion around a single point) do not coincide with the centers of blobs; these two subsystems (CO blobs and orientation systems) are spatially independent, although the iso-orientation contours cross borders of ocular-dominance columns at approximately right angles, and the orientation pinwheel centers and the blob centers tend to lie along the midline of ocular-dominance columns (Bartfield and Grinvald, 1992). The ‘hypercolumn’ modules as Hubel and Wiesel proposed, each including two complete sets of orientation columns in a set of left-right ocular dominance columns and two CO blobs (one for each eye), cannot be the primary unit of cortical organization (Bartfield and Grinvald, 1992).

In fact, a multitude of columns in the visual cortex have been discovered. For example, in V1, aside from the columnar organization of orientation, ocular dominance, and CO blobs, other stimulus parameters, such as direction of movement, spatial frequency and disparity, have been revealed (Tootell et al., 1981, 1988a; Shoham et al., 1997; LeVay and Voigt, 1988). Increasing evidence suggests that it is not possible to map all the dimensions of a stimulus to a common modular unit with all possible combinations of stimulus features represented at least once in each ice-cube like module (Swindale, 1998). A more fluid arrangement has been proposed in which multiple columnar systems or functional maps are superimposed with relatively weak geometric linkages and there exists no common subunit (Swindale, 1998). A key concept from

Hubel and Wiesel's model, however, still holds in that these multiple maps are interleaved so as to ensure that all combinations of the different parameters are represented as completely and uniformly as possible to subserve visual perception across visual space (Swindale, 1998; 2000).

It should be noted that functional architecture of visual cortex varies within and between species (Casagrande and Kaas, 1994; Preuss, 2004). For example, the presence or absence of ocular dominance columns in primate visual cortex has been studied in a wide variety of species (See Horton and Hocking, 1996a for summary). Macaque monkeys have been found to have a strong ocular dominance columnar organization, but New World monkeys such as owl monkeys and squirrel monkeys generally fail to demonstrate robust ocular dominance columns (Horton and Hubel, 1981; Horton and Hocking, 1996a,b). Also, there may be major differences in V2 functional organization between prosimian and simian primates (see Casagrande and Kaas, 1994). For both diurnal monkeys such as macaque monkeys and squirrel monkeys and nocturnal owl monkeys, V2 has both clear CO light and dark bands that may correspond to stripes of high and low orientation selectivity (Tootell et al., 1985; Ts'o et al., 1990; Malach et al., 1994; Roe & Ts'o, 1995). No functional compartments have been revealed by CO staining and/or orientation selectivity in V2 in prosimians, although there exists connectional evidence in prosimians (bush babies) to suggest that V2 in this species is not uniform in spite of the lack of CO and orientation defined modules (Condo and Casagrande, 1990; Preuss et al., 1993; Preuss and Kaas, 1996; Bosking et al., 1996; Collins et al., 2001).

Remaining questions

Greatly aided by new emerging techniques in the last few decades, we have made great progress in understanding the functional organization of visual cortex, as outlined above. Still, there remain some important and/or controversial issues, which need to be examined further. Below I will introduce these issues. The first one is partly related to the new methodological developments; the other issues directly concern functional organization of visual cortex.

First, I would like to look into the reliability and effectiveness of optical imaging by systematically mapping V1 and extrastriate cortex and comparing these results to traditional microelectrode mapping. The microelectrode mapping method has provided much information about visuotopic organization of primate visual cortex, but it has major limitations such as the difficulty of sampling from a large number of recording sites and accurately locating those sites in cortex. Optical imaging is a powerful tool to map visual cortex, since it can directly visualize global visuotopic organization as well as reveal detailed functional features. In fact, it has been used successfully to study the retinotopic organization of V1 in several species of mammals (Bosking et al., 1997; Blasdel and Campbell, 2001; Schiessl and McLoughlin, 2003). Nevertheless, it is not known how accurately the visuotopic maps produced by optical imaging match with those produced by microelectrode mapping, since optical imaging measures indirect metabolic signals and not neuronal activity directly (Bonhoeffer and Grinvald, 1996). In order to study details of visuotopic organization and understand whether optical imaging can be used as a reliable and high-resolution tool, I, along with my colleagues, mapped the visuotopic organization of V1 and MT in bush babies. These animals are ideal subjects for such

studies because they have small smooth brains, and many of the proposed visual areas are exposed on the brain surface of these primates.

Second, although orientation selectivity is one of the best understood response properties of most visual cortical neurons, there remain some interesting questions regarding how orientation selectivity is organized in primate visual cortex. For example, in diurnal primates it has been proposed that cytochrome oxidase (CO) blobs in the primary visual cortex (V1) and CO stripes in the second visual area (V2) segregate color selective cells from cells with selectivity for orientation (see Livingstone and Hubel, 1984; DeYoe and Van Essen, 1985; Ts'o and Gilbert, 1988; Roe and Ts'o, 1995). Unlike diurnal primates, however, nocturnal primates such as the simian primate, owl monkey, and the prosimian primate, bush baby, have rod-dominated retinas with only a single cone type and no color vision (Wikler and Rakic, 1990; Jacobs et al. 1996). It is unclear whether the same type of functional organization is found in the early visual areas of these animals. It is also not clear how nocturnal lifestyle or phylogenetic difference impacts the functional organization of visual cortex. We explored these issues by using optical imaging of intrinsic signals to quantitatively examine the organization of orientation preference domains in relationship to CO compartments in nocturnal owl monkeys. In addition, maps and modular organization of functional properties could vary with visual eccentricity. For example, it is known that more area of cortex is devoted to representation of central vision and less area of cortex is devoted to peripheral vision (McIlwain, 1985). It also has been suggested that in macaque V1 the organization of orientation and spatial frequency and their relationship with CO blobs vary with eccentricity (Tootell et al, 1988a; Vanduffel et al., 2002). Given this proposal, we

wanted to examine how eccentricities affect the organization of orientation preference in bush baby V1.

Third, compared with orientation selectivity and ocular dominance, the cortical organization of spatial frequency preference in primates is less clear and has not been well characterized. In cats, several layouts for spatial frequency preference within primary visual cortex have been described including laminar (Maffei and Fiorentini, 1977), clustered (Tolhurst and Thompson, 1982) and columnar organization (Tootell et al., 1981; Bonhoeffer et al., 1995). Recently, two models of spatial frequency organization were proposed based upon optical imaging in cat primary visual cortex: 1) Spatial frequency is organized into clusters representing high and low frequencies; 2) Spatial frequency is represented continuously, with independent multiple processing domains (Hubener et al., 1997; Shoham et al., 1997; Everson et al., 1998; Issa et al., 2000). Previous studies using either 2-deoxyglucose labeling or single unit recording in macaque monkeys have suggested that spatial frequency is organized into columns in V1 (Tootell et al., 1988a; Born and Tootell, 1991). Some electrophysiological studies in macaque monkeys and bush babies also suggest that cells in CO blobs and interblobs have different spatial frequency preferences (Edwards et al., 1995; DeBruyn et al., 1993). Since the cortical organization of spatial frequency has not been directly examined using optical imaging in primates, we examined this organization in bush baby V1 and also examined the relationship between spatial frequency preference and CO modules (blobs and interblobs).

Finally, since much of the knowledge about the visual cortical organization comes from studies in a very limited set of animal models (e.g. domestic cats and macaque

monkeys), it is important to compare distantly related primate species. We studied two nocturnal primates with long-standing but independent lineages, the prosimian bush baby and the New World simian owl monkey in order to characterize patterns of evolutionary conservation and change.

Thesis overview

This thesis consists of a series of studies designed to address the following questions:

(1) What features of visuotopic organization can optical imaging reveal in primate visual cortex? Do the visuotopic maps produced by optical imaging match with those produced by microelectrode mapping?

(2) Is orientation preference in V1 and extrastriate cortex organized differently in different primate species (e.g., owl monkeys, bush babies and macaque monkeys)?

(3) Does eccentricity affect the relationship between functional modules in primate visual cortex?

(4) How is spatial frequency preference organized in the primate visual cortex?

This thesis consists of 7 chapters, including this introductory chapter. Chapter II examines whether optical imaging can be used as a reliable and high-resolution tool when compared with prior microelectrode mapping results. Chapter III focuses on the second question by examining three visual areas (V1, V2 and V3) in owl monkey visual cortex and comparing cortical organization across primate species. Chapter IV further examines the second question by investigating the orientation and direction preference organization of the middle temporal (MT) visual area in bush babies. Chapter V addresses the issue of

whether orientation preference is organized differently at different eccentricities in bush baby V1. Chapter VI studies how spatial frequency is represented in bush baby V1 and what relationships may exist between the cortical maps of spatial frequency preference, orientation preference and CO blob compartments. The final chapter (VII) summarizes the key findings of the thesis and considers the implications of these findings.

CHAPTER II

OPTICAL IMAGING REVEALS THE VISUOTOPIC ORGANIZATION OF V1 AND MT IN BUSH BABIES

Introduction

The visual cortex of primates is widely recognized as containing a number of visual areas, each specialized to contribute uniquely to visual function (see Felleman and Van Essen, 1991; Rosa, 1997; Kaas and Lyon, 2001 for review). Traditionally, microelectrode mapping of the visuotopic organization has played a major role in defining visual areas (e.g., Allman and Kaas, 1971a,b; Allman et al., 1973). Mapping with single electrodes, however, has some significant limitations. It is hard to reveal global retinotopic patterns given limited sample recordings. It is also hard to accurately reconstruct recording sites in cortex. In addition, it is not easy to obtain receptive fields with clear and reliably defined locations in extrastriate cortex due to the large receptive field sizes in these areas.

Optical imaging of intrinsic signals is a relatively new and powerful technique, and has many advantages over more conventional electrophysiological and anatomical techniques (Bonhoeffer and Grinvald, 1996). It can map a relatively large region in one camera view, and it has the potential for revealing global retinotopic patterns of visual areas with a high spatial resolution. Also, successive maps can be obtained in response to different stimuli in the same cortical area. It also has been used recently to study the retinotopic organization of V1 and some extrastriate areas (Bosking et al., 1997, 2002; Blasdel and Campbell, 2001; Lyon et al., 2002; Schiessl and McLoughlin, 2003).

Nevertheless, as in other types of functional imaging methods (e.g. fMRI in humans), optical imaging is an indirect measure of neural activity derived from a combination of blood flow related changes (Bonhoeffer and Grinvald, 1996). Some studies in cat visual or auditory cortex reported that there are large discrepancies or mismatches between the spatial distribution of optical and single unit responses (Toth et al., 1996; Das and Gilbert, 1995; Spitzer et al., 2001). Thus, how the spread or distribution of stimulus-induced intrinsic signals (detected by optical imaging) relates to spiking activity is an important issue and needs further investigation.

In this study, we used optical imaging of intrinsic signals to map the visuotopic organization of V1 and MT in bush babies. Given that V1 and MT have been well established and there are previous microelectrode mapping studies in both V1 and MT in bush babies, we would like to address two questions: (1) Can optical imaging be used as a reliable and high-resolution tool when compared with prior microelectrode mapping results? (2) Does optical imaging detect subthreshold neural responses?

Bush babies are ideal subjects for such studies because they have small and smooth brains, and many of the proposed visual areas are exposed on the brain surface. By using optical imaging with topographically limited visual stimuli, we were able to reveal aspects of visuotopic organization of both V1 and MT in these animals.

Materials and Methods

General preparation

The 8 bush babies used in this study were handled according to an approved

protocol from the Vanderbilt University Animal Care and Use Committee. The animals were initially anesthetized with isoflurane (2-4% in O₂) and, after tracheal intubation and implantation with two femoral catheters, were mounted in a stereotaxic apparatus. Neuromuscular blockade was initiated by i.v. injection of 1-1.5 mg kg⁻¹ vecuronium bromide (Norcuron). Animals then were artificially ventilated with a mixture of 75% N₂O and 25% O₂ delivered at a rate sufficient to maintain the peak end tidal CO₂ level at around 4 %. Paralysis was maintained by intravenous infusion of vecuronium bromide (0.1-0.3 mg kg⁻¹ hr⁻¹) mixed in 5% dextrose lactated Ringer's. Propofol (2,6,-di-isopropylphenol: 10 mg kg⁻¹ hr⁻¹) was used for anesthetizing bush babies during experiments. In order to ensure that adequate levels of anesthesia were maintained throughout the experiment, heart rate, peak end tidal CO₂, and temperature were monitored continuously after paralysis, and the level of anesthetic increased if necessary. Pupils were dilated with 1% atropine eye-drops and clear gas permeable contact lenses were used to render the retina conjugate with the viewing screen 28.5 or 57 cm distant. Lenses with 3mm artificial pupils were used for most animals. An opening was made in the skull over V1 and was sealed with 1% agarose under a cover glass.

Optical imaging and visual stimuli

Intrinsic optical imaging signals were acquired with the Imager 2001 differential video-enhancement imaging system and VDAQ/NT data acquisition software (Optical Imaging Inc.). Reference images of cortical vasculature were acquired with a 540 nm green light. The cortex was illuminated with a 611 nm light during data acquisition. The camera was focused on the cortical surface, and the depth of field was subsequently increased by closing the lens diaphragm. Visual stimuli were generated using a VSG

system (Cambridge Research Systems, Rochester, UK), and were presented on a 21" video screen (SONY FD Trinitron, Model GDM-F400) in 120 Hz non-interlaced mode with a mean luminance of 30 cd/m².

In order to map V1, topographically limited horizontal or vertical grating stimuli were presented monocularly either within 1° or 2° rectangular windows or 2° patches at eccentricities ranging from 0° to 15°. High-contrast square wave gratings (spatial frequency 0.5 cyc/deg, drift velocity 2 Hz, duty cycle: 20%) of a single orientation were moved back and forth within the windows at different locations. At each location mapped, stimuli consisted of two orthogonally oriented gratings. In order to understand how well optical imaging can resolve visual stimuli, we used very thin gratings (0.5°, 0.25° or 0.1° wide, full screen high) presented monocularly to measure the "line spread" of optical signals in cortex. The "line spread function" can provide critical information about how the system represents or responds to stimuli. The thin grating stimuli were selected because they were spatially restricted in one dimension yet were still capable of providing cortical activation.

Similarly, for creating visuotopic maps in area MT, different sizes of topographically limited stimuli such as circles, annuli, wedges and rectangles were monocularly presented at different visual field locations at eccentricities ranging from 0° to 40°. Drifting gratings (fundamental spatial frequency, 0.2 cycles per degree; drift velocity, 2 Hz; duty cycle, 20%) were presented at two orientations, 0° and 90°, inside the spatially restricted areas.

Video images were acquired at a rate of 30 frames/sec, but all frames acquired for each condition during the 8-sec period of stimulation were summed together for 8 data

frames before further analysis. Individual data frames included 744 x 480 pixels, with a resolution of either 87 pixels per mm for the lens combination (50-mm top, 50-mm bottom) or 174 pixels per mm for the same lens combination used with the addition of a 2x converter on the top. These data acquisition periods were preceded by 10-12 sec interstimulus intervals. Stimulus sets were repeated 10-20 times.

Image analysis

Two approaches were used to create visual field maps. (1) Using Winmix software (Optical Imaging, Inc.), all activity images associated with stimuli of the same orientation were summed and divided by the “pure blank” obtained by summing the images of the blank control to create single-condition maps. (2) The summed activity images acquired during the presentation of one orientation were divided by the summed activity images acquired during presentation of the orthogonal orientation at the same location to create differential maps. Maps constructed either way gave consistent activation patterns.

Custom programs written in Matlab were used to further process the data. The resulting maps were routinely “clipped” (1.5-2 standard deviations around the mean), smoothed by using a Gaussian filter at a radius of 2-3 pixels and scaled in the range of 0–255 gray levels for appropriate display. No further processing was done on the derived maps unless specified.

In some cases, to help reduce vascular artifacts, we used the data images to create a mask over the location of the major blood vessels in the single condition maps. The grayscale value for each pixel in the data images that was located in the mask was replaced by the mean of the grayscale values of the appropriate surrounding pixels

outside the mask (Bosking et al., 2000; Blasdel and Campbell, 2001). Regions located within masked areas were excluded for quantification.

CMF calculation

The cortical magnification factor, CMF, can provide a quantitative assessment of topographical organization. The relationship between CMF and eccentricity tells the relative difference in the amount of tissue devoted to the representation of each degree in visual space (Daniel and Whitteridge, 1961; Van Essen et al, 1984). CMF can be a linear measure (mm of cortex per degree of visual field) (Daniel and Whitteridge, 1961; Van Essen et al, 1984; Albright and Desimone, 1987) or an areal measure, mm^2 of cortex per deg^2 of visual field (Van Essen et al., 1984). For V1, the cortical magnification factor (CMF) was measured based upon visual field maps and calculated as the average linear distance in the cortex representing 1° in visual space (mm/deg) at a particular eccentricity. The distance between two adjacent points on topographical maps of cortex (in mm) was divided by the corresponding distance in degrees of visual space. For MT we calculated the areal CMF as the ratio of the difference in cortical activation areas (mm^2) obtained from two adjacent stimuli and the difference of area sizes of these two stimuli (deg^2). For V1, we used rectangular windows to calculate CMF and for MT, we used circular and annular stimuli.

Histology and alignment

At the termination of each experiment, the animal was deeply anaesthetized with an overdose of sodium pentobarbital and perfused transcardially with a saline rinse followed by 2% paraformaldehyde in 0.1 M phosphate buffer. The brain was removed and the imaged area of cortex was separated and flattened. The imaged piece of cortex

was then frozen and cut with the surface vascular pattern preserved in the first 100 - 150 μ m section. Subsequent sections were cut at 50 μ m. Either CO staining, myelin staining or both were performed using methods described previously (Wong-Riley, 1979; Gallyas, 1979; Boyd and Matsubara, 1996).

Surface and radial blood vessels were the primary landmarks used to align histological sections to the optical reference images of the imaged area. Differences between images and sections due to distortion or tissue shrinkage (about 10 -15%) were handled by global scaling and rotation. After the optical images were aligned with the histological data, we examined the corresponding locations or patterns of the imaged brain areas to see if the anatomical delineation of each visual area matched the optical imaging results.

Results

In this study, we found that high resolution topographic maps of V1 and MT could be produced using optical imaging of intrinsic signals. Visuotopic maps produced by optical imaging of intrinsic signals matched those produced by microelectrode mapping, while at the same time revealing detailed retinotopic features. Below we describe these data in more detail.

Visuotopic organization of V1

General Visuotopy

Figures 1 and 2 show a series of activation patterns evoked by stimulation using either topographically limited vertical gratings (2°, full screen height [40°]) presented at different locations parallel to the vertical meridian (VM), or topographically limited

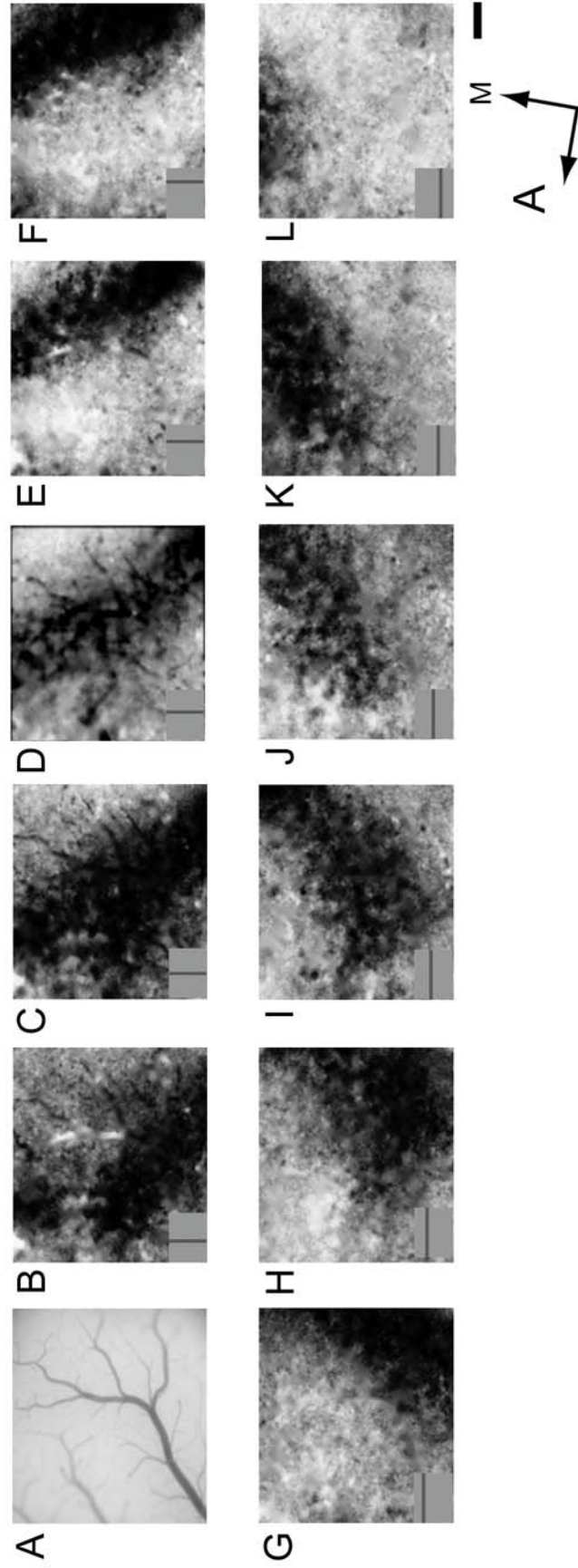


Figure 1. Optical imaging of topographically limited stimuli (Case 1). **A:** A surface reference image. **B-F:** A series of activation patterns evoked by topographically limited vertical gratings (2° , full screen height) at different locations parallel to the vertical meridian (VM): VM 0° , VM $+1^\circ$, VM $+2^\circ$, VM $+4^\circ$, VM $+5^\circ$. **G-L:** A series of activation patterns evoked by topographically limited horizontal gratings (2° , full screen width) parallel to horizontal meridian (HM): HM $+1^\circ$, HM, HM $+1^\circ$, HM $+2^\circ$, HM $+3^\circ$, HM $+3^\circ$. By mapping both vertical and horizontal dimensions of the visual field, we were able to construct a visual field map and determine the visual field representation in cortex. The small insets in lower left corners (B-L) indicate the mapping stimulus positions relative to the display monitor. Scale = 1mm.

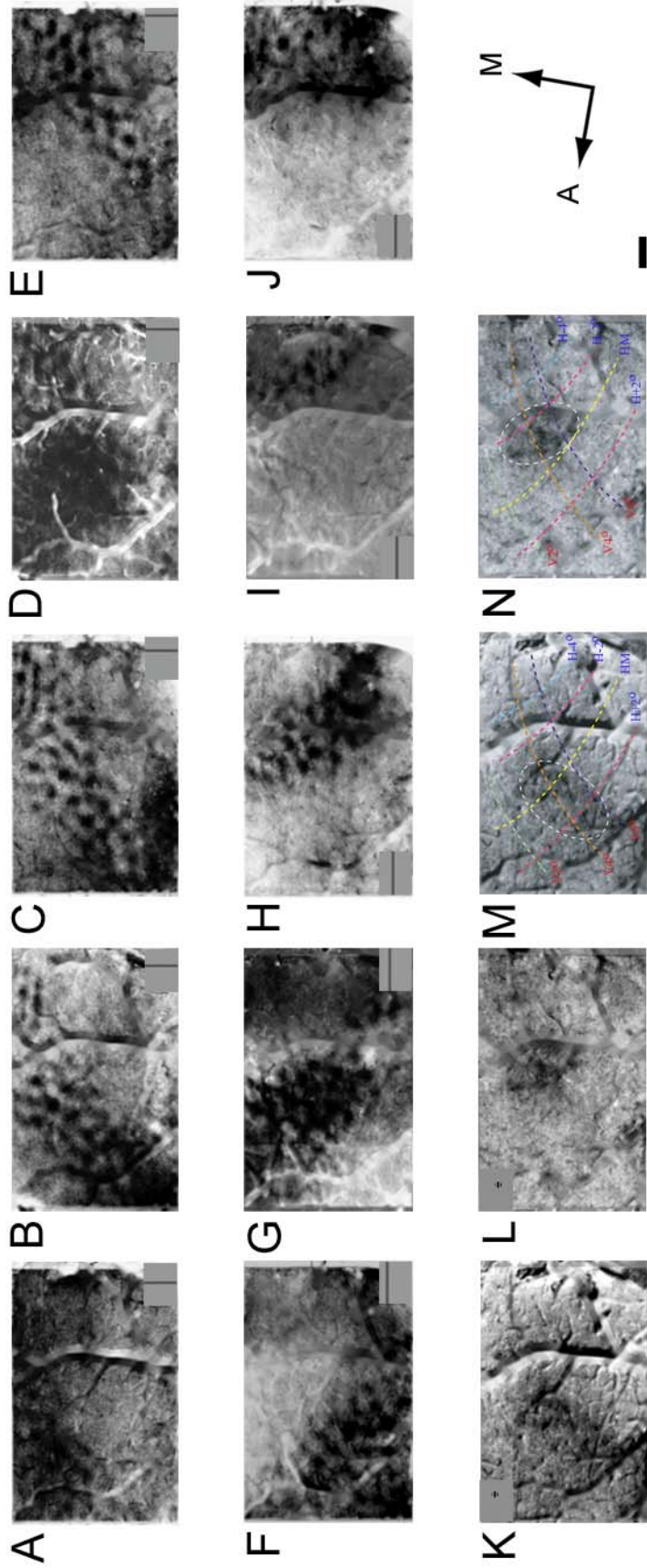


Figure 2. Optical imaging of topographically limited stimuli (Case 2). A-E: A series of activation patterns resulting from stimulation with topographically limited vertical gratings (2°, full screen in height) at VM 2°, VM 3°, VM 4°, VM 5°, VM 6°. F-J: A series of activation patterns resulting from stimulation with topographically limited horizontal gratings (2°, full screen width) at HM+2°, HM 0°, HM-2°, HM-4°, HM-6°. K and L are activation maps produced following stimulation with 2° circular patches located at (x: 4°, y: 0°) and (x: 5°, y: -1°). M and N show the same activation maps with visual field location contours (derived from A-E and F-J) superimposed. Scale = 1mm.

horizontal gratings (2° high, full screen width [57°]) presented parallel to the horizontal meridian (HM) in two different cases. As can be seen clearly in Figure 1, when the stimulus is moved from the vertical meridian to more eccentric points, the activation stripe moves from anterior to posterior in V1. As the stimulus is moved from just above the horizontal meridian into the lower visual field, the band of activation moves from ventral to dorsal V1. Since most V1 neurons are orientation selective, the topographically limited vertical and horizontal gratings produced periodic response patterns (e.g., Figures 1 and 2), which correspond to the layout of orientation domains in this region of cortex.

The average spread of activation in V1 resulting from the stimulus bars (either 2° in width or height) were 1.4 ± 0.18 (mean \pm std) mm/deg at 0- 6° eccentricity. Shifting the stimuli by as little as 1° produced discrete shifts in activation foci in cortex, although stimuli in adjacent positions activated highly overlapping regions in V1. As can be seen by the tapering of the activation zone at greater eccentricities, the same size stimuli activated more cortical territory when presented close to the *area centralis* (e.g. see Figures 1I and Figure 2G).

By mapping both vertical and horizontal dimensions of the visual field, we constructed visual field maps (see Figure 3A, Figure 2M and N). The validity of such visual field maps could be confirmed by matching activation foci produced by small circular patch stimuli presented at specified locations as demonstrated in Figure 2K-N. Stimulation using 2° circular patches located 4° from VM and on the HM, and 5° from VM and 1° below HM, activated distinguishable cortical regions in a predicted pattern (Figure 2 K and L). These activation patterns were centered at the intersections

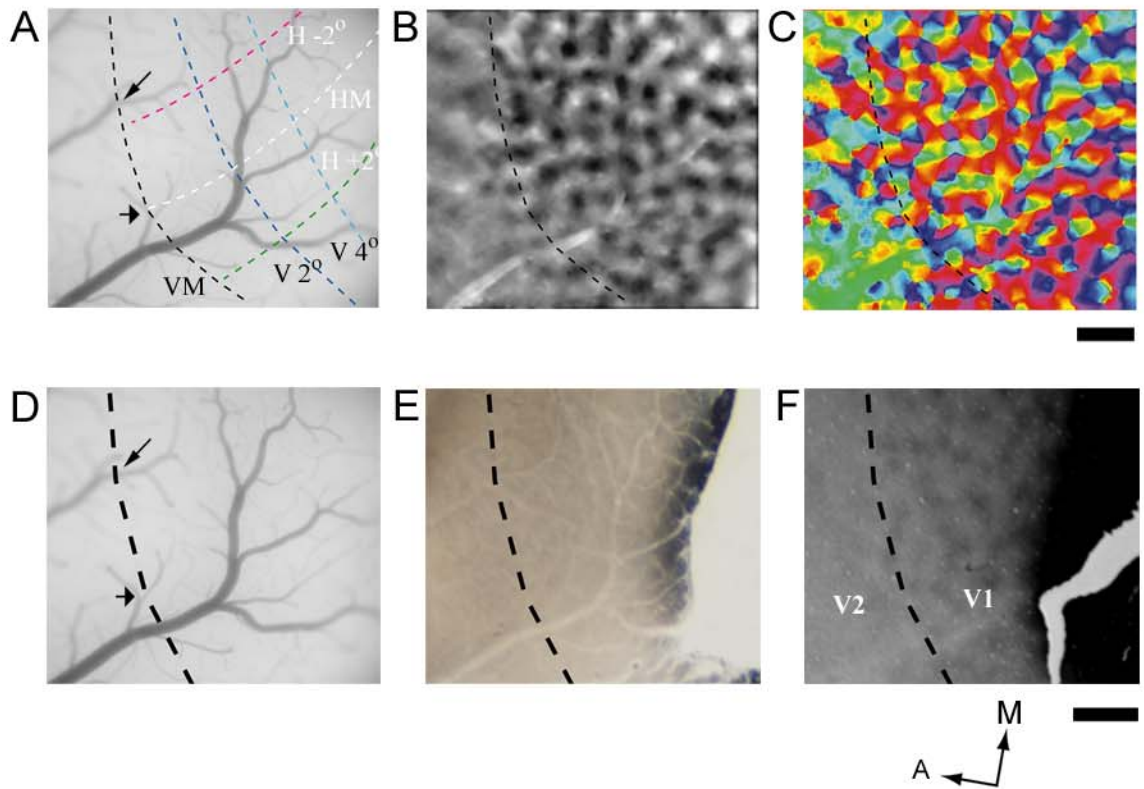


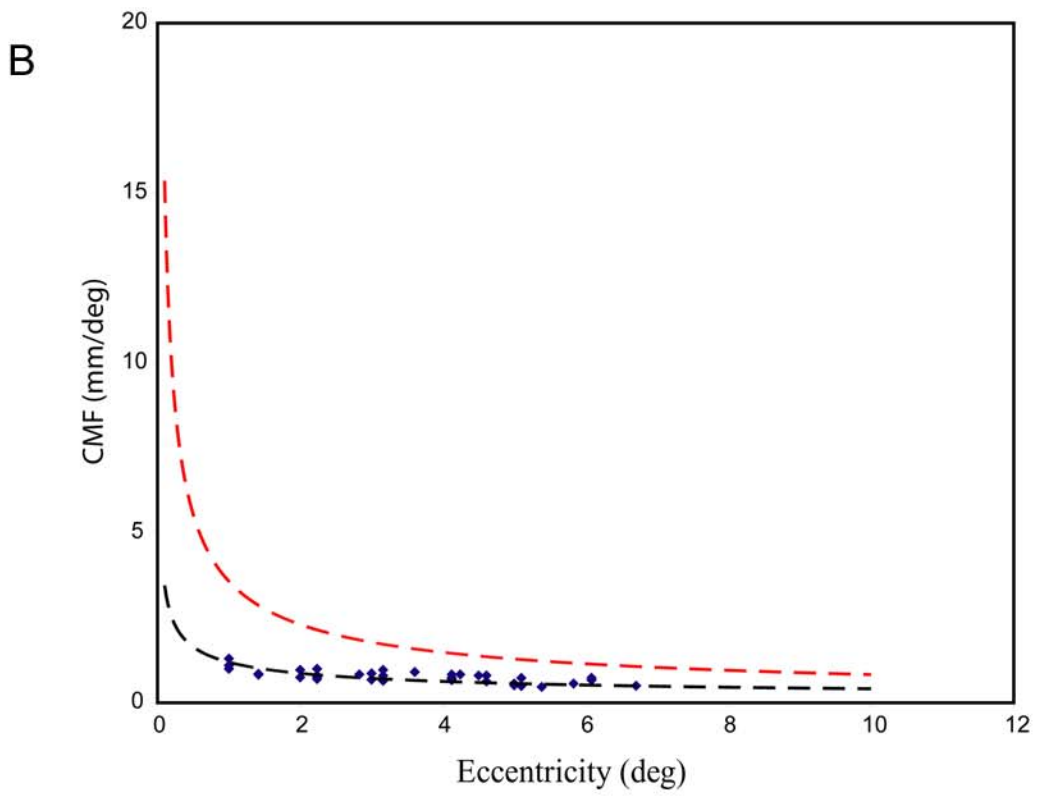
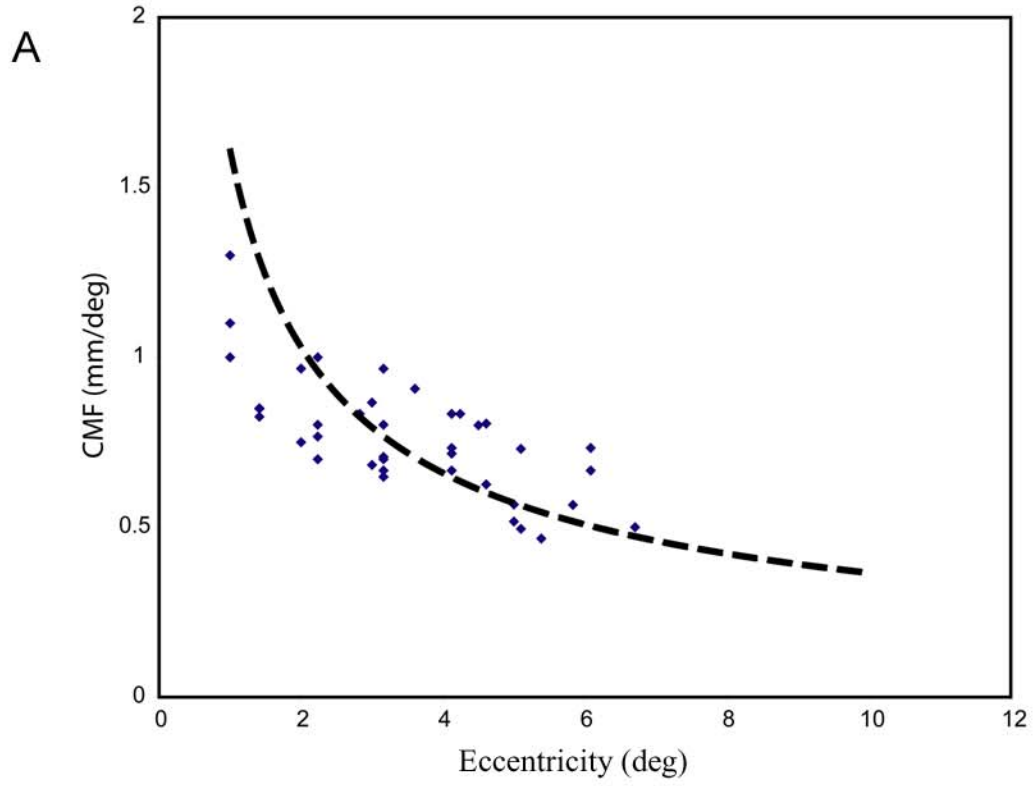
Figure 3. The V1/V2 border determined by the topographical mapping. **A:** A reference image with the visual field location map constructed based upon the series of activation patterns shown in **B-F** and **G-L** in Case 1. For the visual field map, H -2° and H 2° are 2 degrees below and above the horizontal meridian (HM) representation, respectively; V 2° and V 4° are 2 and 4 degrees away from the vertical meridian (VM) representation, respectively. **B** and **C** are an orientation difference map of $0^\circ/90^\circ$, and a color-coded orientation preference map from the same imaged area, respectively. The dashed black line in **A**, **B** and **C** is the midline of VM representation. **D**, **E** and **F** are the reference image, the image of the superficial brain section (with blood vessel patterns) and the image of a deeper cytochrome oxidase (CO) stained section, respectively. The thick dashed black line delineates the V1/V2 border. The short and long arrows in **A** and **D** point to matching landmarks. The border of V1/V2 determined by intrinsic imaging is consistent with that observed for the full screen orientation map and with the anatomical boundary determined by CO staining. Scale bar = 1 mm

of activation bands at VM +4° and HM 0°, at VM +4° and HM +1°, respectively (Figure 2M and N). Also, the border of V1/V2 determined by intrinsic imaging was consistent with that observed based on the anatomical boundary determined by CO staining (Figure 3). Bush baby V1 and V2 can be easily distinguished based upon CO staining because V1 has a periodic staining pattern (CO blobs) and V2 does not. Also, since iso-orientation domains in V2 are larger than in V1 (see also Chapter III), the border of V1/V2 could be determined simply by the visible difference in functional maps between these areas (Figure 3B and C). The thick dashed black lines in Figure 3D, E and F delineate the V1/V2 border.

CMF comparisons

We measured the cortical magnification factor (CMF) and compared the results with those produced by microelectrode recordings (Rosa et al., 1997). We did not find any significant difference in the CMF that related to azimuth or elevation, which suggests that there are no local anisotropies in cortical representation in bush baby V1. This result agrees with the finding of microelectrode mapping in bush baby V1 (Rosa et al., 1997), but differs from that reported in both optical imaging and microelectrode mapping studies for macaque V1 (Van Essen et al., 1984; Blasdel and Campbell, 2001). As shown in Figure 4A, the CMF measured at 1- 7° eccentricity matched the function of CMF vs eccentricity taken from Rosa et al. (1997). Our measurement of average CMF for eccentricities of 1-7° was 0.77mm/deg, which is close to the extrapolated value (0.81 mm/deg) of Rosa et al. (1997) at the same eccentricities. Figure 4B compares the microelectrode mapping results of Van Essen et al. (1984) in macaque monkeys, Rosa et al. (1997) in bush babies and the present study. The CMF in bush babies is much less

Figure 4. Comparison between the cortical magnification factor (CMF) measured by optical imaging mapping and microelectrode recordings. **A.** The CMF measured from optical imaging at a particular eccentricity (blue diamonds) matches well with the function of CMF vs eccentricity (E) from Rosa et al. (1997): $CMF = 2.36 \cdot (E + 0.73)^{-0.8}$. **B.** A comparison of CMF results obtained from the microelectrode mapping results of Van Essen et al. (1984) in macaque monkeys (red dashed line, plotted as $CMF = 10 \cdot (E + 0.82)^{-1.14}$), Rosa et al. (1997) in bush babies (black dashed line) and the present study. The CMF in bush babies is much less than that reported in macaque monkeys in the representation of central vision.



than that reported in macaque monkeys for the central vision representation.

Resolution of optical imaging

We found that activation patterns could be produced by gratings of 0.5° and 0.25° in width (Figure 5A-D). We also could see shifts in activation foci in cortex, responding to stimulus positions moved by as little as 0.25° . In fact, optical imaging resolved ultra thin gratings down to 0.1° (compare Figure 5E with Figure 5F), although the activation pattern using such fine gratings was weak. Note that different widths of the limited horizontal gratings (0.5° , 0.25° , 0.1°), centered at the same location in visual space, had a peak of activation at the same exact cortical location (compare the arrows in Figure 5B and D, and the arrow heads in Figure 5C and E).

We measured the ‘line spread’ function in response to very thin grating stimuli. The activation spread produced by the 0.5° and 0.25° gratings showed no obvious differences, although the activation produced by the 0.5° gratings was stronger than that resulting from the 0.25° gratings. The ‘line spread’ measurements (defined based upon outlining the distinctive modular patterns of activation produced by 0.5° gratings) were about 1.4 mm in cortex, which is about twice that based upon microelectrode mapping (0.63 mm) using 0.5° gratings (Rosa et al., 1997). Thus, the spread of activation in V1 measured via optical imaging is about twice that predicted based upon recording from small groups of cells extracellularly.

Visuotopic organization of MT

General retinotopic organization

Bush baby MT is exposed on cortical surface and has a complete representation of the contralateral visual hemifield. Thus, we could also use optical imaging to extensively

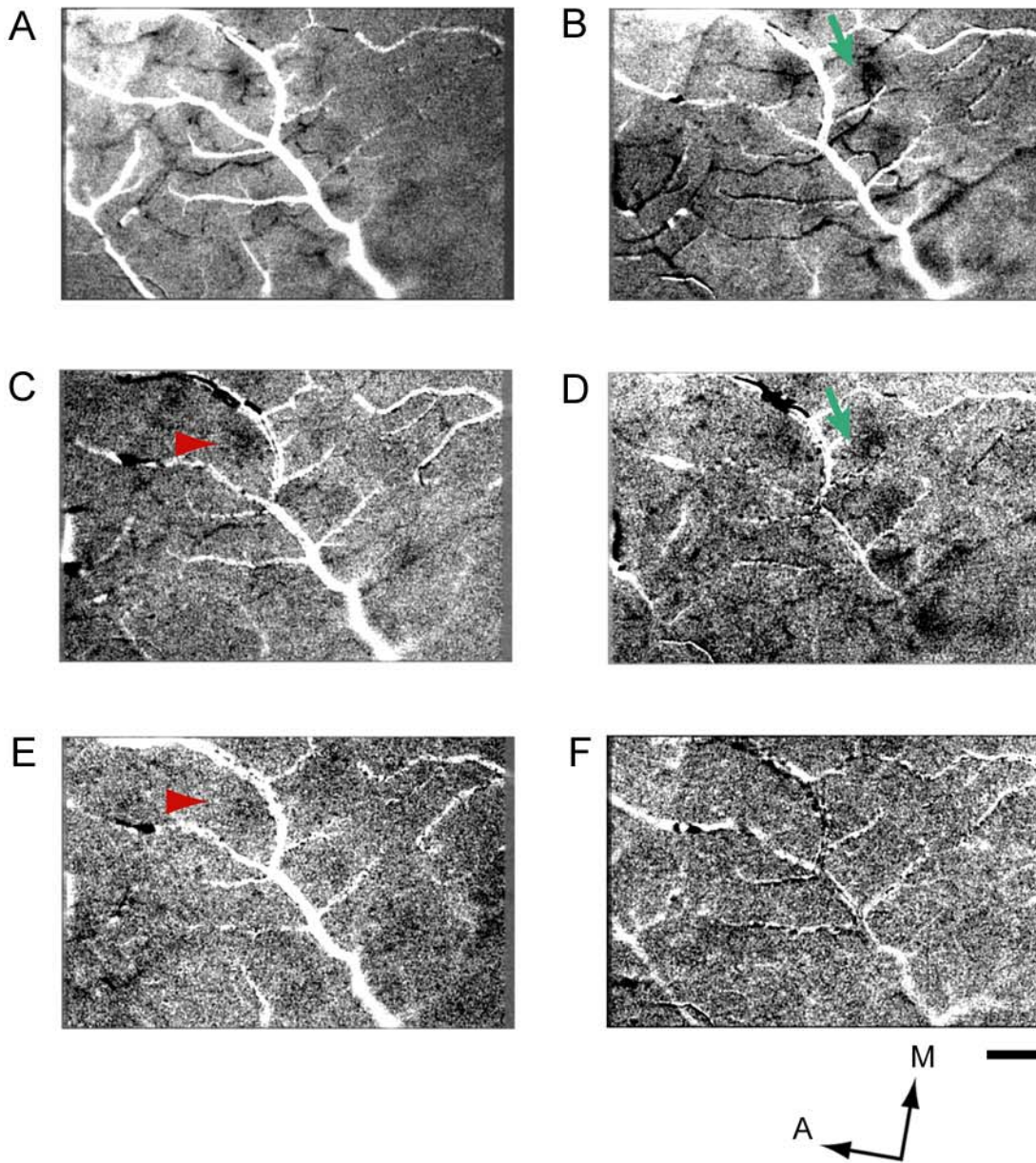


Figure 5. High resolution of visuotopic mapping. **A** and **B** are optical activation maps from stimulation using horizontal gratings of 0.5° height, full screen width at positions of 3° and 3.5° parallel to HM. **C** and **D** are activation maps produced by horizontal gratings of 0.25° height, full screen width at positions of 3.25° and 3.5° parallel to HM. **E** is an activation map produced by horizontal gratings of 0.1° height, full screen width at positions of 3.25° parallel to HM, and **F** is a control map without any visual stimulation. The green arrows in **B** and **D** point to the activation module produced by stimulation using limited horizontal gratings of 0.5° and 0.25° in height (full screen width) at the position of 3.5° parallel to HM; and the red arrow heads in **C** and **E** point to the activation module produced by stimulation using limited horizontal gratings of 0.25° and 0.1° in height (full screen width), centered at the position of 3.5° parallel to HM. Scale bar is 0.5mm.

characterize the visuotopic organization of MT. The first finding was that MT was activated by drifting gratings of different orientations in patterns that clearly distinguished MT from surrounding areas. MT is located in the middle of the upper temporal lobe of bush babies (Figure 6A), where it can be delimited as a myelin-dense area (Figure 6B). The same region of cortex was activated when full screen (40°) drifting gratings were viewed. The activation was patchy and modular (Figure 6D) and the locations of activated patches varied with the orientations of the drifting grating (see below). The full screen grating most strongly activated the dorsocaudal 2/3 of MT, representing central and paracentral vision, while weakly activating the ventrorostral 1/3 of MT, largely representing peripheral vision beyond the 40° of the stimulating screen. Although some areas beyond MT showed activation, none of the areas of cortex surrounding MT were as highly activated by the gratings, indicating that such stimuli effectively distinguish MT and identify most of its extent (Figure 6D). Defined by imaging, the size of MT (18 mm² with a rostrocaudal length of 4.1 mm, and a dorsoventral height of 6.3 mm) corresponds with previous portrayals of MT in bush babies (Beck and Kaas, 1998), and with the size of MT judged from histological boundaries in the present cases (Figure 6D).

The second major finding was that stimuli restricted to parts of the visual field effectively revealed features of the retinotopic organization of MT. The overall retinotopic organization of MT in bush babies (Allman et al., 1973) and other primates (Allman and Kaas, 1971a; Van Essen et al., 1981) is known from relating receptive field locations of neurons to recording sites in MT, but optical imaging provides a richer understanding of the ways that stimuli in different parts of the visual field activate MT.

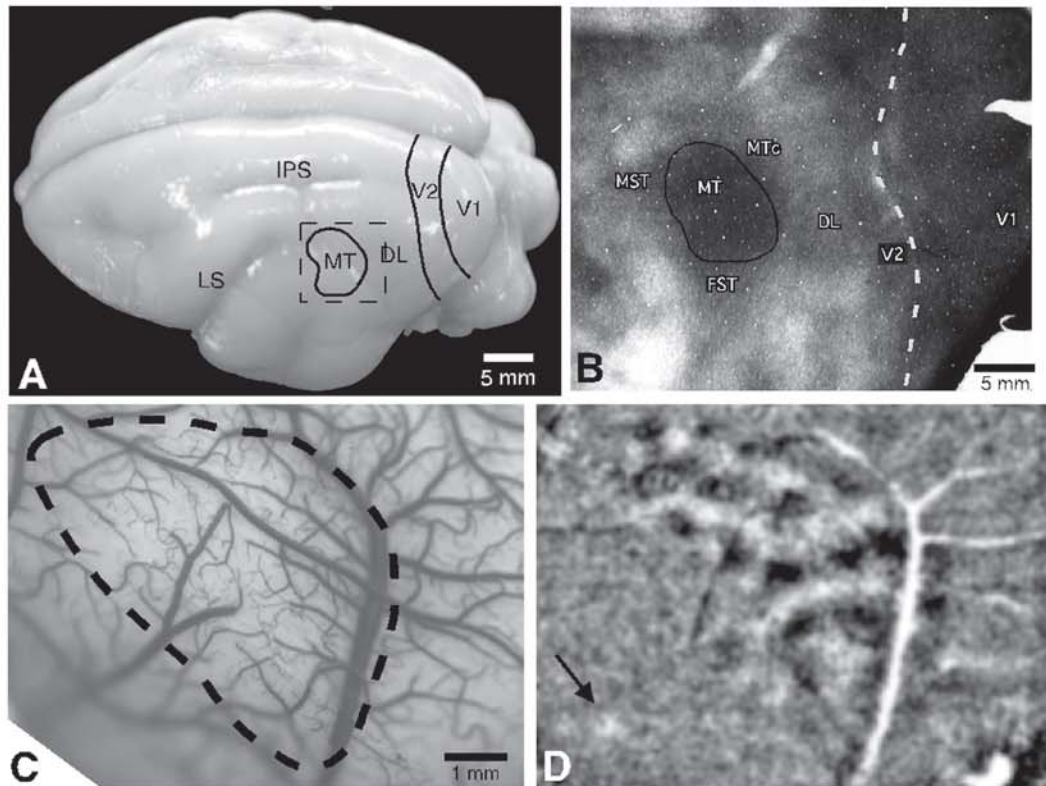


Figure 6. Visualization of area MT in vivo by optical imaging of intrinsic signals

A. A dorsolateral view of the bushy baboon brain showing approximate locations of the first visual area, V1, the second visual area, V2, the dorsolateral area, DL, and the middle temporal area, MT. The dashed box indicates the estimated camera view for the optical images acquired in case 03-01. The intraparietal sulcus, IPS and lateral sulcus, LS, are also indicated. Scale bar is 5mm. **B.** A section of flattened cortex stained for myelinated fibers is shown with architectonically-defined boundaries of MT and surrounding areas. Scale bar is 5mm. **C.** The cortical surface of the imaged area, showing the blood vessel patterns and the approximate boundary of the area MT (dashed line), which was revealed by activation patterns resulting from binocular stimulation of full screen drifting gratings at 4 different orientations (0° , 45° , 90° , 135°). **D.** shows one of the orientation difference maps ($90^\circ/0^\circ$) (case 03-01). Dark patches are areas with selective responses to orientation 90° ; white patches are areas with selective responses to orientation 0° . The region highly responsive to oriented, drifting gratings closely approximates MT as identified architectonically in the same case. Less pronounced activity occurs in surrounding cortex. Arrow in **D** marks a small focus of activity rostral to MT.

Oriented drifting gratings of a few degrees of visual angle, continued to maximally activate small patches in MT, but as few as 1-3 patches were well-activated, with the location of the patches depending on where in the visual field the stimulus is (Figure 7A). Successively larger stimuli activate successively larger arrays of patches (compare Figure 7A, B and C), and similarly located stimuli of different orientations activate different patches in the same cortical region (Compare Figure 7B and E). Gratings that changed from a small disc in central vision to larger and larger rings activated patches in MT that progressed rostrally (Figure 7E-H), while gratings in the lower visual field activated patches dorsal to those in MT activated by upper field gratings (Figure 7I-L). These results demonstrate the differing effects of various stimulus locations and orientations when stimulating MT, and indicate that at least several patches of neurons are highly activated by small restricted stimuli. An additional result is that these stimuli also activate patches of cortex outside of MT, although less strongly, and that these patches appear to be parts of additional retinotopic areas. These patches may reflect activity in proposed visual areas MST, FST, MTc, and DL (Figure 7B).

Other aspects of the visuotopic organization in MT were revealed by comparing full screen stimulation to vertical or horizontal, slit-like windows of stimulation. Again, the full screen (40°) gratings activated patches over most of MT (Figure 8A), while a narrow (4°) vertical window centered on the vertical meridian passing through the center of gaze activated a broad strip of MT along its outer border (Figure 8B), where the vertical meridian is represented (Allman et al., 1973). The same stimulus also activated regions well into MT, indicating that the responsive neurons are not tightly confined to the MT border. Moving the vertical window 4° into the contralateral visual

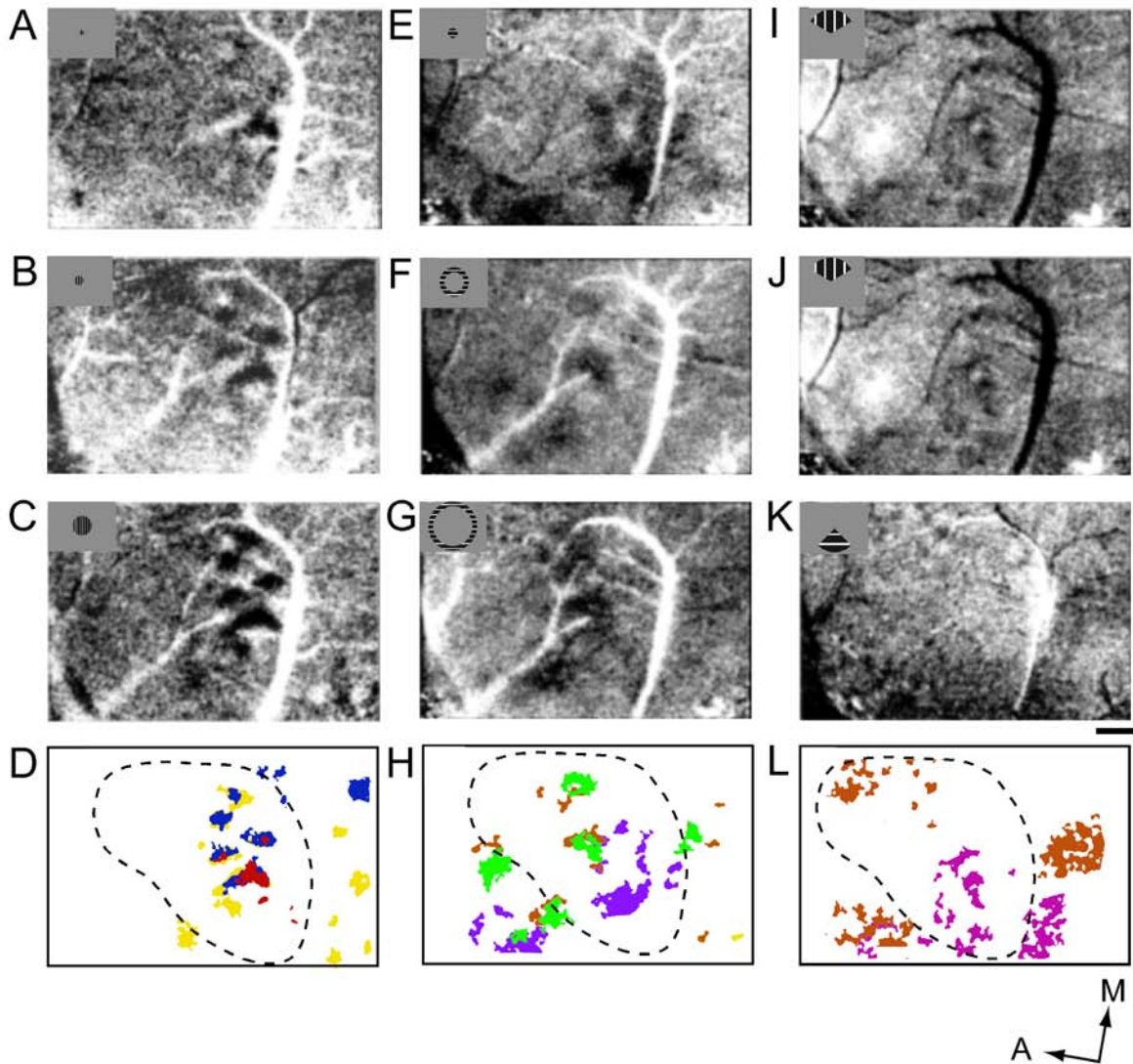


Figure 7. The retinotopic organization of MT and surrounding cortex revealed by stimuli restricted to part of the visual field. Scale bar in A is 1mm. **A-D.** Differential activation maps ($0^\circ/90^\circ$) resulting from binocular stimulation of drifting gratings in a disc centered on the representation of area centralis. **A.** 2.5° (radius) disc; **B.** 5° disc; **C.** 10° disc. Note that difference maps tend to show the most robust activation patterns. **D.** Summary of high activity patterns (red, 2.5° ; blue 5° ; yellow 10°). **E-G.** Single condition maps resulting from monocular stimulation of drifting vertical gratings in (**E**) a 5° radius disc; (**F**) a 10° - 15° annulus; (**G**) a 20° - 25° annulus; all centered on the representation of the area centralis. High activity patterns are summarized in **H** (5° , blue; 10 - 15° green; 20 - 25° orange). **I-L.** Activation patterns resulting from stimulation by a wedge in the upper visual field (**I.** 120° wedge ; **J.** 90° wedge, radius= 25°) and a wedge in the lower visual field (**K.** 90° wedge, radius= 25°) with the apex centered on the area centralis. **L.** Summary of high activity patterns from **I-J** (upper field in purple, lower field in brown). All the optical images here are from the same case as shown in Figure 6. The dashed contours in **D**, **H** and **L** indicate the approximate MT extent. Scale bar is 1mm.

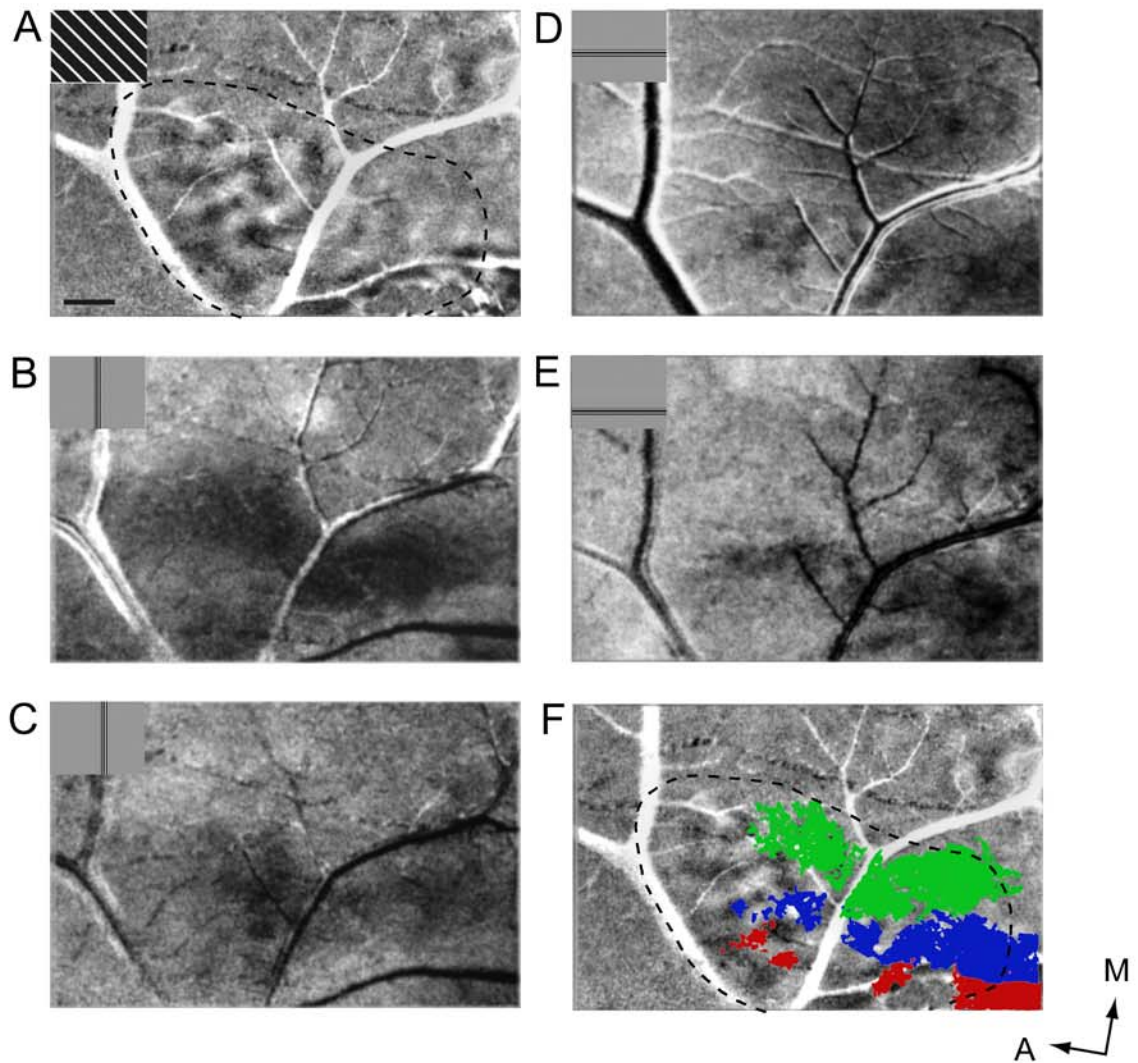


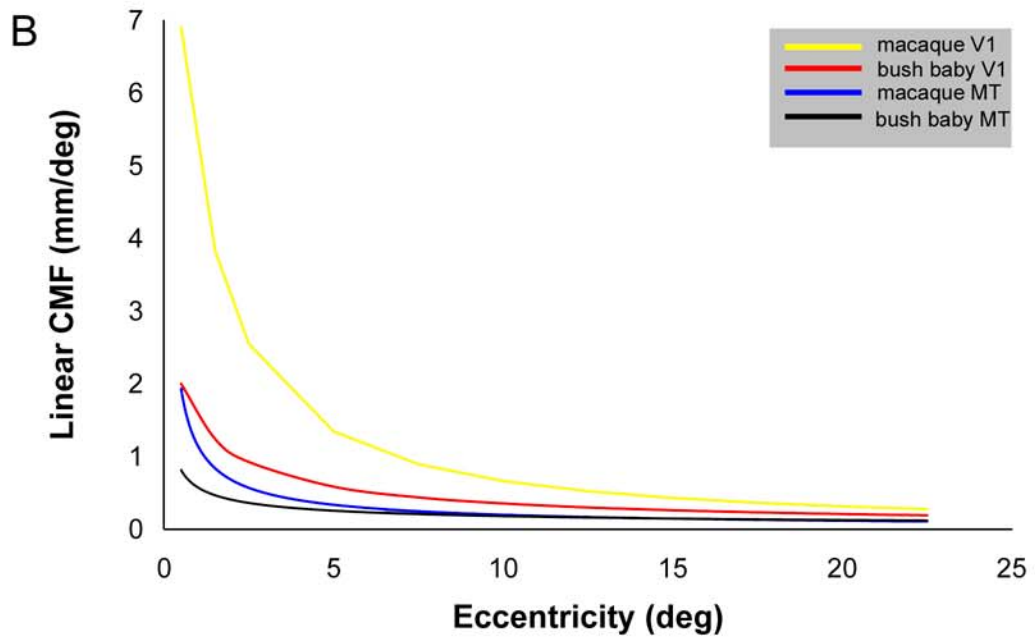
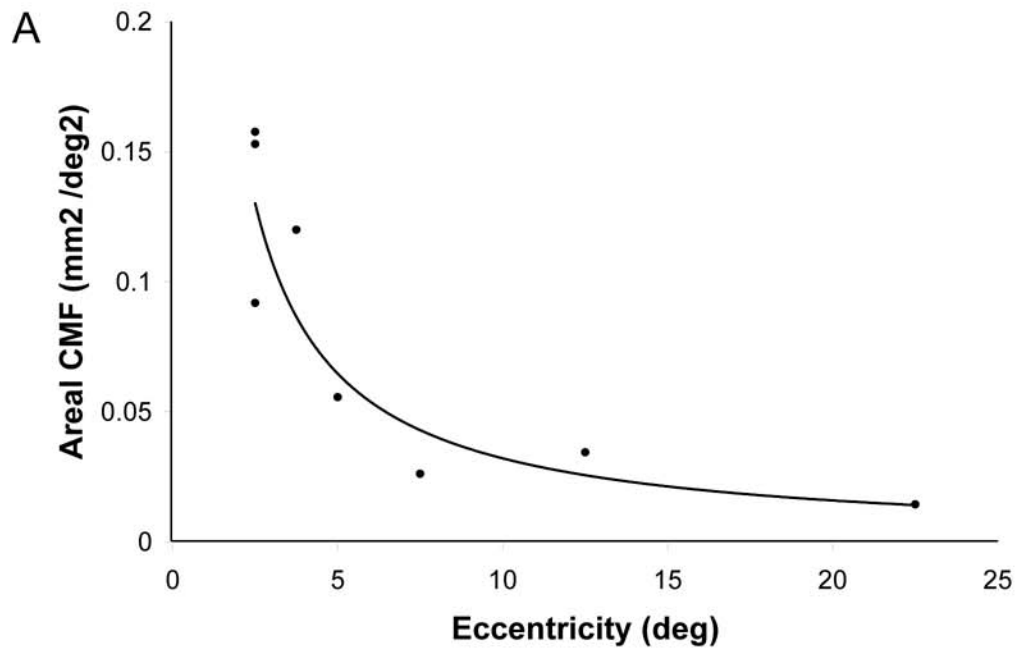
Figure 8. The retinotopic organization of MT revealed by drifting gratings in horizontal or vertical windows in different locations. **A.** The extent of MT (dashed line, case 03-02) revealed by full screen stimulation with a drifting grating (a $135^{\circ}/45^{\circ}$ differential map). **B-C.** Activity patterns as the 4° wide, full screen wide, vertical window is shifted from centered on the vertical meridian (**B**) to 4° to the right (**C**). **D-F.** Activity patterns as the 4° high, full screen wide, horizontal window is shifted from 0° horizontal (**D**), to -4° (**E**). **F.** Colorized, thresholded images of activation resulting from 0° VM stimulation (green), 0° HM stimulation (red), and 0° HM – 4° stimulation (blue). Scale bar is 1mm.

hemifield showed only a modest shift in activation (Figure 8C). Narrow horizontal windows of stimulation also activated patchy bands of tissue in MT, with the band activated by a window on the zero horizontal meridian (Figure 8D) located more ventral than the band activated by the horizontal window displaced 8° into the lower visual quadrant (Figure 8E). The color-coded summary in Figure 3F illustrates the band (green) activated by the vertical window placed at the zero vertical meridian was along the dorsal border devoted to the lower visual quadrant (the ventral border of MT would also be expected to be activated by this stimulus, but it was out of the view of the camera). In contrast, the red band corresponds to the zero horizontal activation, effectively dividing MT into dorsal and ventral halves. The -8° horizontal window shifted activation (blue) into the dorsal half of MT as predicted. Thus, optical imaging showed detailed features of MT visuotopic organization and demonstrated that bush baby MT had an orderly and global retinotopic organization.

CMF and point image sizes

Restricted stimuli of the same size activated more cortical tissue in MT when presented to central than peripheral vision, and activations produced by adjacent stimuli overlapped more in central vision than in the representation of paracentral and peripheral vision. We found that the areal CMF (aCMF) in MT systematically decreased with increasing eccentricity: $\text{aCMF} = 0.328 \cdot (\text{eccentricity})^{-1.0}$ ($R^2 = 0.88$) (Figure 9A). The CMF in MT reached $\sim 0.16 \text{ mm}^2/\text{deg}^2$ at the representation of 2.5° eccentricity, and dropped off quickly at the representation of 5° eccentricity, reaching $\sim 0.05 \text{ mm}^2/\text{deg}^2$, and then dropped off much less rapidly beyond 10° , reaching $\sim 0.025 \text{ mm}^2/\text{deg}^2$ at 20° eccentricity.

Figure 9. The cortical magnification factor as a function of eccentricity in areas V1 and MT. **A.** Areal CMF is plotted versus eccentricity (black dots) in bush baby MT from the present study. The power function that best fits the data is: $CMF = 0.338 \cdot (\text{eccentricity})^{-1.0}$ ($R^2 = 0.88$). The areal CMF systematically decreased with increasing eccentricity. **B.** The square root of the areal CMF (in **A**) approximates a linear CMF. The resultant function ($CMF = 0.57 \cdot (\text{eccentricity})^{-0.5}$, black solid line) is plotted for comparison with a function obtained from macaque MT ($CMF = 1.14 \cdot (\text{eccentricity})^{-0.76}$, blue solid line) (Albright & Desimone, 1987), a function obtained from bush baby V1 ($CMF = 2.36 \cdot (\text{eccentricity} + 0.73)^{-0.8}$, red solid line) (Rosa et al., 1997), and a function obtained from macaque V1 ($CMF = 10 \cdot (\text{eccentricity} + 0.82)^{-1.14}$) (Van Essen et al., 1984)



The square root of the areal CMF approximates a linear CMF. In Figure 9B, the black line is the linear CMF plotted as a function of eccentricity from 0.5°- 22.5° ($CMF = 0.573 \cdot (\text{eccentricity})^{-0.504}$) in bush baby MT from the present study, the blue solid line is the linear CMF plotted versus eccentricities ($CMF = 1.14 \cdot (\text{eccentricity})^{-0.76}$) from macaque MT in the study of Albright and Desimone (1987). Comparison of the function of CMF vs eccentricity shows that bush baby MT has much less cortical magnification than macaque MT in the central visual representation, but has comparable CMF in the peripheral visual representation (Figure 9B). When the CMF plots of bush baby MT (blue line) and V1 (red line) are compared, we can see that the V1 CMF is 2-3 times of that found in area MT.

We approximated the point image size (the amount of cortex related to processing a single point in space) of MT in bush babies by the product of the cortical magnification factors (ranging from 0.55 mm/deg at 2.5° eccentricity to 0.13 mm/deg at 25° eccentricity) by the aggregate receptive field size (roughly 5° to 15° (Allman et al., 1973), as ~2.57 mm for central vision and ~3.25 mm for peripheral vision in MT, respectively).

Discussion

In the present study, we used the optical imaging technique to extensively examine topographic maps of V1 and MT in bush babies. When compared to previously established data, we found that optical imaging was a reliable, efficient and high-resolution mapping tool capable of revealing detailed retinotopic features of both visual cortical areas. Below we consider the details of these results in light of prior studies.

V1

Both the present study and the microelectrode mapping studies (Rosa et al., 1997) indicated that the visuotopic organization of V1 in the bush baby shares many features described for simian primates (owl monkeys: Allman and Kaas, 1971a; macaque monkeys: Van Essen et al., 1984; marmosets: Fritsches and Rosa, 1996). V1 contains a continuous representation of the contralateral visual hemifield with the vertical meridian marking the V1/V2 border and the horizontal meridian bisecting V1 into the lower and upper quadrant representation. Central vision representation is located at the anterior and lateral portion of V1, and peripheral vision is represented more posteriorly and medially in V1.

V1 has an expanded representation of central vision, that is, proportionally, more V1 tissue is devoted to the central $\leq 5^\circ$. We found that activation of the same size stimuli occupied more cortical territory when stimuli were presented close to the *area centralis*, as can be seen by the tapering of the activation zone at greater eccentricities. This is not seen in tree shrew V1 (Bosking et al., 2002), but agrees with a previous report that the spread of functional activity with 2-DG labeling is greater near the foveal representation than near or greater 5° eccentricity in macaque V1 (Tootell et al., 1988b).

Surprisingly, optical imaging can resolve stimuli as narrow as 0.1° and detect shifts of stimulus position by as little as 0.25° . This is much smaller than the average receptive sizes (1° to 3°) for bush baby V1 cells at eccentricities of $\leq 10^\circ$ (Rosa et al., 1997). We also found that the optically detected activity covered a much larger area than that predicted from previous single unit recording studies, being about twice that predicted based upon microelectrode recording. This suggests that optical imaging

measures spike activity and neuronal responses that are subthreshold to extracellular recording. This observation agrees with two earlier studies of cat visual cortex that provide evidence that intrinsic optical signals reflect both sub- and suprathreshold neuronal activity (Das and Gilbert, 1995; Toth et al., 1995). The latter studies demonstrated, as we found, that stimulation in part of visual field evokes optical signals distributed over a much larger cortical area than the corresponding estimates of neuronal spiking responses. In fact, Das and Gilbert (1995) reported that the point spread measured with recordings accounted for only 5% of that measured from optical imaging, and they speculated that the remaining 95% was probably generated by subthreshold activation or was due to long-range intrinsic horizontal connections. As mentioned above, we did not find as large a discrepancy between the spatial distribution of optical and unit responses as reported by Das and Gilbert (1995). One possible reason accounting for the discrepancy may be species difference between cats and bush babies.

MT

Our optical imaging results in bush baby MT demonstrate the existence of an orderly retinotopic map, confirming results of earlier microelectrode mapping studies in this prosimian primate (Allman et al., 1973), as well as in New World owl monkeys, cebus monkeys and marmosets (Allman et al., 1971a, Diogo et al., 2003, Fiorani et al., 1989), and in Old World macaque monkeys (Van Essen et al., 1981, Gattass et al., 1981). The existence of such an orderly map is also supported by anatomical tracing connections from V1 in a number of prosimian and simian primates including bush babies (Symonds and Kaas, 1978), squirrel monkeys (Tigges et al., 1981), owl monkeys (Weller et al., 1984), marmosets (Spatz, 1977) and macaque monkeys (Ungerleider and Mishkin, 1979).

In Old World simians such as macaque monkeys and in humans, reports have been conflicting concerning whether visuotopy is smooth and orderly and whether all of MT corresponds in macaque monkeys to the area of densest myelin or CO staining.

Functional magnetic resonance imaging has been used to provide evidence of visuotopy in MT of humans, although such a map is not always apparent due to resolution issues (Huk et al., 2002). Thus it seems reasonable to conclude that there is an orderly visuotopic map of the contralateral visual hemifield in MT of all primates.

CMF and point image size

In bush babies, the CMF in V1 is much larger than in MT. Both V1 and MT CMFs systematically decrease with increasing eccentricity as reported in macaque monkeys (Albright and Desimone, 1987). However, CMFs of V1 and MT in bush babies are markedly less than those in macaque monkeys at representations of central vision. This may reflect species differences and may reflect less central specialization or a much shallower gradient of ganglion cell density changes in bush baby retinas (DeBruyn et al., 1980; See Chapter 5).

In both bush babies and macaque monkeys, V1 CMF curves are much steeper than those of MT. It has been known that as an important stage for the motion processing system within the dorsal stream, MT mostly receives M pathway dominant inputs via V1 cortical circuitry (See Merigan and Maunsell, 1993; Casagrande and Kaas, 1994). Given that retinal M cell density representing central and peripheral vision is much less steep than that found in P cells (Silveria, 2004), the shallower CMF curve in MT may reflect the preferential indirect M pathway projections from V1 to MT.

Both V1 and MT point image sizes in bush babies do not vary much with eccentricity. In V1, its point image size varies from ~ 1mm (central) to 0.8 mm (peripheral); in MT, its point image size does not seem to vary much either (see the Results). In contrast, it has been reported that in macaque V1 and MT the point image size in the central visual field is a few times that found in the peripheral field (V1, ranging from 5 mm in central regions to 1 mm in peripheral regions; MT, ranging from 7 mm in central regions to 3 mm in peripheral regions) (See Albright and Desimone, 1987).

For both macaque monkeys and bush babies, the larger point image size in MT compared to that in V1 likely reflects the much larger receptive field sizes of cells in MT than those found in V1 (e.g., 1:5 for bush babies). The larger point image size in MT would mean that two closely spaced points in the visual field could result in separate foci of activity in V1 but a common focus of activity in MT. Given that MT is only one tenth the size of V1, the coverage of the visual field must be achieved at the expense of a loss of spatial resolution, as the larger MT receptive field sizes already suggest.

CHAPTER III

FUNCTIONAL ORGANIZATION OF ORIENTATION PREFERENCE IN OWL MONKEY VISUAL CORTEX

Introduction

A common feature of early visual areas is the existence of modules wherein cells that have similar functional properties are grouped together. For example, it has long been demonstrated by single-cell recordings, metabolic labeling and optical imaging that visual cortical neurons with similar orientation selectivity tend to group together and form a modular organization. (Hubel and Wiesel, 1977; Tootell et al., 1988a; Blasdel and Salama, 1986; Roe and Ts'o, 1995). Also, anatomically functional modules often have been defined in relationship to compartments stained by cytochrome oxidase (CO) (e.g., CO blobs within V1 and CO stripes in V2) (Horton and Hubel, 1981; Livingstone and Hubel, 1984). How orientation modules are organized in relationship to CO compartments, however, has been the subject of considerable controversy, especially in V1 with some investigators supporting a strong relationship and others finding no relationship (Livingstone and Hubel, 1984; DeYoe and Van Essen, 1985; Ts'o and Gilbert, 1988; Roe and Ts'o, 1995; Lennie et al. 1990; DeBruyn et al., 1993; Edwards et al. 1995; Leventhal et al. 1995). In addition, most studies investigating the functional organization of V2 are limited to macaque monkeys. There have been no studies of the functional organization of V3 outside of macaque monkeys; only a few investigations have been limited to single unit recording in macaque V3 (Felleman and Van Essen, 1987; Roe and Ts'o, 1997; Gegenfurtner et al., 1997; Adams and Zeki, 2001). Therefore,

we examined the functional organization of orientation preference of V1, V2 and V3 using optical imaging of intrinsic signals and investigated relationships between orientation preference domains and CO modules in these cortical areas in New World owl monkeys.

Owl monkeys offered several advantages for these studies. First, with the exception of macaque monkeys, the visual system of owl monkeys has been studied in the most detail (for review see Casagrande and Kaas, 1994). Second, owl monkeys have relatively small, lissencephalic brains. This feature allowed us to easily access extrastriate areas for optical imaging. Finally, owl monkeys are special because they are the only nocturnal simians in existence. They have only a single cone type and lack color vision, but have well defined CO modules in many visual areas (e.g. V1, V2 and V3) (Tootell et al., 1985; Wikler and Rakic, 1990; Casagrande and Kaas, 1994; Jacobs et al. 1996; Lyon and Kaas, 2002).

Materials and Methods

General preparation

The 10 owl monkeys used in this study were handled according to an approved protocol from the Vanderbilt University Animal Care and Use Committee. Animals were prepared for surgery, paralyzed and anesthetized as described in detail previously (Xu et al., 2001). In these animals V1 was imaged in 9 hemispheres, V2 in 8 hemispheres and V3 in 4 hemispheres.

The animals were initially anesthetized with isoflurane (2-4% in O₂) and, after tracheal intubation and implantation with a femoral catheter, were mounted in a

stereotaxic apparatus. Neuromuscular blockade was initiated by i.v. injection of 1-1.5 mg kg⁻¹ vecuronium bromide (Norcuron). Animals then were artificially ventilated with a mixture of 75% N₂O, 23.5% O₂ and 1.5% CO₂ delivered at a rate sufficient to maintain the peak end tidal CO₂ level at around 4 %. In most cases, paralysis and anesthesia were maintained by intravenous infusion of vecuronium bromide (0.1-0.2 mg kg⁻¹ h⁻¹) and sufentanil citrate (Sufenta: 12-15 mg kg⁻¹ h⁻¹) mixed in 5% dextrose lactated Ringer's delivered at a rate of about 2.7 ml/h. For a minority of cases, anesthesia was maintained by intravenous infusion of propofol (2,6-di-isopropylphenol: 10 mg kg⁻¹ hr⁻¹) through a separate infusion line. In order to ensure that adequate levels of anesthesia were maintained throughout the experiment, heart rate, peak end tidal CO₂ and temperature, as well as EEG, were monitored continuously after paralysis and the level of anesthetic increased if necessary. Pupils were dilated with atropine eye-drops and clear gas permeable contact lenses were used to render the retina conjugate with the stimulus monitor 28.5 or 57 cm distant. In most animals, 3mm artificial pupils were used. The optic disks and *areae centralii* were plotted on the screen.

A craniotomy was made over V1, V2 and V3 and surrounding visual areas, and the dura was reflected. An optical imaging chamber was cemented to the skull and filled with artificial CSF (using the following composition (in mM)): NaCl, 118; KCl, 4.8; CaCl₂, 2.5; NaHCO₃, 25; MgSO₄, 1.2; KH₂PO₄, 1.2; glucose, 10) and sealed with a glass coverslip. In some cases, openings were simply sealed with 1% agarose under a glass coverslip without a chamber.

Visual stimuli and optical imaging

Intrinsic optical imaging signals were acquired with the Imager 2001 differential video-enhancement imaging system and VDAQ/NT data acquisition software (Optical Imaging, Mountainside, NJ, USA). Surface reference images of cortical vasculature were acquired with a 540 nm green light. The cortex was illuminated with a 611 nm orange light during data acquisition and was visualized with a tandem lens microscope attached to a low noise video camera. The camera was focused slightly beneath the cortical surface, and the depth of field was subsequently increased by closing the lens diaphragm. Visual stimuli were generated using a VSG system (Cambridge Research Systems, Rochester, UK), and were presented on a 21" video screen (SONY FD Trinitron, Model GDM-F400) in 120 Hz non-interlaced mode with a mean luminance of 30 cd/m².

To study the functional organization of orientation preference, high-contrast rectangular gratings (fundamental spatial frequency 0.5 cyc/deg, drift velocity 2 Hz, contrast, 100%, duty cycle: 20%) of 4 or 8 orientations were displayed on the full screen and presented binocularly. Each grating was moved back and forth along an axis that was orthogonal to the orientation of the grating. A single trial consisted of data acquisition during continued presentation of the drifting grating stimulus for 8-10 sec, and an interstimulus interval of 10-12 sec using a blank screen of mean luminance. Stimulus sets were made up of 10-30 trials. In some trials all orientation conditions and a blank control were presented in randomized order. In other trials, only orthogonal pairs of orientations (e.g., 0°/90°, 45°/135°) were presented on separate trials.

For retinotopic optical image mapping, retinotopically limited horizontal and vertical grating stimuli were presented monocularly either within 1°- 2° rectangular

windows or 2° - 4° patches at eccentricities ranging from 0° to 20° (see also Lyon et al., 2002). Given the limitations of our camera view we imaged only the dorsal cortex which represents the lower visual field in all three visual areas (V1, V2, V3) at eccentricities ranging from 0° to 20°. Considering recent concerns over the precision and limits of resolution of optical imaging (see Grabquist-Fraser et al., 2003) we also compared the region of cortex activated by stimuli presented on the vertical meridian with the V1/V2 border defined by CO staining. The zone of activation defined optically was always centered on this border defined anatomically suggesting the optical imaging can be used to map visual cortex without distortion.

Video images were acquired at a rate of 30 frames/sec, but all frames acquired for each condition during the 8 sec period were summed together into 4-8 data frames before further analysis. Individual data frames included 744×480 pixels, with a resolution of either 87 pixels per mm for the 50-mm top, 50-mm bottom lens combination or 174 pixels per mm for the same lens combination used with the addition of a 2X converter.

Image Analysis

To construct maps of orientation preference, we summed together all images associated with the same orientation using Winmix software (Optical Imaging, Inc.); the summed images acquired during the presentation of one orientation were divided by the summed images acquired during presentation of the orthogonal orientation to create orientation difference maps (Blasdel, 1992a; Bosking et al., 1997). The difference images were “clipped” at 1-2 standard deviations around the mean of the image pixel distribution and scaled in the range of 0–255 gray levels.

Programs written in NIH Image and Matlab were used to further process the data. Orientation difference images were smoothed using a 40 μ m radius of mean filter kernel. Low frequency noise was reduced by convolving the image with a 450 μ m radius of mean filter kernel and subtracting the result from the original image (Bosking et al., 1997). Vector summation of the difference images was done on a pixel by pixel basis to create a color coded orientation preference (angle) map and a magnitude map coding the degree of orientation selectivity by brightness, with strong orientation selectivity being represented as the brightest and weak orientation selectivity as the darkest (see Bosking et al., 1997 for details). The two maps were combined to create a polar map, which contains information about both orientation preference (color) and magnitude of orientation selectivity (brightness). Rate of change orientation maps were also constructed for the same regions of cortex with the highest rate of change represented as white and the lowest as black. Location of pinwheel centers were determined by thresholding the rate of change map to pinpoint those areas where the rate of change was greatest. These were defined as pinwheel centers, assuming that all orientations presented were represented at these points (Blasdel, 1992b)

In some cases, in order to reduce vascular artifacts, we used reference images or a stack of optical images to create a mask indicating the location of the major blood vessels; the grayscale value for each pixel in these images that was located in the mask was replaced by the mean of the grayscale values of the appropriate surrounding pixels outside the mask (Bosking et al., 2000; Blasdel and Campbell, 2001). Grayscale values for those pixels that were not in the mask were not changed during this filtering.

Electrophysiological verification

Following optical imaging sessions, multiunit or single unit electrode recordings were made to test cell responses within regions of specific orientations defined by the imaging. Cells were recorded in the superficial cortical layers with Parylene-coated tungsten electrodes of 1-2.5 M Ω impedance (Micro Probe, Inc., Potomac, MD, USA). Recordings of orientation preference were consistent with the optical imaging results.

Histology, alignment and data analysis

At the termination of each experiment, the monkey was deeply anaesthetized with an overdose of sodium pentobarbital and perfused transcardially with a saline rinse followed by 2 % paraformaldehyde in 0.1 M phosphate buffer. The brain was removed and the imaged area of cortex was separated and flattened. The imaged piece of cortex was then frozen and cut with the surface vascular pattern preserved in the first 100 - 150 μ m section. Subsequent sections were cut at 50 μ m. CO staining was performed using methods described previously (Boyd and Matsubara, 1996).

Surface and radial blood vessels were the primary landmarks used to align histological sections to the reference images. Differences between images and sections due to distortion or tissue shrinkage (about 10 -15%) were handled by global scaling and rotation. After the optical images were aligned with the histological data, regions of interest were chosen for further quantification. These regions were selected because they contained dense and even CO staining and could be aligned with optical images that were relatively free of blood vessel artifacts. Comparisons between cases were always made at the same relative visual field location (eccentricity).

In V1, the CO image was high-pass filtered at slightly larger than the average blob size (at a radius of 70-170 μ m) and low pass filtered at slightly smaller than the smallest blobs (at a radius of 35-70 μ m). This image was then thresholded and posterized into 3 gray levels: dark (CO blob proper), white (CO interblob proper), and grey (border area) (see Figure. 13B) (see also Boyd and Casagrande, 1999). Using Igor Pro 4.0 (WaveMetrics, Inc.), we encoded the X-Y coordinates of pinwheel centers (defined as described above) and then transferred these coordinates to the CO threshold image to examine the relationship between pinwheel centers and blob, interblob, and blob/interblob border areas. Chi-square analyses was then performed to assess the probability of pinwheel centers falling within each of these compartments. Additionally, to compare the degree of orientation selectivity between compartments, we performed a statistical analysis (Kruskal-Wallis test) on the relationship between CO modules (CO blobs and interblobs) and orientation response selectivity using the magnitude map. In the magnitude map, the degree of orientation selectivity is coded by brightness, with stronger orientation selectivity being represented as the higher value (brighter) pixel. We estimated the orientation selectivity index of each individual pixel by simply normalizing its pixel values by the maximum pixel value on the magnitude map. The orientation selectivity index ranged from 0 - 1 (lowest - highest).

The relationship between orientation selectivity and CO intensity was analyzed in a similar manner in areas V2 and V3. CO images were appropriately band-pass filtered (high pass at a radius of 340-680 μ m; low pass at a radius of 100-200 μ m) and thresholded into dark CO bands, interbands, and border areas. We then transferred contour plots of

CO maps in V2 and V3 to the optical images to qualitatively and quantitatively examine the correspondence of orientation selectivity with different CO compartments.

A one-way ANOVA with post hoc mean difference tests (Tukey tests) was performed, provided that the data did not violate the prerequisite of variance homogeneity across groups. For groups with both unequal variances and unequal samples, we used the Kruskal-Wallis test. Alpha levels of $P \leq 0.05$ were considered significant.

Results

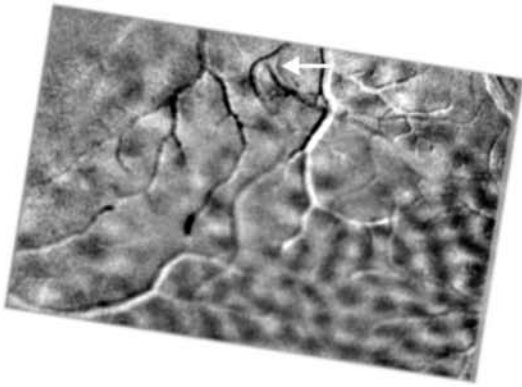
Our most significant finding was that the modular functional organization of V1 and V2 of owl monkeys was strikingly similar to that described in other simian primates, suggesting that differences in lifestyle (nocturnal versus diurnal), including the presence or absence of color vision, is not a driving force behind the existence of these functional modules. We also demonstrated for the first time that V3, like V2, consists of zones of high and low orientation that are oriented perpendicular to the V2/V3 border. In all three areas the basic geometric arrangement in regions of high orientation selectivity was similar and consisted of pinwheels and linear zones although the size of individual orientation domains increased significantly from V1 to V2 to V3. Below we consider these results in more detail.

Defining visual areas

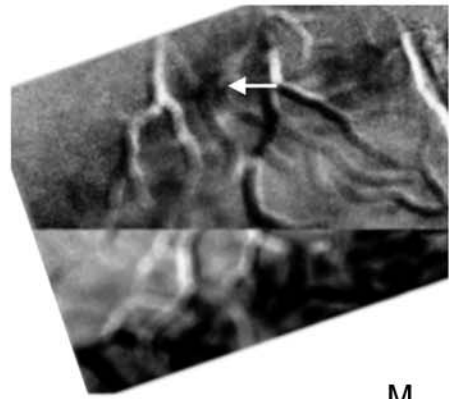
We defined visual areas based upon a combination of visuotopic mapping and functional imaging, histological landmarks, and predictions concerning the extent of each area determined by connectional anatomy (Lyon and Kaas, 2001; 2002). Figure 10A shows that there are clear differences in orientation preference organization between V1,

Figure 10. Visuotopic organization of V1, V2 and V3. **A** shows an orientation difference map of 0°/90° for V1, V2 and V3 where 0° activation is shown as light patches and 90° as dark patches. **B** is a montage from two camera positions showing cortical activation patterns resulting from stimulation of 2° stimuli presented separately along the vertical meridian and the horizontal meridian. The white arrows in **A** and **B** indicate the common blood vessel patterns used for alignment of the two images. **C** shows the vertical meridian activation (V1/V2 border), in red and the horizontal meridian activation (V2/V3 border), in blue superimposed on the orientation map taken from **A**. Due to camera angle limitations we imaged only the dorsal portion of visual cortex (corresponding to the representation of the lower visual field). **D** shows a CO section with V1, V2 and V3 delineated by thin and thick dashed lines from a different case. The modules in V1 are blob-like; the ones in V2 are stripe-like; and the ones in V3 are larger, patch-like and more irregular than in V2. A, anterior; M, medial. Scale bar is 1.0 mm for **A, B, C**, and 2.0 mm for **D**.

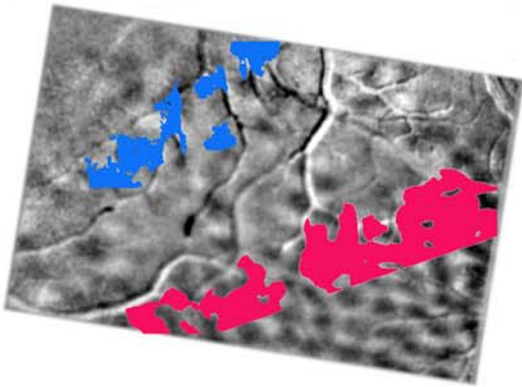
A



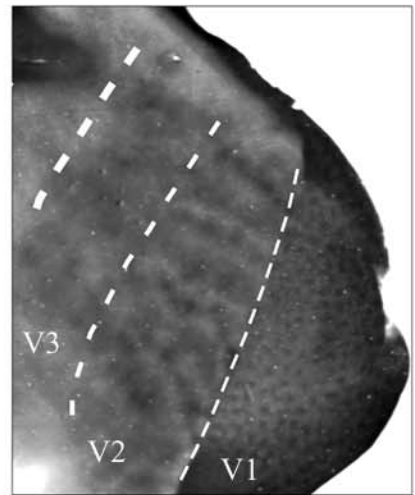
B



C



D



V2 and V3 (see details below). Figure 10B shows cortical activation patterns resulting from stimulation of the vertical meridian and the horizontal meridian; and Figure 1C shows the overlay of these activation patterns on the orientation map in Figure 10A. Consistent with the known retinotopies of these areas, restricted stimuli presented along the vertical meridian activated cortex on the V1/V2 border as well as along the anterior border for V3; restricted stimuli presented along the horizontal meridian crossed through V1 and activated cortical tissue marking the border of V2 and V3 (see Lyon et al., 2002 for details). In CO stained sections, V1 was easily distinguished from V2 based upon the presence of CO blobs; compared with stripe-like CO patterns in V2, there were larger light and dark patches within V3 (Figure 10D).

The general organization of orientation preference in V1, V2 and V3

Figure 11 shows 4 orientation difference maps in owl monkey V1 and V2. The borders of V1/V2 and V2/V3, indicated by thin and thick dashed lines in these images, respectively, were determined based upon both CO histochemistry and topographic mapping using optical imaging of spatially restricted stimuli as described above. In these orientation difference maps, dark areas indicate areas that responded strongly to a particular orientation and light areas indicate areas that responded strongly to the orthogonal orientation. In both V1 and V2, visual stimuli of different orientations elicited clear patches of orientation specific activity. As illustrated in Figure 11, there were marked differences in the organization of orientation preference domains between V1 and V2. For example, the size and spacing of iso-orientation domains in V2 appeared to be about twice as large as those found in V1. Furthermore, while iso-orientation domains in V1 formed a continuous map of high orientation selectivity, in V2 clear bands

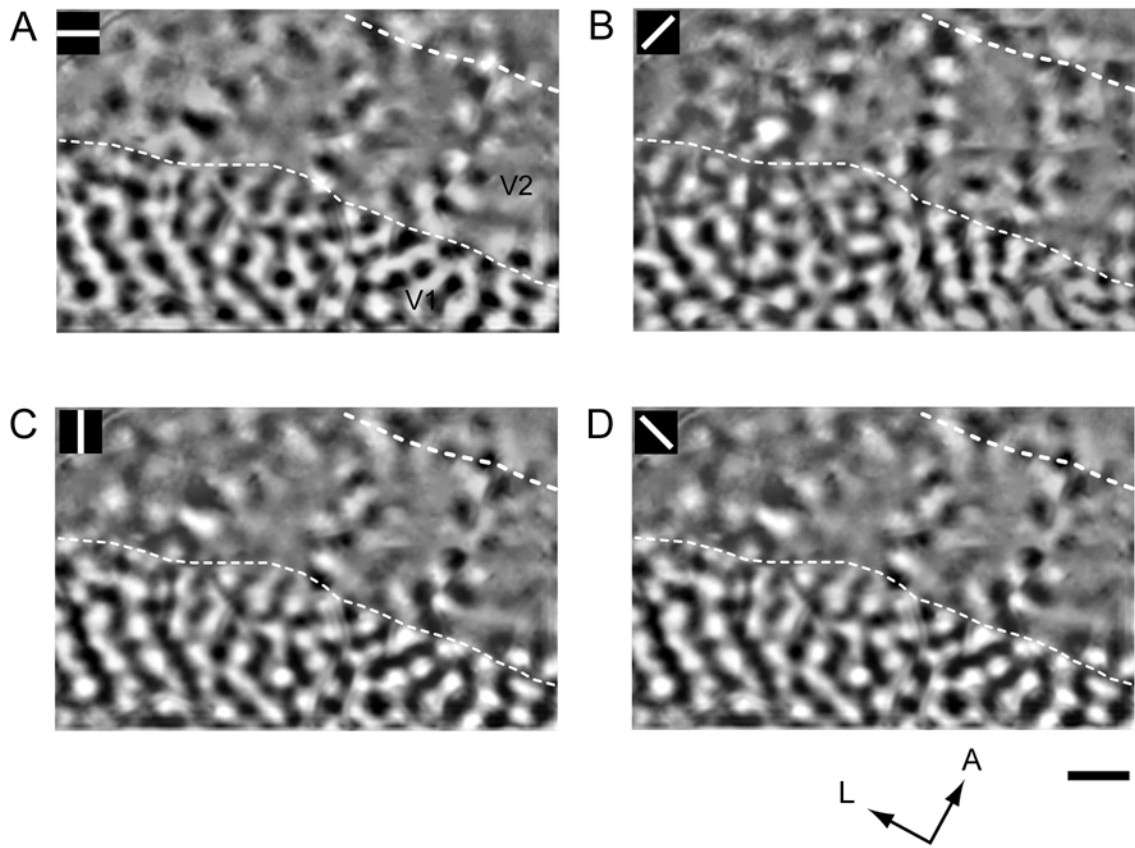
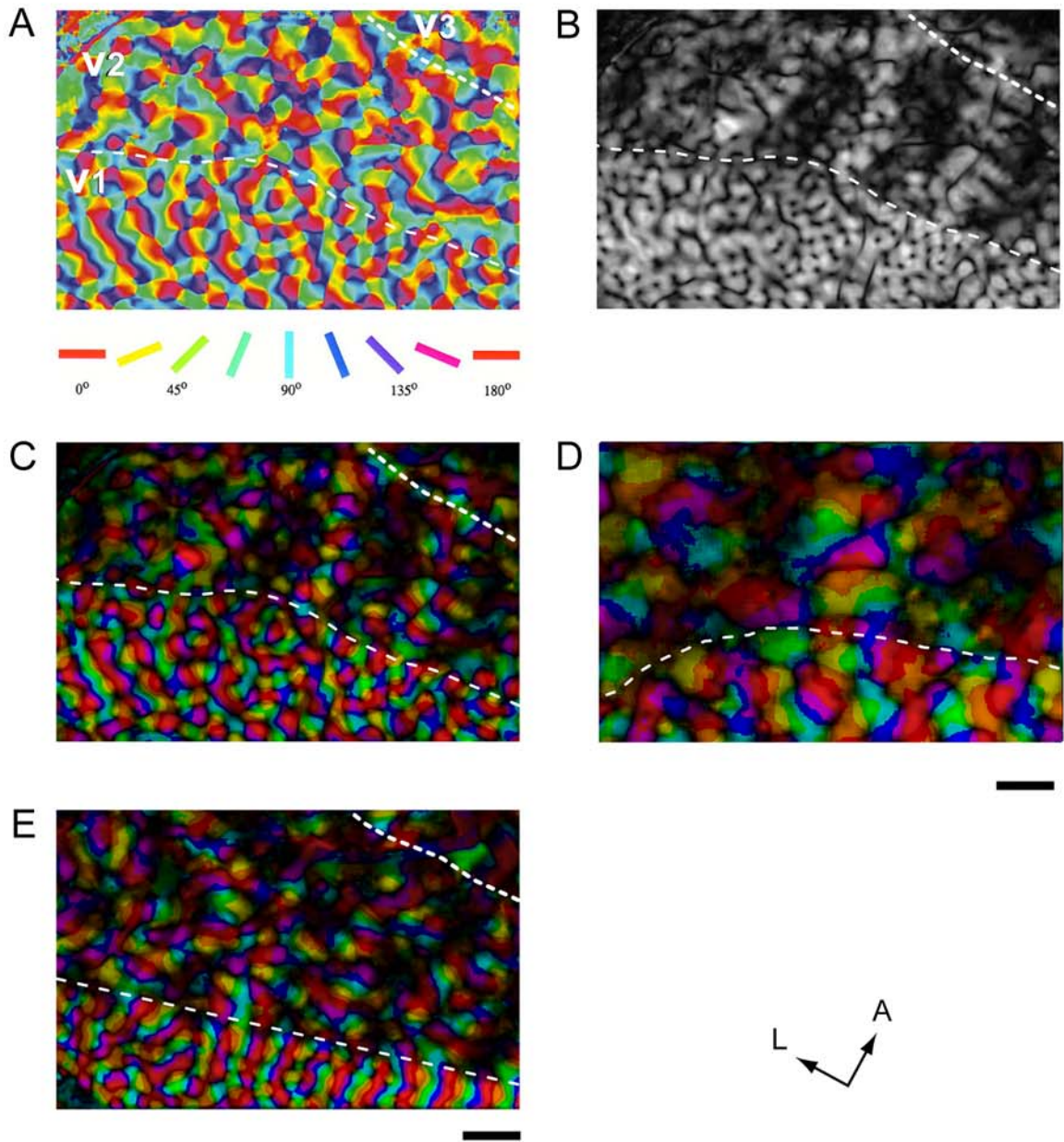


Figure 11. Orientation difference maps of V1 and V2. Four orientation difference maps from the same case shown in Figure 1 are as follows: **A.** $0^\circ/90^\circ$ **B.** $45^\circ/135^\circ$ **C.** $90^\circ/0^\circ$ and **D.** $135^\circ/45^\circ$. The data were obtained from full field rectangular gratings (duty cycle 0.2; spatial frequency 0.5 c/deg, temporal frequency 2 Hz). The thin and thick dashed lines delineate the V1/V2 and V2/V3 borders, respectively. Note that orientation preference is represented continuously throughout V1 but in a series of alternating bands of high and low selectivity within V2. See text for details. A, anterior; L, lateral. Scale bar = 1.0 mm.

of high and low orientation selectivity were evident that resembled the pattern of high and low CO stained bands in this area running perpendicular to the V1/V2 border. This organization of orientation selectivity in V2 is strikingly different from that demonstrated in another nocturnal primate (bush baby) where the organization of V2 shows no bands of low and high orientation selectivity and resembles the organization of V1 (Bosking et al., 1996), but is similar to that described in diurnal primates such as macaque monkeys and squirrel monkeys (Ts'o et al., 1990; Malach et al., 1994; Roe and Ts'o, 1995).

Figure 12 shows the maps of orientation preference in V1 and V2 in more detail. Figure 12A, B and C show, respectively, an orientation preference map, a magnitude map and a polar map, for the same case shown in Figure 11. As reported in other primate and non-primate species (Blasdel, 1992b; Chapman et al., 1996; Bosking et al., 1997; Shmuel and Grinvald, 2000), the owl monkey V1 map contained regions where orientation preference changed linearly (linear zones), and regions where orientation preference was organized radially (pinwheels) (Figure 12A, C, D and E; see also Figure 13B, D). Linear zones were often prominent along the V1/V2 border, and iso-orientation contour lines in these linear zones tended to intersect the border at right angles (Fig 12E). The average size of iso-orientation domains in V1 (N=5 cases) was $0.076 \pm 0.046 \text{ mm}^2$ (mean \pm std).

V2 bands of high and low orientation selectivity, which were evident under both low (Figure 12B, C and E) and high (Figure 12D) magnification, were present in all 10 cases studied. Nevertheless, the regularity of these bands varied somewhat between cases (compare Figure 12E with Figure 12C and D). In many cases, as also described in macaque monkey (Roe and Ts'o, 1995), the V2 bands in owl monkey had irregular



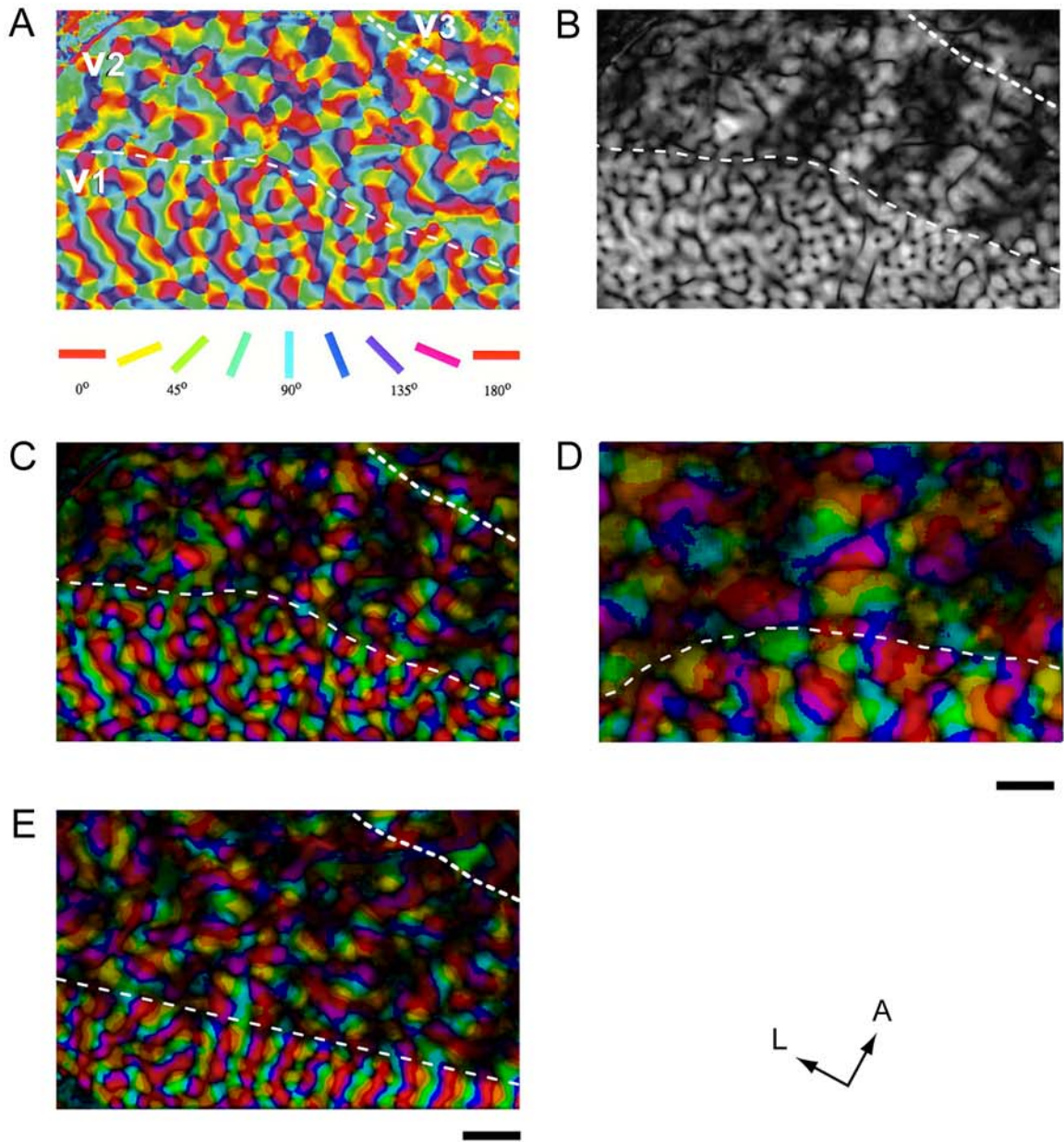
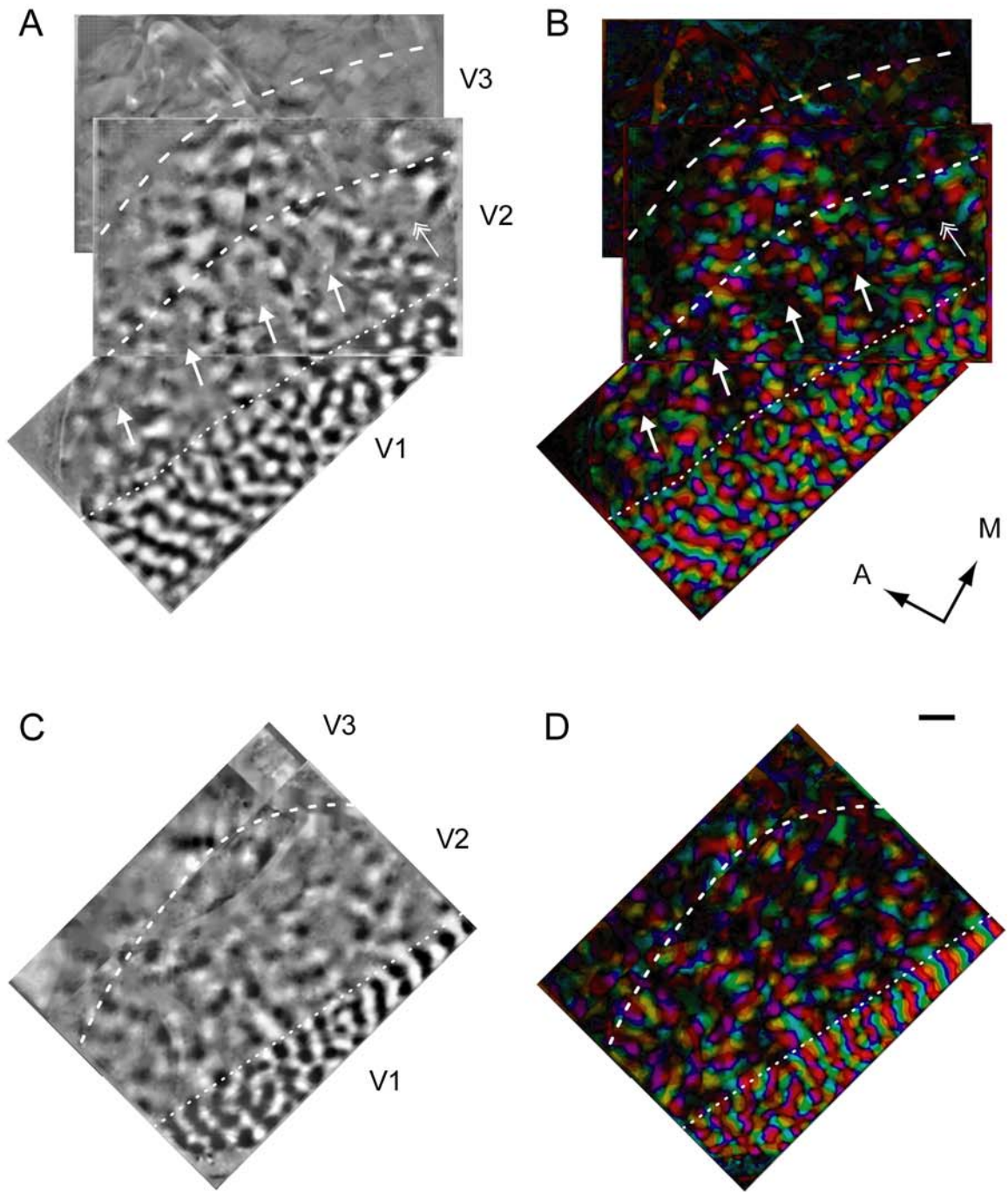


Figure 13. Comparison of the organization of orientation preference in V1, V2 and V3. **A** is an orientation difference map ($90^\circ/0^\circ$). **B** is a polar map showing both orientation preference (color) and magnitude of orientation selectivity. **A** and **B** are montages of data from three camera positions from the same case shown in figures 1 and 2. The borders of V1/V2, V2/V3, and the outer border of V3, are indicated by one thin and two thick dashed lines. These borders were determined based upon both topographic mapping and CO staining patterns. The single white arrows indicate V2 bands of low orientation selectivity that stop at the V2/V3 border; the double white arrow indicates a V2 band of low orientation selectivity that continues across the V2/V3 border. **C** and **D** are montages of data from two camera positions that show an orientation map ($0^\circ/90^\circ$) and a polar map from the same case shown in Figure 12E. In this case regions of high and low orientation selectivity were less stripe-like in V2 and V3. A, anterior; M, medial. Scale = 1.0 mm.



shapes suggestive of internal substructures. The same irregular patchy appearance often was seen in the CO stained bands as well (see below). Average widths of bands of high and low orientation selectivity in V2 measured in 4 cases parallel to the V1/V2 border were 1.7 ± 0.5 (mean \pm std) mm and 1.0 ± 0.3 mm, respectively, which differed significantly ($P < 0.0007$, t-test). Quantitative analysis matched our qualitative impression that the size of V2 iso-orientation domains (0.10 ± 0.034 mm²) was significantly larger than those of V1 ($P < 0.0005$, t-test). The basic geometric arrangement of the map of orientation preference (within regions of high selectivity) was, however, quite similar across V1, V2 and V3, with all three visual areas showing both pinwheels and linear zones (Figures 12 and 13).

V3 was similar to V2 and distinct from V1 in that it contained zones of high and low orientation selectivity that ran perpendicular to the V2/V3 border. V3 could be further distinguished from both V1 and V2 by its significantly larger iso-orientation domains (Figure 13A and C). The average iso-orientation domain size for V3 measured in 3 cases was 0.126 ± 0.055 mm². One way ANOVA and post-hoc mean difference tests indicated that iso-orientation domain sizes in V1, V2 and V3 differed significantly (one-way ANOVA, $P < 0.0001$; Tukey tests, V1 vs V3 ($P < 0.001$), V2 vs V3 ($P = 0.006$)). These differences were also reflected in the differences in pinwheel density between areas. Overall, pinwheels occurred at a density of 7.7 ± 1.2 (mean \pm std) pinwheels/mm² in V1 (for 0-12° of eccentricity), 3.04 ± 0.55 pinwheels/mm² in V2 and 2.36 ± 0.1 pinwheels/mm² in V3.

Although V3, like V2, exhibited zones of high and low orientation selectivity, the V3 zones were not simple continuations of the V2 bands of high and low orientation

selectivity. Instead, as shown in Figure 12, V2 bands of high orientation selectivity appeared to fuse into larger zones of high orientation selectivity in V3. Some V2 bands of low orientation selectivity stopped abruptly at the V2/V3 border and other V2 bands of low orientation selectivity continued uninterrupted across the V2/V3 border (see single and double arrows in Figure 12A and B). The average widths of regions of high and low orientation selectivity in V3 measured parallel to the V2/V3 border from two cases in which these zones were particularly well defined were 2.8 ± 0.6 (mean \pm std) mm and 1.3 ± 0.2 mm, respectively (data measured from 3 cases). Thus, the high orientation selectivity zones in V3 were, on average, about twice the size of those found in V2, while the low orientation selectivity V3 zones were on average about the same as those in V2.

Relationship between pinwheel centers and CO blobs in V1

We examined the relationship between the map of orientation preference and the distribution of CO blobs. As shown in Figure 14, the average density of pinwheel centers in CO blobs was $8.65 /\text{mm}^2$, in interblobs it was $7.4 /\text{mm}^2$, and in border areas between blobs and interblobs it was $7.95 /\text{mm}^2$ (Figure 14). A Chi square analysis indicated that there was no significant relationship in the distribution of pinwheel centers to CO blobs, interblobs or border areas ($P = 0.54$). Similar results were obtained from 3 other cases at matching eccentricities of $\leq 12^\circ$ (Table 1). These results, indicating the lack of a relationship between the map of orientation selectivity and CO blobs, are consistent with two previous studies that also examined relationships between pinwheel centers and CO blobs in primate V1 (macaque, Bartfeld and Grinvald, 1992; bush baby, Bosking et al., 1996; however, see Blasdel and Salama, 1986).

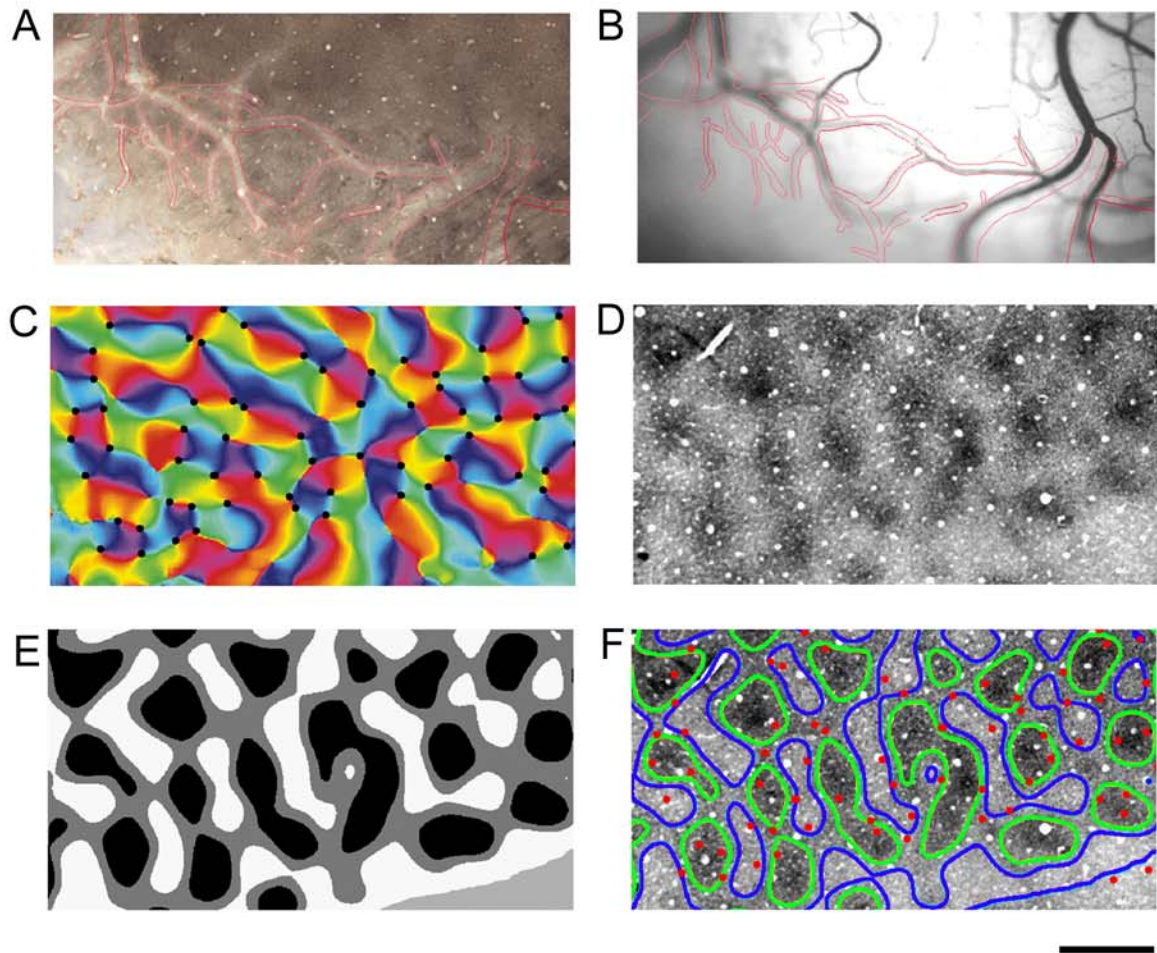


Figure 14. The relationship between pinwheels, CO blobs and interblobs in V1. **A** shows a histological brain section with superficial blood vessel contours traced in red. **B** is the optical reference image with the overlay of the superficial blood vessel patterns (red contours) corresponding to the brain area shown in **A**. The matching line-up between the histological section and optical image ensures the accuracy of our subsequent analysis. **C** is a polar map with pinwheel centers identified (black dots) from the image area. **D** is a CO section from the imaged area. **E** is the CO thresholded image of a well-stained portion of the CO section in **D**. **F** is the CO section with contour plots transferred from the CO thresholded image and with pinwheel center locations indicated (red dots). Green contours encircle CO blobs, blue contours encompass CO interblobs, border areas lie between the two colors. In the area analyzed, the pinwheel density was 8.65 /mm² for CO blobs, 7.4 /mm² for interblobs and 7.95 /mm² for border areas. The distributions do not differ significantly ($p = 0.54$, chi square analysis). Scale bar = 1.0 mm.

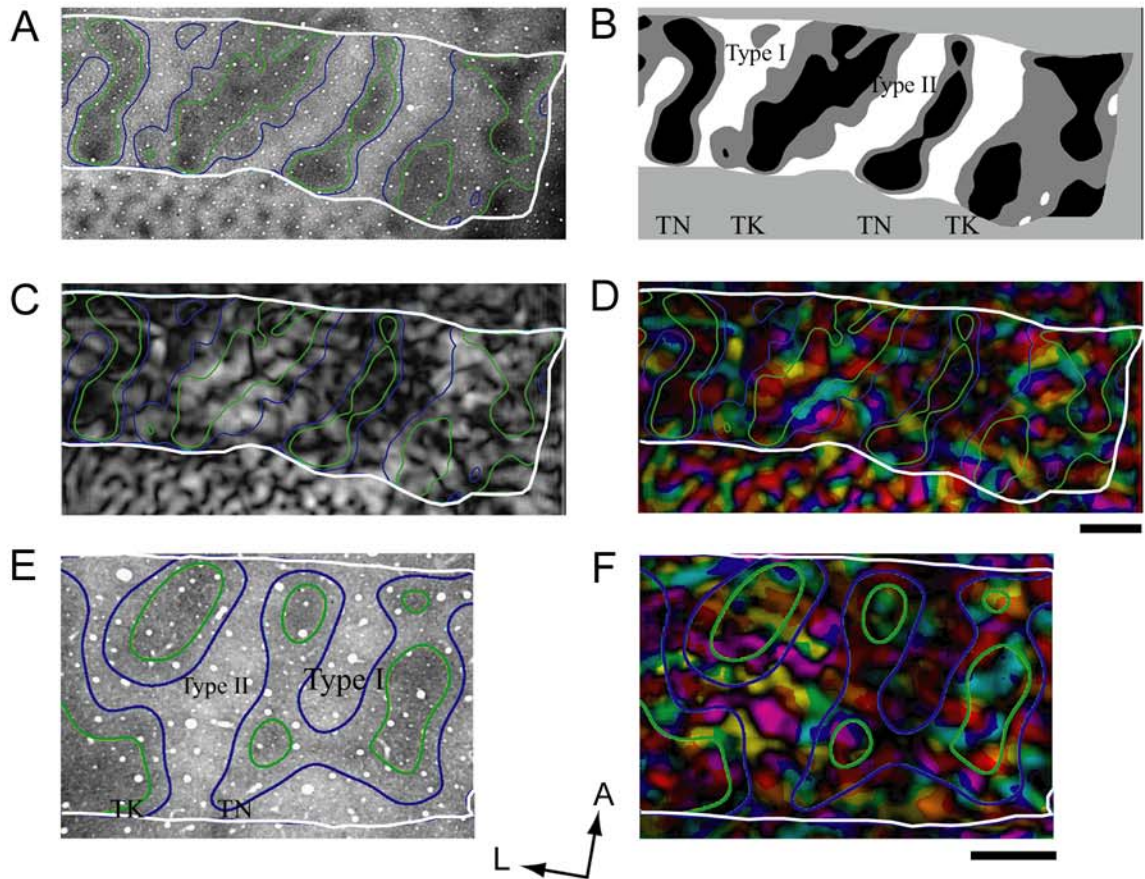


Figure 15. The relationship between zones of high and low orientation selectivity and CO light and dark bands in V2. **A, B, C** and **D** are from one case, **E-F** are from another. **A** is a CO section with contour plots transferred from the thresholded image of the same CO stained region of V2 as shown in **B**. The acronyms in **B** and **E** are defined as follows: TN, thin CO dark band; TK, thick CO dark band; Type I, CO pale band with low orientation selectivity; Type II, CO pale band with high orientation selectivity. **C** is a magnitude map with contour plots transferred from **B**. Light areas denote regions of high selectivity and dark areas low selectivity. **D** is a polar map with contour plots transferred from **B**. Green contours encircle CO dark bands, blue contours encompass the CO light bands; border areas lie between the two colors. The white lines in **A, C, D** denote the border for the selected area. Similarly, **E** is a CO section with contour plots transferred from its thresholded image, and **F** is a polar map with contour plots transferred from the thresholded CO image of **E**. Note that 4 types of bands are visible, light and dark CO bands which exhibit either high or low levels of orientation selectivity, suggesting that there are 4 functional compartments in V2. See text for quantitative details. A, anterior, L, lateral. Scale bar = 1.0 mm.

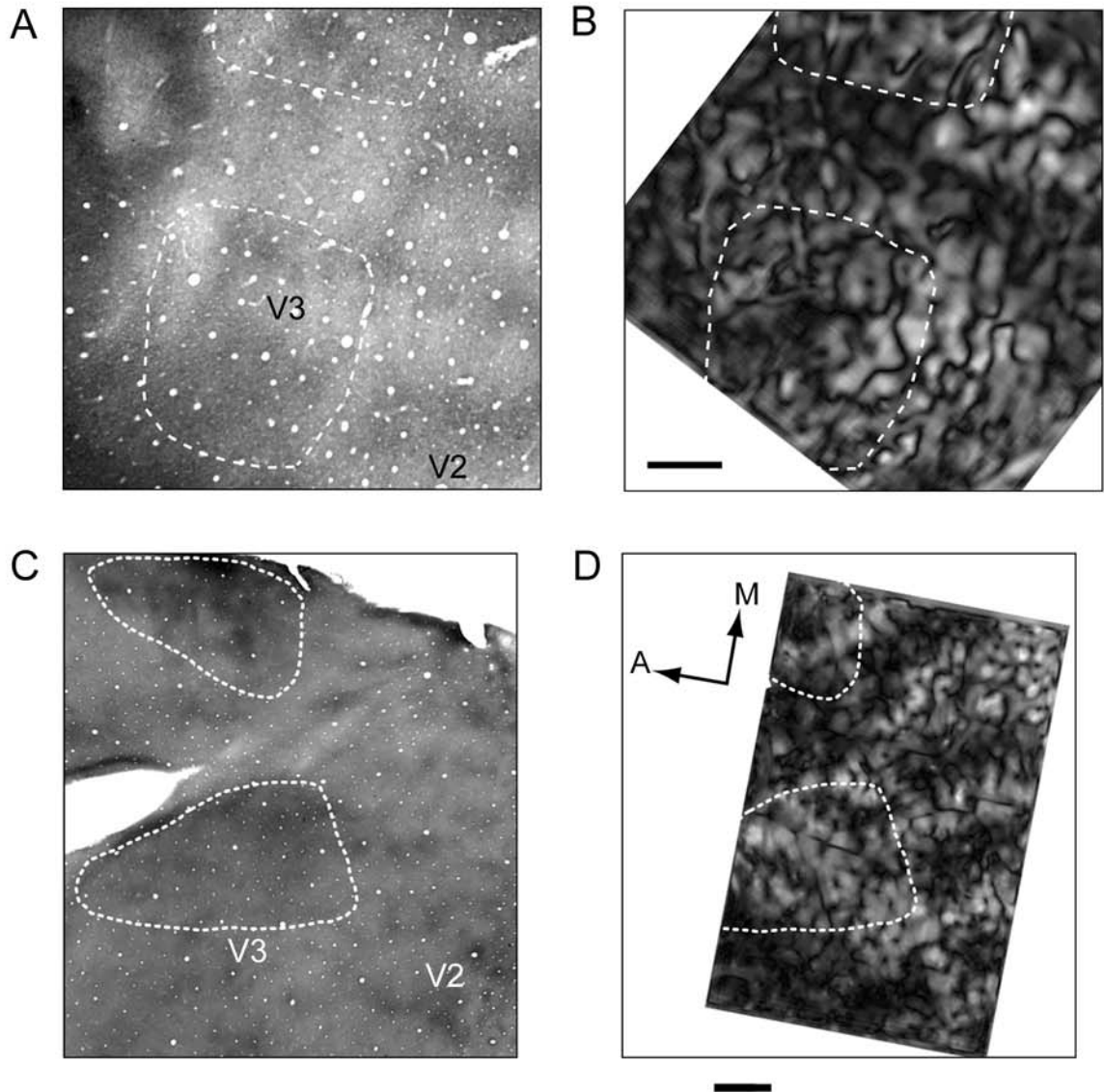


Figure 16. Comparisons between CO modules and orientation preference domains in owl monkey V3. This figure presents two cases: **A** and **B** (case 1), **C** and **D** (case 2). **C** and **D** are from the same case shown in Figures 1 and 2. The white dashed lines in **A** and **C** encircle the V3 CO dense zones; these lines are transferred onto the V3 orientation magnitude map in **B** and **D**. These panels show the correspondence of V3 CO dense and pale zones to regions of high and low orientation selectivity in the V3 magnitude map. Scale bars for **A** and **B** (in **B**) and for **C** and **D** (in **D**) equal 1.0 mm..

Table 1. The relationship between pinwheel centers and blobs. The V1 areas selected for analysis ranged from 5 mm² - 12 mm². Alpha levels of $P \leq 0.05$ are considered significant.

Case #	Estimated eccentricity of the area analyzed	Orientation pinwheel center density (/mm ²)			χ^2 analysis P value
		within CO Blobs	within CO interblobs	within border areas	
01.15.02	5-10 deg	8.68	7.40	7.96	0.54
11.07.01	5-10 deg	5.60	5.47	7.83	0.38
12.06.01	6-12 deg	6.78	6.40	7.40	0.68
11.01.01	5-10 deg	7.93	8.05	7.27	0.78
02.26.02	0-3 deg	8.54	5.12	4.02	0.07

We also performed a statistical analysis on the relationship between CO modules and orientation response selectivity based upon the magnitude maps. The orientation selectivity indices (see methods) for pixels aligned with CO blobs did not differ significantly from those aligned with interblobs across cases. This result is in agreement with studies of single-unit recordings in owl monkey and bush baby V1, which showed little difference in the orientation selectivity of individual neurons in blob and interblobs regions (DeBruyn et al., 1993; O'Keefe et al., 1998).

Relationship of orientation preference domains to the CO bands in V2 and V3

Based upon qualitative analyses, V2 CO thin bands in macaque monkeys and squirrel monkeys have been reported to correspond to zones of low orientation selectivity and high chromatic selectivity, while V2 CO thick bands have been reported to correspond to zones of high orientation selectivity (DeYoe and Van Essen, 1985; Ts'o et al., 1990; Malach et al., 1994; Roe and Ts'o, 1999; Xiao et al., 2003; see however, Roe, 2004). Areas V2 and V3 of owl monkeys are also characterized by bands of light and dark CO staining (Tootell et al., 1985; Lyon and Kaas, 2002; also see Figures 15 and 16). These bands also appeared to correspond qualitatively to zones of high and low orientation selectivity. In order to facilitate quantitative comparisons, we divided V2 (as we had done in V1 for CO blobs) into dark CO bands, interbands, and border areas with appropriate thresholding of CO images (see methods and Figure 15). We also subdivided CO dark bands into two types: CO thick bands and CO thin bands, based upon the assumption that if two functional compartments exist they should alternate in sets in order to map all functional compartments efficiently without "holes" at each eccentricity. It is noteworthy that quantifying these relationships was more complex in V2 due, in part, to the fact that each "band" was not uniform either in CO staining or in its degree of

orientation selectivity. Rather, these bands often appeared more like a string of smaller patches. The results of our analyses are illustrated in Figure 15, where the dark areas (low selectivity) in the polar map were centered on the CO dark patches in the thin bands, while the bright areas (high selectivity) in the magnitude and polar maps (Figure 15C, D, F) were centered principally on CO dark patches of the thick bands. We performed statistical analysis on the relationship between V2 CO modules (CO thick bands, CO thin bands and pale bands) and orientation response selectivity in the V2 magnitude map. In Figure 15C, the orientation selectivity indices for map pixels over dark patches of CO thick bands were significantly higher than those over CO dark patches in thin bands (thick CO dark patches: 0.32 ± 0.16 (mean \pm std); thin CO dark patches: 0.18 ± 0.13 ; $P < 0.0001$, Kruskal-Wallis test). It was consistent with 3 other cases examined, suggesting that CO thick and thin dark bands represent distinct functional compartments.

As Malach et al. (1994) observed in squirrel monkey V2, we also noted that the distribution of orientation preference did not appear to be constrained by the borders between CO thick, thin and pale bands but bridged the transition between these sets of bands. In owl monkeys, pale bands adjacent to CO thick bands exhibited high orientation selectivity whereas pale bands adjacent to CO thin bands tended to exhibit low orientation selectivity (Figure 15C, D, and F). Statistical analysis confirmed our qualitative impression that Type II CO pale bands (lateral to thin CO band) had much higher orientation selectivity than Type I CO pale bands (lateral to thick CO band). In Figure 15C, the orientation selectivity indices for V2 magnitude map pixels over the Type II CO pale bands differed significantly from those over the Type I CO pale bands (Type II CO pale bands: 0.31 ± 0.17 ; Type I CO pale bands: 0.21 ± 0.13 ; $P < 0.001$,

Kruskal-Wallis test). The pattern of bands appeared to alternate as follows: a thin CO dark band of low orientation selectivity, a pale band of low orientation selectivity (Type I); a thick CO dark band of high orientation selectivity, a pale band of high orientation selectivity (Type II). From these data, one would conclude that there are actually four functional compartments in V2, two associated with CO dark bands and two associated with CO pale bands.

Figure 16A shows an example of the different CO staining patterns found in V1, V2 and V3. In V3, the large CO dense zones always appeared to correspond to zones of high orientation selectivity, while the CO pale zones in V3 correlated with regions of low orientation selectivity (see Figure 16B and C). We applied a similar quantitative analysis to V3 that we described above for V2. The orientation selectivity indices of the corresponding V3 magnitude map over the CO dense zones were different significantly from those over the CO pale zones (Case1, V3 CO dense zones: 0.21 ± 0.24 ; V3 CO pale zones: 0.12 ± 0.20 ; Case2, CO dense 0.35 ± 0.19 ; CO pale 0.20 ± 0.14 . Both cases: $P < 0.005$, Kruskal-Wallis test). Thus, CO dense zones in V3 matched regions of high orientation selectivity while CO pale zones matched regions of low orientation selectivity.

Discussion

In this study we had two goals: 1) to determine if the functional organization of V1, V2 and V3 differ in owl monkeys and 2) to quantify the geometry of orientation domains in relationship to compartments defined by CO in these 3 areas. Our results suggest that most, but not all, elements of the functional organization of areas V1, V2 and

V3 are shared across primate species; differences appear to relate more to evolutionary relationships than to lifestyle. Our quantitative results in owl monkeys suggest that the in V1, CO blobs and orientation pinwheels do not show a 1:1 relationship and they are not spatially aligned. In V2 the relationships between CO and orientation preference provide evidence for four functional domains. In V3, CO compartments are correlated with orientation organization. In the discussion that follows, we consider the implications of these findings in light of results reported by others.

Orientation preference and CO blobs in V1

Our results revealed that in V1 of owl monkeys orientation preference maps are organized into pinwheels and linear zones similar to what has been described across a range of mammals including squirrel monkeys, macaque monkeys, bush babies, cats, tree shrews and ferrets (Blasdel, 1992a,b; Malach et al., 1994; Chapman et al., 1996; Bosking et al., 1997; Shmuel and Grinvald, 2000), suggesting that these functional compartments in V1 have a common early evolutionary history. It is likely that the organization of orientation into pinwheels and linear zones is a product of the competing pressures to represent sensory attributes without visuotopic gaps, but still represent each orientation with adequate resolution (Blasdel, 1992b). If so, one might predict more linear zones to occur where visual space is mapped anisotropically such as along the vertical meridian. In fact, as reported in cats, tree shrews and squirrel monkeys (Malach et al., 1994; Bosking et al., 1997; Shmuel and Grinvald, 2000; Blasdel and Campbell, 2001), linear zones in owl monkeys were prominent along the V1/V2 border, and iso-orientation contour lines in these linear zones tended to run across the border orthogonally. In

Table 2. Relationship between V1 size, number of CO blobs and pinwheels.

Numbers shown are means from several studies. Estimates of V1 size and CO blob density for all primates are from Condo and Casagrande (1990, see Figure 11 for list of references). V1 size for tree shrews is from Lyon et al, 1998 and for cat is from Tusa et al., 1978. CO blob density for macaque monkey is from Murphy et al., 1998 and Van Essen et al., 1984 and for cat is from Boyd and Matsubara, 1996. Pinwheel densities are averages calculated from the following sources (bush baby: Bosking et al., 1996, Soc. Neurosci. Abstr. 22, 1610; owl monkey: present study; squirrel monkey: Blasdel and Cambell 2001; macaque monkey, Obermayer and Blasdel, 1997, tree shrew, Bosking et al., 1997; cat, Muller et al., 2000. There is a strong linear correlation between the total CO blobs and the total pinwheels (total pinwheels = $1.85 \cdot \text{total CO blobs} + 399$; $r^2 = 0.96$).

Species	V1 size (mm ²)	CO blob density (/mm ²)	Total CO blobs in V1	Pinwheel density (/mm ²)	Total pinwheels in V1
Bush baby (<i>Ottoplemur garnetti</i>)	139	2.75	382	6.4	890
Owl monkey (<i>Aotus trivirgatus</i>)	287	3.6	1030	7.4	2124
Squirrel monkey (<i>Saimiri sciureus</i>)	637	4.5	2867	11	7007
Macaque monkey (<i>Macaca nemestrina</i> , <i>Macaca fascicularis</i> , <i>Macaca mulatta</i>)	1269	4.4	5584	8.0	10152
Tree shrew (<i>Tupaia belangeri</i>)	60	NA	NA	9.4	564
Cat (<i>Felis domesticus</i>)	380	1.5	570	3.0	1140

macaque monkeys this arrangement fits with the anisotropic visuotopic map in which visual space is magnified parallel to the V1/V2 border (Blasdel and Campbell, 2001).

Since pinwheels are a common feature of V1, their density should bear some relation to the density of functional columns within V1, given that each pinwheel represents all orientations. Table 2 compares the density and number of pinwheels in V1 across species. Also shown are the density and number of CO blobs. Even though variability is high between cases and studies (the table simply shows averages), some interesting trends emerge. For each species, the number of pinwheels is approximately double the number of CO blobs with a strong linear correlation between the total CO blobs and the total pinwheels. From these numbers it is obvious that pinwheels cannot be uniformly distributed and also be centered on blobs (as our quantitative data indicate for owl monkey). One could argue that the relationships between blobs and pinwheels are eccentricity dependent (see Vanduffel et al., 2002) but our measures in owl monkey would suggest that if there is a relationship it would have to occur beyond 10 degrees of eccentricity. Although the numerical estimates of pinwheel number, blob number and V1 size are based upon very few species and involve across-animal and across-study comparisons it is unlikely that these estimates are so inaccurate that pinwheels would end up matching the distribution of CO blobs. If the 2:1 estimates are accurate they suggest that the relationship between CO blobs and orientation is not completely random supporting the idea these represent real functional compartments and not accidents of development (See Purves et al., 1992 for review). Although not the main purpose of this paper, it is noteworthy that what is represented in the CO blobs has been the subject of considerable debate. Since all primates, regardless of the presence or absence of color

vision, have CO blobs, it is likely that they serve some function that transcends the representation of this property. Given that lower spatial frequencies appear to preferentially be associated with CO blobs even in non-primates (i.e. cats) (Shoham et al., 1997), one speculation is that properties that would require relative constant metabolic expenditure such as color contrast, brightness contrast and other surface properties are represented separately within CO blobs (see Allman and Zucker, 1990 for discussion). Regardless, one would like all estimates of CO blob and pinwheel number to be made from several members of the same species under conditions where tissue shrinkage and other potential technical problems were taken into account to be certain about relationships.

The organization of orientation and CO compartments in V2

We had originally predicted that the pattern of orientation domains in V2 of owl monkeys would resemble the continuous pattern of orientation domains reported in V2 of the nocturnal bush baby because bands of low orientation selectivity in V2 in diurnal primates appear to mark compartments with color selective cells (Ts'o et al., 1990; Roe and Ts'o, 1995). Clearly, low orientation selectivity bands in owl monkeys cannot contain cells selective for color since these primates have only a single cone type (Wikler and Rakic, 1990; Jacobs et al. 1996). Nevertheless, V2 in owl monkeys is organized in a similar manner to V2 in diurnal macaque monkeys and squirrel monkeys (Ts'o et al., 1990; Malach et al., 1994). Thus, there is clear evidence that both CO light and dark bands contain stripes of high or low orientation selectivity and that the difference in V2 organization in bush babies (prosimians) and monkeys (simians) evolved over 60 million years ago. While simian V2 organization may be unrelated to color vision it also is

possible that the simian V2 organization in owl monkeys was retained from an ancestor of the owl monkey that had color vision (Ross, 2000). If true, this raises a further question concerning the function of the compartments containing cells which are not selective for orientation or color in owl monkeys, a question we will return to below.

Our data indicate that four functionally distinct compartments exist in V2, two containing cells selective for orientation and correlating with the “thick” CO bands and one class of pale bands and the other two containing cells with low orientation selectivity and correlating with the CO “thin” bands and the second class of pale bands. This conclusion also is supported by evidence from reported connection patterns of V2. In owl monkeys as in all primates studied, more than 80% of input connections to V2 come from V1 (see Casagrande and Kaas, 1994 for review). As in macaque monkeys, different compartments in V2 of owl monkeys appear to receive projections from either CO blobs or interblobs supporting the idea that at least two functional divisions exist in V2 that originate in separate compartments in V1 (Krubitzer and Kaas 1990a,b). In macaque monkeys, however, a number of studies have provided evidence that CO blobs in V1 contain non-oriented color selective cells and project to the thin stripes in V2 (see Livingstone and Hubel, 1984; Ts’o and Gilbert, 1988; Roe and Ts’o, 1995; Sincich and Horton, 2002). The functional aspect of this conclusion, however, is mainly based upon multiunit recording and has not been supported by more recent recording results (Lennie et al. 1990; Edwards et al. 1995; Leventhal et al. 1995; Gegenfurtner et al., 1996) or the results of optical imaging (Blasdel and Salama, 1986; Ts’o et al., 1990; Bartfeld and Grinvald, 1992; Landisman and Ts’o 2002a). Moreover, although the same anatomical connections appear to exist between CO compartments in V1 and V2 in owl monkeys and

macaque monkeys, there is no evidence from optical imaging or single unit recording in owl monkeys (see O'Keefe et al., 1998) to support the idea that cells in CO blobs are purely/primarily non-oriented. Thus, the lack of orientation selectivity in V2 compartments in owl monkeys must be created at this level either via wiring from V1 or intrinsic wiring in V2 itself.

As in macaque monkeys, the outputs of V2 to areas MT and DL in owl monkeys indicate that V2 has at least three compartments as V2 projections to MT originate from every other CO dense band and interbands appear to project to DL (V4) (Krubitzer and Kaas, 1990a,b). The current view of V2 in macaque monkeys is that it is divided into three functional compartments that support motion vision (CO thick bands), form vision (CO interbands) and color vision (CO thin bands) (see Roe and Ts'o, 1997 for review). Evidence for a tripartite organization comes from a number of anatomical and physiological studies (see Livingstone and Hubel, 1984; DeYoe and Van Essen, 1985; Roe and Ts'o, 1995). A recent study in cebus monkey, however, provides evidence for at least four V2 functional compartments (Nascimento-Silva et al., 2003; see also Roe and Ts'o, 1995 and Roe, 2004 for evidence of four V2 compartments in macaque monkeys). Nascimento-Silva et al., 2003 showed that cells in the CO pale bands consist of two types, those that project to visual area PO and those that project to V4. No cells were found that projected to both areas suggesting that there are *two types of CO pale bands*. Similarly they found that area MT received input almost exclusively from CO thick bands while area V4 received input from CO thin bands. All cells projected only to one of these areas, again supporting the idea that 4 compartments may exist. While it is still uncertain if all simians have 3 or 4 compartments in V2, our results indicate that several

different properties are likely segregated within V2 in simians that do not depend on color vision.

The functional organization of V3

No prior optical imaging studies have been done to determine the functional organization of V3. The present study provides evidence for two functional compartments in V3 of owl monkeys consisting of large zones containing cells with high orientation selectivity separated by narrower zones containing cells with low orientation selectivity. The V3 zones of high orientation selectivity showed a similar geometric organization to those in owl monkey V2 with both pinwheels and linear zones but the domain sizes were much larger. Additionally, zones of high orientation selectivity in V3 corresponded to CO dense zones while regions of low orientation selectivity matched CO pale zones.

Electrophysiological recordings from V3 in macaque monkeys have found both non-oriented cells and orientation sensitive cells (Baizer, 1982; Adams and Zeki, 2001). Also, a 2-deoxyglucose study of orientation selectivity in macaque monkeys suggested that regions of high and low orientation selectivity exist in V3 (Vanduffel et al., 2002), suggesting that the compartmental organization of V3 that we see in owl monkeys may generalize across simian primates. No evidence was reported for compartments of low and high orientation selectivity in the V3 region of prosimian bushbabies (Bosking et al., 1996).

CHAPTER IV

ORIENTATION AND DIRECTION PREFERENCE ORGANIZATION IN BUSH BABY MT

Introduction

The cerebral cortex of all studied primates contains a number of functionally distinct visual areas, but only a few of these areas are so well defined that they are widely recognized as present in all primates. These areas include primary and secondary areas, V1 and V2, which appear to be characteristic of nearly all mammals, and the middle temporal (MT) visual area (also termed V5), which has been only identified in primates (See Kaas, 2004 for review). The restricted distribution of this area suggests that MT appeared as a distinct visual area with, or just before, the emergence of the first primates. Comparative studies have identified a number of features of MT that are present in all studied primates and thus are likely to have been conserved since the last common ancestor. For example, MT receives direct inputs from V1, contains a global representation of the contralateral visual hemifield, has dense myelination, and contains a preponderance of neurons selective for direction of stimulus movement (Kaas, 2004).

Prosimian primates represent a major branch of primate evolution that diverged from the anthropoid branch (monkeys, apes, and humans) over 60 million years ago (Purvis, 1995). As optical imaging has been used to extensively characterize the organization of orientation and direction in area MT of the New World monkey, owl monkey (Malonek et al., 1994), it is possible to compare MT in this simian with

prosimian bush babies in detail, and identify ancient, ancestral features of MT cortical organization that are common to both lines of evolution.

To do so, we used the method of optical imaging of intrinsic signals in MT of prosimian bush babies that were evoked by different stimulus conditions.

Materials and Methods

General preparation

The 3 bush babies (greater galagos, now referred to as *Otolemur garnetti*) used in this study were handled according to an approved protocol from the Vanderbilt University Animal Care and Use Committee. Briefly, bush babies were initially anesthetized with isoflurane (2-4% in O₂), and paralysis induced by intravenous injection of 1-1.5 mg/kg vecuronium bromide (Norcuron). Bush babies were artificially ventilated with a mixture of 75% N₂O and 25% O₂ delivered at a rate sufficient to maintain the peak end tidal CO₂ level at around 4%. Paralysis and anesthesia were maintained by intravenous infusion of vecuronium bromide (0.2-0.4 mg/kg/h) mixed in 5% dextrose lactated Ringer's and propofol (10-20 mg/kg/hr) through separate lines. Pupils were dilated with 1% atropine and gas permeable contact lenses rendered the retina conjugate with the 28.5 cm distant stimulus monitor. During experiments the optic disks and *areae centralii* (AC) were plotted on the screen and 3 mm artificial pupils were placed in front of the eyes. A craniotomy exposed MT and surrounding visual areas, and openings were sealed with 1% agarose under a glass coverslip.

Optical imaging and visual stimuli

The functional organization of MT was imaged in 5 hemispheres. Each experimental session lasted from 36 to 60 hours. Intrinsic optical imaging signals were acquired with the Imager 2001 differential video-enhancement imaging system and VDAQ/NT data acquisition software (Optical Imaging, Mountainside, NJ, USA). Surface reference images of cortical vasculature were acquired with a 540 nm green light. The cortex was illuminated with either a 611 nm or a 689 nm light during data acquisition and was visualized with a tandem lens microscope attached to a low noise video camera. Visual stimuli were generated using a VSG system (Cambridge Research Systems, Rochester, UK), and were presented on a 21" video screen (SONY FD Trinitron, Model GDM-F400) in a 120 Hz non-interlaced mode with a mean luminance of 30 cd/m².

To study responses to stimuli of different orientations, high-contrast rectangular gratings (fundamental spatial frequency 0.2-0.4 cyc/deg, drift velocity 2 Hz, duty cycle: 20%) of 4 orientations at intervals of 45° were displayed on the full screen and presented binocularly. Each grating was moved back and forth along an axis that was orthogonal to the orientation of the grating. A single trial consisted of data acquisition during continued presentation of the drifting grating stimulus for 8 sec and an interstimulus interval of 12 sec using a blank screen of mean luminance. Stimulus sets were made up of 10-30 trials. To study responses to different directions of motion, high-contrast rectangular gratings were moved in 8 directions at intervals of 45° on the full screen, presented binocularly. In addition, high-contrast randomly positioned dots were drifted in 8 directions (dot density, 3-6 % surface area) within a circular window of 20°-30° centered on the AC representation and viewed binocularly.

Video images were acquired at a rate of 30 frames/sec, but all frames acquired for each condition during the 8 sec period were summed together for 8 data frames before further analysis. Individual data frames included 744 x 480 pixels, with a resolution of 87 pixels per mm.

Image Analysis

Using Winmix software (Optical Imaging, Inc.), all images associated with stimuli of the same orientation were summed and divided by the summed images acquired during presentation of the orthogonal orientation to create differential maps (Blasdel, 1992a). To construct maps of direction preference, all images associated with the same stimulus direction (drifting gratings or random dots) were summed. The summed images acquired during the presentation of one direction were divided by a 'cocktail' blank (the average summed images of all the stimulus directions) to create single direction maps (Malonek et al., 1994). We also created differential direction maps by dividing the images associated with one direction by those associated with the opposite direction.

Orientation and direction maps were smoothed using a 7 x 7 pixel mean filter kernel. Low frequency noise was reduced by convolving the image with an 80 x 80 pixel mean filter kernel and subtracting the result from the original image. Filtering was done in the floating point range before the maps were clipped and scaled in the range of 0-255 gray levels. Vector summation of the orientation or direction maps on a pixel by pixel basis was used to create a color coded orientation or direction preference (angle) map. A magnitude map of the degree of orientation or direction selectivity was coded by brightness, with strong orientation or direction selectivity being the brightest (see Chapter

III for details). The two maps were combined to create a polar map, which contains information about both orientation or direction preference (color) and magnitude of selectivity (brightness).

Histology and alignment

At the termination of each experiment, the bush baby was deeply anesthetized with an overdose of sodium pentobarbital and perfused transcardially with 0.9% saline in 0.1M phosphate buffer (PB) followed by 2 % paraformaldehyde in 0.1M PB. The brain was removed and the cortex was separated and flattened. The cortex was frozen and cut with the surface vascular pattern preserved in the first 100 μm section. Subsequent sections were cut at 40 μm . Sections were processed for cytochrome oxidase (CO) (Wong-Riley, 1979) and myelin (Gallyas, 1970).

Surface and radial blood vessels were the primary landmarks used to align histological sections to the optical reference images of the imaged area. Differences between images and sections due to distortion or tissue shrinkage (about 10 -15%) were handled by global scaling and rotation. After the optical images were aligned with the histological data, we examined the corresponding locations or patterns of the imaged brain areas to see if anatomical delineation of MT matched with optical imaging results. In each case, the CO and myelin patterns identified boundaries of MT that were consistent with those estimated from imaging results.

Results

MT was activated by full screen drifting gratings of different orientations in ways that clearly distinguished MT from surrounding areas; the activation pattern was patchy

or modular across the surface of MT, and the locations of activated patches varied with the orientations of the drifting gratings (Figures 17 and 18). The iso-orientation domains formed elongated ovals (Figure 17, Figure 18A and 18B). The average size of iso-orientation domains of the 4 orientations was $0.2 \pm 0.015 \text{ mm}^2$ (mean \pm sd). Drifting grating stimuli also caused additional activation in 2–3 surrounding cortical areas (possibly MTc, MST and DL), suggesting that these areas contain neurons sensitive to stimulus orientation. The black arrow in Figure 17C points to some activation foci in one of the areas.

The relationship of sets of patches activated by different orientations to each other was most effectively illustrated by orientation maps produced by dividing activity patterns from orthogonal orientations (Figure 17, Figure 18A and 18B) and combining results based on different orientations in a single color-coded summary (Figure 18C). The summary shows how systematic rotations of stimulus orientations produce systematic shifts in activation patterns, with clusters of activation for orientation arrays corresponding in number to the activation patches for any orientation (Figure 18C). The iso-orientation domains shifted from one to the next in orientation pinwheels where orientation preference changes in a radial fashion around a single point and linear zones where orientation preference changes slowly along a straight line (Figure 18C). When activation strengths for all orientations were considered, the surface-view map was divided into an additional patchwork of highly activated and poorly activated territories. This result suggests that MT of bush babies has a second type of modular organization consisting of a patchwork of regions where neurons are not highly sensitive to oriented drifting gratings. Single neuron recordings and 2-deoxy glucose labeling patterns in owl

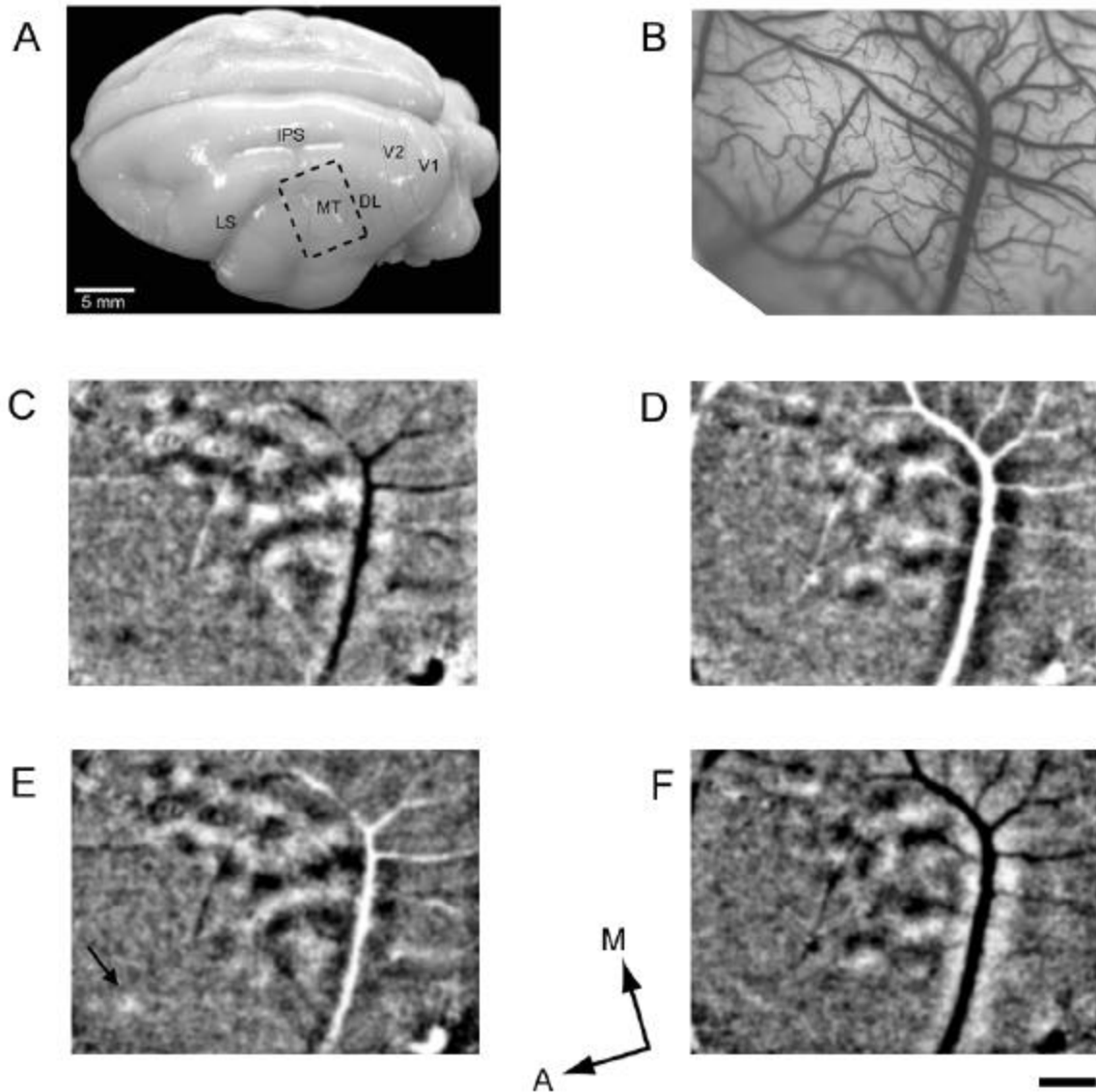


Figure 17. Activation patterns in MT by using full screen drifting gratings of different orientations. **A** is a photograph of a bushy baby brain with a few visual areas marked on the surface. The black dashed box outlines the estimated camera view for the optical images acquired for the experimental case. IPS, intraparietal sulcus; LS, lateral sulcus; MT, middle temporal visual area; DL, dorsolateral area. **B**. A reference image of the cortical surface area showing the blood vessel pattern. **C-F** show orientation difference maps, $0^\circ/90^\circ$, $45^\circ/135^\circ$, $90^\circ/0^\circ$, $135^\circ/45^\circ$, resulting from binocular stimulation. These activation patterns delineate the approximate extent and boundaries of MT. Additional activation in surrounding cortical areas reveals at least 2–3 other visual areas with neurons sensitive to stimulus orientation. The black arrow in **E** points to one of the areas. Scale bar for **B-F** is 1mm.

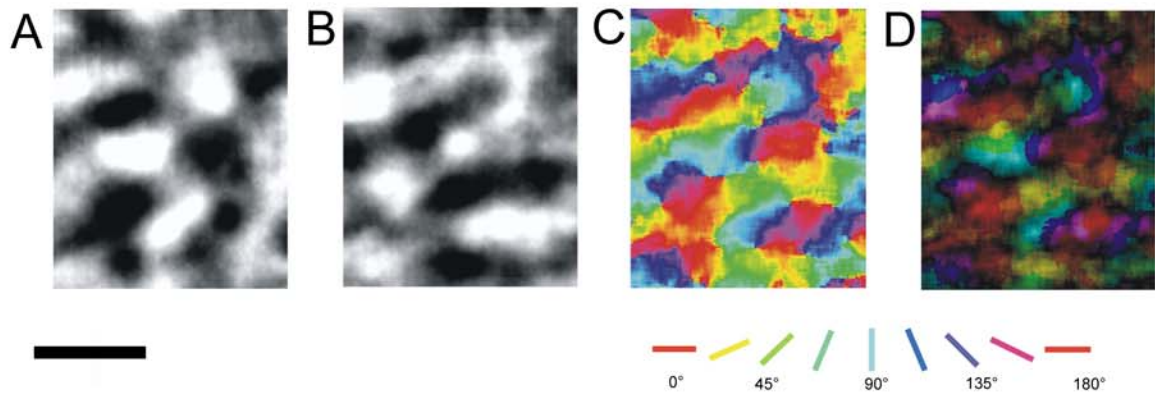


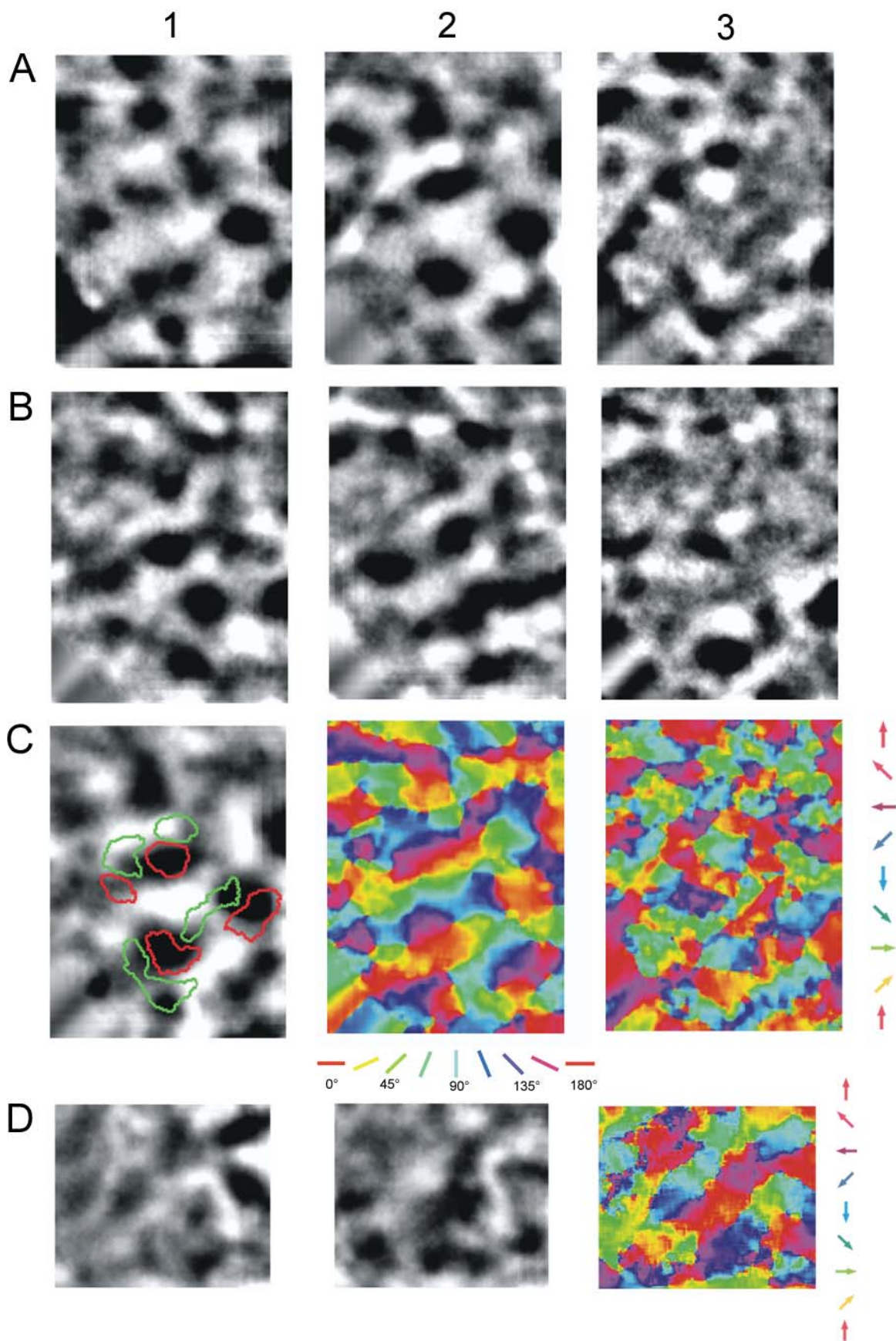
Figure 18. Functional maps of orientation preference in MT. Orientation difference maps were obtained from full-field, drifting gratings at four orientations, with $0^\circ/90^\circ$ shown in **A** and $45^\circ/135^\circ$ in **B** ($90^\circ/0^\circ$ and $135^\circ/45^\circ$ not shown). Dark areas responded strongly to the first orientation, while light areas responded strongly to the second, orthogonal grating orientation. **C.** A color-coded orientation preference map produced from vector summation on a pixel by pixel basis from the four difference maps noted above. The key shown below the map indicates orientation preference. **D.** The polar map of orientation preference contains information about both orientation preference (color) and magnitude of orientation selectivity (brightness, dark to light = weak to strong). Scale bar = 1mm

monkey suggest that MT contains segregated modular groups of neurons more effectively activated by either global or local motion (Born and Tootell, 1992; Born, 2000). The gratings and arrays of moving dots used in the present experiments may have best activated the MT modules that are sensitive to global motion.

The orientation maps of MT reflect the movement of oriented stimuli back and forth in two opposite directions. A further finding of the present study was that the movement of an oriented stimulus in one direction did not activate the same territories as movement in the opposite direction (Figure 19A1-3, and 19B1-3). Instead, patches of MT best activated by a particular orientation were divided into parts preferring motion in one direction or the other (Figure 19C1). In general, iso-orientation domains had a more band-like appearance, and were typically larger in size and more uniform in their distribution than iso-direction domains. In a way similar to the color-coded orientation preference map (Figure 19C2), the color-coded direction preference map (Figure 19C3) consisted of numerous regions within which direction preference changes in a slow, continuous fashion. There also were some regions separated by winding boundaries across which direction preference shifts abruptly, often by 180 degrees. The vertical and horizontal direction preference domains appeared to account for a large portion of the cortical map (Figure 19C3).

MT also demonstrated direction selective domains when stimulated by moving random dot patterns (Figure 19D1-2), although random dots induced weaker responses than directional grating stimuli. Nevertheless, the direction preference map produced with dots shared similar, but not identical, features to that produced from the gratings (Figure 19D3).

Figure 19. The relation of orientation preference maps to direction of movement maps in MT. The regions illustrated in panels **A**, **B**, and **C** are identical. Panels **D1-3** are from a different region of MT. **A**. Single condition direction of movement maps for upward (**A1**) and downward (**A2**) grating movement, and the differential direction of movement map (upward/downward) (**A3**). **B**. Single condition direction-of-movement maps for upward oblique (**B1**) and downward oblique (**B2**) gratings of the same orientation, and the differential direction of movement map (**B3**) (upward oblique / downward oblique). In **A3** and **B3**, the dark regions correspond to particular iso-direction domains, and the white regions correspond to the opposite iso-direction domains. **C1**. Orientation difference maps ($0^\circ/90^\circ$) with selected contours of iso-direction domains from **A3** shown above (green, 90° iso-direction domains; red, 270° iso-direction domains). **C2** is an orientation preference map, created from vector summation of 4 orientation difference maps. **C3** is a direction preference map, created from vector summation of 8 differential direction of movement maps (e.g. $90^\circ/270^\circ$ and $135^\circ/315^\circ$ shown in **A3** and **B3**). **D1** and **D2** are single condition maps of direction of movement from moving random dot stimuli in the directions of 0° and 180° . **D3** is a color-coded direction preference map from vector summation of 8 single condition maps of direction resulting from random dot stimuli moving in 8 different directions. Scale bar = 1mm



Discussion

The present results indicate that MT of prosimian bush babies is functionally organized in a manner very similar to MT of simian primates. In the present optical imaging experiments, moving gratings selectively activated arrays of orientation preference domains across MT. Sequences of orientation preference domains systematically rotated around pinwheel centers or changed along a straight line, with each orientation domain divided into separate territories for opposite directions of movement preference. Moving arrays of random dots activated similar direction of movement territories.

Overall, these results are remarkably similar to optical imaging results reported for MT of owl monkeys, a New World monkey (Malonek et al., 1994), results that are highly consistent with data from microelectrode recording experiments in New World cebus monkeys (Diogo et al., 2003) and Old World macaque monkeys (Zeki, 1974; Baker et al., 1981; Felleman and Kaas, 1984; Albright, 1984; Allman et al., 1985; Snowden et al., 1992). Orientation domains in MT of bush babies are organized very much like those of V1 in monkeys, being represented continuously as a series of pinwheels and linear zones. However, the orientation domains in MT ($\sim 0.2\text{mm}^2$) are much larger than those in V1 ($\sim 0.09\text{mm}^2$). A very similar organization for orientation domains was reported for MT in owl monkeys using optical imaging procedures (Malonek et al., 1994). This arrangement of orientation contrasts with that described in areas V2 and V3 of simians where domains of high orientation selectivity are separated by distinct bands of low orientation selectivity (See Chapter III). While orientation domains have been examined only in bush babies and owl monkeys, microelectrode recordings from both New World

and Old World monkeys have previously demonstrated that a majority of neurons in MT are well tuned for orientation (Albright, 1984; Felleman and Kaas, 1984), although this is not widely recognized. Our data in bush babies also demonstrate that regions surrounding MT, including both MTc and MST, contain cells selective for orientation as reported by others in owl monkeys and macaque monkeys (Lyon et al., 2002; Roy and Wurtz, 1990; Roy et al., 1992).

Our results also demonstrate a systematic representation of direction of stimulus movement in MT of bush babies that is similar to that demonstrated by using optical imaging in the New World owl monkeys (Malonek et al., 1994) and by electrophysiological recording in the New World cebus monkeys (Diogo et al., 2003). In Old World macaque monkeys directionally selective cells also are organized into columns in area MT (Albright, 1984; Albright et al., 1984). In cebus monkeys, owl monkeys and bush babies, stimulus direction appears to be represented by continuous changes in directional preference, as well as by breaks and points where there are rapid changes in direction (pinwheel-like). This arrangement of directional domains is similar to that identified for directional domains in cat area 18 (Bonhoeffer and Grinvald, 1991; Shmuel and Grinvald, 1996) and ferret area 17 (Weliky et al., 1996), although we did not find any robust direction selective columns in V1 of either bush babies or owl monkeys in our attempts (and no direction columnar organization has not been reported in the primate V1 literature). This representation of direction is somewhat different from the rectilinear model proposed for the organization of direction in macaque monkey MT by Albright et al. (1984), a difference that likely reflects the difficulties inherent in reconstructing surface-view maps from single unit recordings within a structure buried in

a sulcus. Thus, in an analogous fashion to V1 (Bonhoeffer and Grinvald, 1996), optical imaging has revised our view of the geometry of feature representations in area MT. In addition, optical imaging studies in owl monkeys (Malonek et al., 1994) and bush babies (present study) provide clear evidence that the basic organization of MT emerged with or before early primates and has been retained in both prosimian and anthropoid lines of descent.

CHAPTER V

IS THE MAP OF ORIENTATION PREFERENCE ORGANIZED DIFFERENTLY AT DIFFERENT ECCENTRICITIES?

Introduction

Orientation selectivity is one of the fundamental properties of most visual cortical neurons. It has long been known that visual cortical neurons with similar orientation selectivity tend to group together and form a columnar organization in primary visual cortex, V1 (Hubel and Wiesel, 1962; 1968; 1977; Tootell et al., 1981; Payne et al., 1981; LeVay and Voigt, 1988; Tootell et al., 1988a). Another prominent feature of primate V1 is the distinct periodic pattern of elevated metabolic activity seen with staining for the mitochondrial enzyme cytochrome oxidase (CO), CO blobs and interblobs (Livingstone and Hubel, 1984; 1988; Casagrande and Kaas, 1994). Currently, controversy still exists over how orientation is organized in primary visual cortex (V1) of primates and how the organization of this attribute relates to the organization of other functional properties such as those that correlate with the location of CO blobs and interblobs. For example, some investigators have reported that CO blobs contain mainly non-orientation selective, color selective cells; others find no such relationship (Livingstone and Hubel, 1984; DeYoe and Van Essen, 1985; Ts'o and Gilbert, 1988; Lennie et al. 1990; Edwards et al. 1995; Leventhal et al. 1995). One explanation for these differences might be that different studies were examining different regions of V1 representing different eccentricities. In support of the argument that the organization of V1 varies with eccentricity, Vanduffel et al. (2002) reported several eccentricity dependent differences in the organization of

orientation selectivity in macaque V1 using a double-label deoxyglucose technique in awake behaving monkeys that viewed 2 different orientations. They found the orientation selectivity was about 40% weaker in the foveal representation, and the degree of overlap between the representation of orientations was much greater in the V1 area representing central vision than the area representing peripheral vision. They also found that in the region of V1 representing peripheral vision, orientation columns avoided blobs, while in the foveal representation, orientation columns converged closer to them. These data suggest that the relationship between functional modules changes with retinotopic eccentricity.

In this study we were interested in examining the relationship between orientation modules, CO modules and eccentricity in a species where a large region of V1 was available for optical imaging of intrinsic signals. We chose to examine the prosimian bush baby because more than 15 degrees of the visual field representation in V1 can be imaged in this species. This species is also of interest because it only has a single cone type and therefore does not have color vision (Wikler and Rakic, 1990; Jacobs et al., 1993) but does have very well developed CO blobs in V1. We had three specific questions: (1) Does the magnitude of orientation selectivity or the size of orientation domains vary with eccentricity? (2) Does the spatial arrangement of orientation preference vary with eccentricity? (3) Does the spatial relationship between CO blobs and orientation domains vary with eccentricity?

Optical imaging of intrinsic signals provides a number of advantages over more conventional methods. Optical imaging of intrinsic signals allows responses to visual stimuli to be observed across a wide area of cortex simultaneously with high spatial

resolution. Also, one can examine many different orientations over a wide area whereas metabolic labeling techniques such as 2-deoxyglucose (2-DG) are limited to one or two orientations and single unit recordings such as electrophysiological mapping can examine only one cell at a time (Tootell et al., 1981; Tootel et al., 1988a,c; Grinvald and Bonhoeffer, 1996; Vanduffel et al., 2002).

Materials and Methods

General preparation

The 5 bush babies used in these experiments were handled according to an approved protocol from the Vanderbilt University Animal Care and Use Committee. Animals were prepared for surgery, paralyzed and anesthetized consistent with earlier descriptions (Rosa et al., 1997). Paralysis and anesthesia were sustained by intravenous infusion of vecuronium bromide ($0.1-0.3 \text{ mg kg}^{-1} \text{ h}^{-1}$) mixed in 5% dextrose lactated Ringers delivered at a rate of 2 ml/h and propofol (2,6 -di- isopropylphenol: $10 \text{ mg kg}^{-1} \text{ h}^{-1}$), respectively. The heart rate, peak end tidal CO_2 , temperature, and ECG were monitored continuously after paralysis in order to ensure that proper levels of anesthesia were maintained throughout the experiment. Levels of anesthesia were increased when necessary. 1% atropine eye-drops were used to dilate the pupils, and clear contact lenses with 3 mm artificial pupils were used to make the retina conjugate with the computer monitor 28.5 or 57 cm distant. A craniotomy was made over V1 and its surrounding visual areas, and the dura was reflected. The opening was sealed with 1% agarose under a cover glass.

Optical imaging and visual stimuli

The Imager 2001 differential video-enhancement imaging system and VDAQ/NT data acquisition software (Optical Imaging Inc.) were used to acquire intrinsic optical imaging signals. Reference images of the cortical vasculature were attained with a 540 nm green light. The cortex was illuminated with a 611 nm orange light during data acquisition and was visualized with a tandem lens microscope attached to a low noise video camera. The camera was focused either on the surface or slightly beneath the cortical surface, and the depth of field was subsequently increased by closing the lens diaphragm.

In order to perform the visuotopic mapping, topographically limited horizontal and vertical grating stimuli were presented monocularly within 1-2° rectangular windows or 2° patches at eccentricities that ranged from 0° to 15°. Video images were acquired at a rate of 30 frames/sec, but all frames acquired for each condition during the 8-sec period of stimulation were summed together for 8 data frames before further analysis. These data acquisition periods were preceded by 10-12 sec interstimulus intervals. Stimulus sets were repeated 10-20 times.

To study the functional organization of orientation preference, high-contrast rectangular gratings (fundamental spatial frequency 0.5 cyc/deg, drift velocity 2 Hz, duty cycle: 20%) of 4 orientations were displayed on the full screen and presented binocularly. Each grating was moved back and forth along an axis that was orthogonal to the orientation of the grating. A single trial consisted of data acquisition during continued presentation of the drifting grating stimulus for 8-10 sec, and an interstimulus interval of

10-12 sec using a blank screen of mean luminance. Stimulus sets were made up of 10-30 trials.

To examine intrinsic signal magnitudes in response to orientations, we recorded all video frames for the 18-20 sec period (8 sec drifting grating stimulation plus 10-12 sec blank screen); video frames were summed into 36-40 data frames before further analysis. Stimulus sets were made up of 10-20 trials.

Image Analysis

To create visuotopic maps, all activity images associated with stimuli of the same position were summed and divided by the “pure blank” obtained by summing the images of the blank control to create single-condition maps. The map was clipped at 1-2 SD from the mean and was scaled and displayed at 0-255 grey levels. The resulting images were smoothed using a 7 x 7 pixel mean filter kernel. By mapping both vertical and horizontal dimensions of the visual field, we could construct visuotopic maps to determine eccentricities of V1 regions (see Chapter 2).

To construct maps of orientation preference, we summed together all images associated with the same orientation using Winmix software (Optical Imaging, Inc.). The summed images acquired during the presentation of one orientation were divided by the summed images acquired during presentation of the orthogonal orientation to create orientation difference maps (Blasdel, 1992; Bosking et al., 1997). Custom programs written in NIH Image and Matlab were used to further process the data. Orientation difference images again were smoothed using a 7 x 7 pixel mean filter kernel. Low frequency noise was reduced by convolving the image with an 80 x 80 pixel mean filter kernel and subtracting the result from the original image (Bosking et al., 1997). Vector

summation of the difference images was done on a pixel by pixel basis to create a color coded orientation preference (angle) map.

In some cases, in order to reduce vascular artifacts, we used reference images or a stack of optical images to create a “mask” indicating the location of the major blood vessels; the grayscale value for each pixel in these images that was located in the mask was replaced by the mean of the grayscale values of the appropriate surrounding pixels outside the mask (Bosking et al., 2000; Blasdel and Campbell, 2001). Grayscale values for those pixels that were not in the mask were not changed during this filtering. Region under the mask were excluded in quantitative measures.

Measurement of iso-orientation domains

In order to compare the orientation preference organization in central and peripheral V1, we first mapped the visuotopic organization of V1. In order to compare with other studies, this study focused mainly on V1 areas representing central eccentricities from 0-3° and peripheral (or paracentral) eccentricities from 3-6°. Iso-orientation domain sizes were measured on orientation difference maps (e.g., 0°/90°, 45°/135°). The same region of interest (ROI), relatively free of blood vessels, was chosen for all four difference maps of the same case. The region of interest then was divided into central and peripheral V1 according to visual field maps obtained earlier. Then the ROI of each image was thresholded to include only the top 25% darkest pixels for further quantitative measurements. The Imaging Processing Toolkit (Reindeer Graphic Company) was used to calculate the domain sizes in central and peripheral ROIs. The average iso-orientation domain size from each case was based upon the measurements of 4 individual orientations (0°, 45°, 90°, 135°). We measured 4 sets of

data from 3 animals. Statistical tests were done by performing t-tests on the 4 iso-orientation data sets from central and peripheral ROIs on the basis of individual cases.

Examination of the distribution of pinwheel centers over CO blobs/interblobs

At the termination of each experiment, the animal was deeply anaesthetized with an overdose of sodium pentobarbital and perfused transcardially with a saline rinse followed by 2 % paraformaldehyde in 0.1 M phosphate buffer. The brain was removed and the imaged area of cortex was separated and flattened. The imaged piece of cortex was then frozen and cut with the surface vascular pattern preserved in the first 100 - 150 μ m section. Subsequent sections were cut at 50 μ m. CO staining was performed using methods described previously (Boyd and Matsubara, 1996).

Surface and radial blood vessels were the primary landmarks used to align histological sections to the optical images. Regions of interest were chosen for further quantification. The CO image was high-pass filtered at slightly larger than the average blob size (at a radius of 10-25 pixels) and low pass filtered at slightly smaller than the smallest blobs (at a radius of 5-10 pixels). This image was then thresholded and posterized into 3 gray levels: dark (CO blobs proper), white (CO interblobs proper), and grey (border areas) (see Boyd and Casagrande, 1999). Using Igor Pro 4.0 (WaveMetrics, Inc.), we encoded the X-Y coordinates of pinwheel centers (defined as described above) and then transferred these coordinates to the CO threshold image to examine the relationship between pinwheel centers and blob, interblob, and border areas. Chi-square analyses were then performed to assess the probability of pinwheel centers falling within each of these compartments.

Results

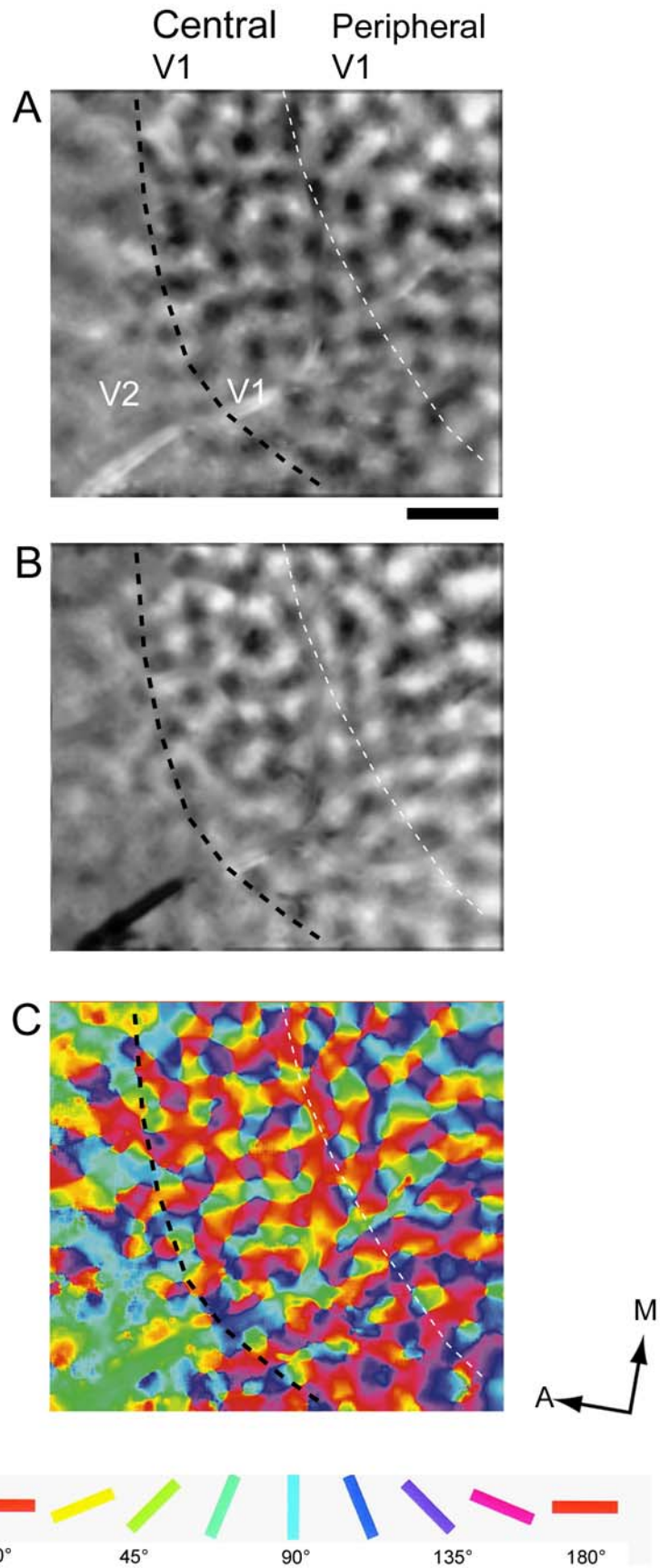
Orientation preference organization in central and peripheral V1

Orientation preference maps from a representative case are shown in Figure 20. Figure 20A is an orientation difference map produced from $0^\circ/90^\circ$ orientations and Figure 20B represents a difference map produced from $45^\circ/135^\circ$ orientations. In both panels, central ($0-3^\circ$) and peripheral ($3-6^\circ$) V1 are delineated by dashed lines. The dark line represents the vertical meridian (VM) (V1/V2 border), while the white line represents the 3° iso-eccentricity line. The region found between the two lines defines the $0-3^\circ$ or central vision. Beyond the white dashed line is the representation of peripheral vision ($3-6^\circ$). The dark and light patches indicate areas responsive to each of the two orientations. Qualitative examination of the two cortical representations suggests that central and peripheral V1 contain zones that are equally well activated by orientation. A color-coded version of the orientation preference map taken from the same imaged area (see Figure 20C) allows one to see the geometric arrangement of the whole cortical area. This map also shows that geometric arrangements of orientation preference in the central and the peripheral zones of V1 are similar. Both zones have pinwheels and linear zones.

Magnitude of orientation selectivity

A quantitative analysis of the magnitude of the orientation response in a representative case is shown in Figure 21. The curves illustrated in Figure 21A and B show the time courses of intrinsic signal strength in central V1 and peripheral V1 to an 8-

Figure 20. Comparison of the maps of orientation preference in central and peripheral V1. **A** and **B** are the orientation difference maps of $0^\circ/90^\circ$ and $45^\circ/135^\circ$, respectively. **C** is a color coded orientation preference map. Orientation preference is color-coded as in the key. The black and white dashed lines in **A**, **B** and **C** divide the representation zone of central vision in V1 ($= 3^\circ$) from the representation zone of peripheral vision (i.e., $3^\circ - 6^\circ$). Scale = 1mm.



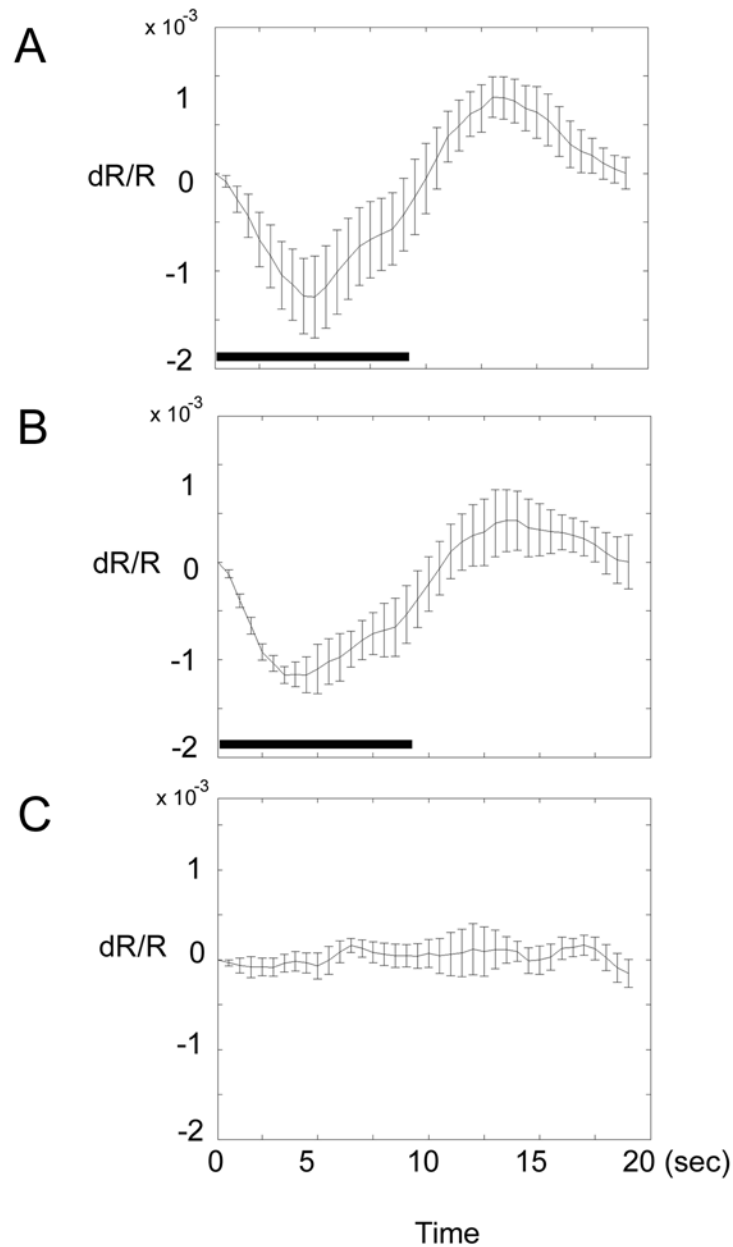


Figure 21. Time course plots of intrinsic signal magnitude at different eccentricities.

A and **B** show the time courses of intrinsic signal strength in central V1 and peripheral V1 to an 8 second stimulation using full screen drifting gratings at 45° , respectively. **C** is the blank control for comparison. For **A** and **B**, each curve represents the average of 5 iso-orientation domains with the signal strength plotted against baseline over 19 seconds. The central ROI peak magnitude is 0.13% [$1.3 \pm 0.42 (10^{-3})$], and the peripheral ROI magnitude is 0.12% [$1.2 \pm 0.09 (10^{-3})$]. There was no significant difference in the magnitude of signal activation when central domains were compared to more peripheral domains.

second stimulation with a 45° stimulus, while Figure 21C shows the blank control for comparison. The curves represent an average across 5 iso-orientation domains with the signal strength plotted against baseline over 19 seconds. In the central region of interest, peak magnitude was 0.13% [$1.3 \pm 0.42 (10^{-3})$], while in the peripheral region of interest the peak signal magnitude was 0.12% [$1.2 \pm 0.09 (10^{-3})$]. Therefore, there was no significant difference in the magnitude of signal activation when central domains were compared to more peripheral domains ($P > 0.05$). We also got non-significant results from the two other cases.

Iso-orientation domain sizes in central and peripheral V1

The average iso-orientation domain sizes from 4 difference maps of orientation (0°/90°; 45°/135°; 90°/0°; 135°/45°) were compared for central and peripheral V1. Iso-orientation domain sizes in central V1 were significantly smaller than those in peripheral V1 with only one exception, as shown in Table 3. This result was interesting given that magnification decreases with increasing eccentricity (see Chapter 2). In addition, the pinwheel density in central V1 tended to be higher than that in peripheral V1 ($5.6 \pm 1.2/ \text{mm}^2$ (mean \pm std) vs 4.8 ± 0.8).

Re-examination of the relationship between CO blobs and pinwheel centers

In this study we also investigated the spatial relationship between CO blobs and orientation domains at different eccentricities. It was reported that pinwheel centers do not correlate with CO blobs in V1 of bush babies, owl monkeys and macaque monkeys, although central and peripheral eccentricities were never strictly differentiated in these studies (Bartfeld and Grinvald, 1992; Bosking et al., 1996; See Chapter 3). To determine if the relationship between pinwheel centers and CO blobs vary with eccentricity, we re-

Table 3. Comparison of iso-orientation domain sizes in central and peripheral V1

Case #	average iso-orientation domain size at eccentricities (0° - 3°)	average iso-orientation domain size at eccentricities (3° - 6°)	Statistical t test - P value
10.19.02	0.04 ± 0.01 mm ² (mean ± SE)	0.08 ± 0.02 mm ²	0.002
11.19.02L	0.13 ± 0.01 mm ²	0.23 ± 0.03 mm ²	0.05
11.19.02R	0.10 ± 0.01 mm ²	0.125 ± 0.01 mm ²	0.01
04.22.03	0.09 ± 0.01 mm ²	0.11 ± 0.01 mm ²	0.07

examined the relationship between CO blobs and pinwheel centers in V1, comparing the maps in the central representation (e.g., 0-3° eccentricity) with the maps in the peripheral representation (e.g., 3-6° eccentricity). We did not find a significant relationship between the distribution of pinwheel centers and CO blobs in either central or peripheral V1 in two cases. An example taken from central V1 is shown in Figure 22. In the selected area, the pinwheel density is 5.7/mm² in CO blobs, 4.7/mm² in interblobs and 6.2/mm² in border areas. The distributions did not differ significantly ($p = 0.51$, chi square analysis). For the same case, the distribution of pinwheel centers in peripheral V1 was non-significant: 5.4/mm² in CO blobs, 4.2/mm² in interblobs and 4.8/mm² in border areas ($p = 0.33$).

Discussion

In the bush baby V1, we did not find any significant eccentricity related variations in the geometric arrangement of orientation or the magnitude of responses to orientation. We did, however, find that orientation domain size varied with eccentricity. We also found that there was no eccentricity dependent relationship between the CO blobs and pinwheels. Below we discuss the significance of these findings in detail.

Species differences in orientation preference organization

Our results differ from previous research reported by Vanduffel et al. (2002) whose results suggest a systemic variation in the geometry of orientation columns and its relationship to CO blobs with eccentricity in macaque V1. There are several possible explanations for the differences between the present study and the results of Vanduffel et al. (2002). First, two obvious differences between our studies are the species used and

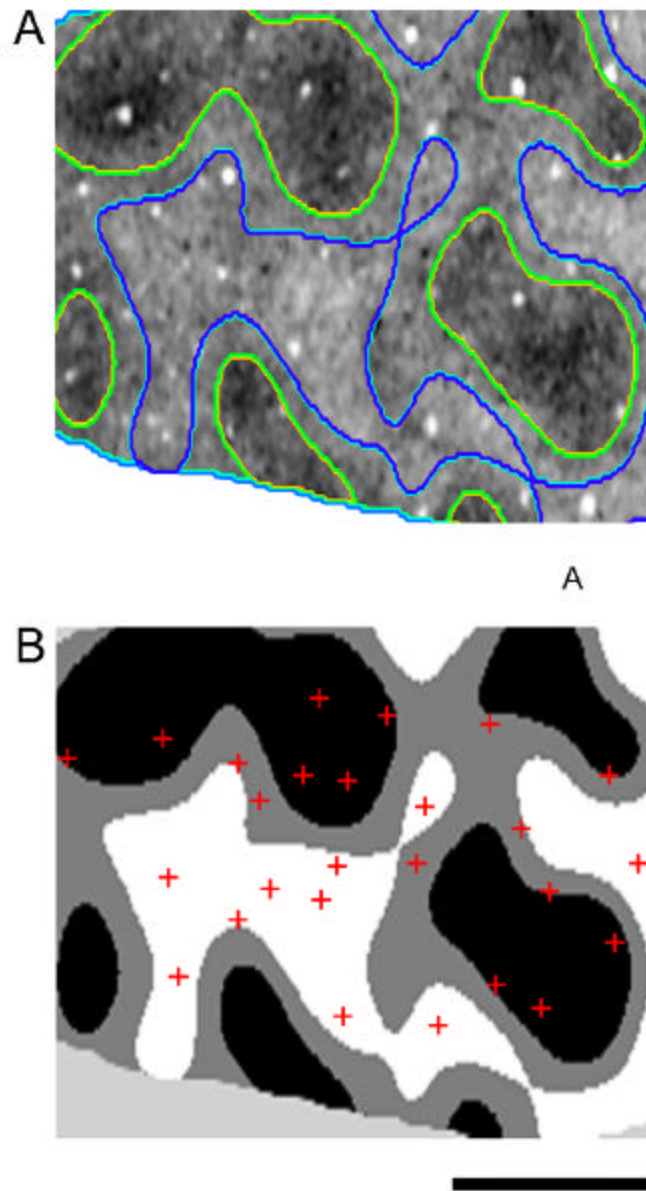


Figure 22. The distribution of orientation pinwheel centers in CO blobs and interblobs in central V1. **A.** A CO section from central V1 (eccentricities $< 3^\circ$) with contour plots transferred from its thresholded image. Green contours encircle CO blobs, blue contours encompass CO interblobs, border areas lie between the two colors. **B.** The CO thresholded image with pinwheel center locations indicated (red crosses). Scale bar = 1.0 mm.

the life styles of those species. Bush babies are tree dwelling nocturnal prosimians with relatively large eyes, a reflective tapetum and a rod-dominated retina. Bush babies contain only a single type of L/M cone (Wikler and Rakic, 1990; Jacobs et al., 1996). In contrast, macaque monkeys are diurnal, mainly ground dwelling, Old World simians with trichromatic color vision. The retinae of nocturnal and diurnal primates (e.g., bush baby and owl monkey vs macaque monkey and human) show marked differences in the distribution of photoreceptor subtypes (Perry et al., 1984; Curcio et al., 1987; Wikler and Rakic, 1990; Wikler et al., 1990). For example, the retina of the macaque monkey possesses an all cone foveola with a peak density of 130,000 cones/mm². This cone density declines about 20 fold toward the periphery. In contrast the peak cone density in bush babies is only 7,500-8,500/mm² and declines to 1,500/mm² in the periphery (the central to periphery gradient in cone density is about 5 fold) (Wikler and Rakic, 1990). Thus the density of foveal cones and the central to peripheral differences in the macaque monkey are much greater than in the retina of the bush baby (Wikler and Rakic, 1990). Also, bush babies do not have well developed foveae. In fact a fovea occurs in only 1 out of 9 members of the species with the remaining members having an *area centralis* (Walls, 1967). In either case this central specialization, unlike that of macaque monkeys, contains both rods and cones (DeBruyn et al., 1980). There are also large differences in the degree of central specialization in terms of the ganglion cell density (DeBruyn et al., 1980; also see Silveria, 2004). For diurnal species like the macaque monkey the ganglion cell density reaches 60,000 cells/mm² in the foveal slope. For the nocturnal species like the bush baby studied here ganglion cell density peaks at about 12,000 cells/mm² (DeBruyn et al., 1980), which is one fifth of that found in the diurnal macaque monkey.

Therefore, compared to bush babies, macaque monkeys have a retinal specialization that emphasizes color and stronger central vision. This may be, in turn, translated to the differences seen in cortical organization.

In addition, electrophysiological studies indicate that the V1 cortical organization differs between macaque monkeys and bush babies. It has been reported that in the central vision representation region ($< 2.5^\circ$) of the macaque V1, there exist many chromatically selective cells with a low percentage of cells that are selective to stimulus orientation and a rising proportion of orientation selective cells with increasing eccentricities (Poggio et al., 1975; Zeki, 1984). In bush baby V1, almost all the recorded V1 cells at different eccentricities are orientation selective and only 6% of the cells are non-oriented (DeBruyn et al., 1993). Bush baby cortical cells also have narrower orientation selectivity than is found in the macaque monkey (DeBruyn et al. 1993). Nevertheless, Vanduffel et al. (2002) claimed that in macaque V1, the magnitude of responses to orientation in the central representation is about 40% less than is seen in more peripheral representations. The markedly lower orientation selectivity in central V1 reported by Vanduffel et al. (2002) is counterintuitive and is not compatible with high discrimination ability (which presumably requires high selectivity to stimulus orientations) in central vision. Our data in bush babies did not show this difference. Instead our data suggest that the magnitude of orientation selectivity does not vary within eccentricities of $= 10^\circ$.

Modular distribution and eccentricity

Another finding in this study is that iso-orientation domain sizes in bush baby V1 are smaller at central eccentricities ($0-3^\circ$) than at more peripheral eccentricities

(paracentral 3-6°). This is interesting and may be related to higher discrimination ability in central vision. Considering that cortical modules that analyze visual attributes of the image in small portions of the visual field have a roughly constant size in V1 representing the central 20° of the visual field (approximately 1-2 mm in diameter) (Hubel and Wiesel, 1977), a single point in visual space may activate more sets of orientation modules due to smaller iso-orientation domain sizes, which may underlie the ability to make fine orientation discriminations in central vision. Note that in our study we only focused on central and paracentral V1 regions and did not systematically examine the more peripheral representation (> 6°). The linear dimension of the cortical point image decreases toward far peripheral V1 (Dow et al., 1981) but is always large enough to contain neurons selective to all orientations. So the orientation module sizes would be predicted to get smaller in the far periphery, which we may examine in a future study.

As far as the possible link between CO blobs and orientation column systems is concerned, the variation of CO blobs with eccentricities has been reported, but the results have been inconsistent across species and across studies. For example, in bush baby V1, the CO blob density increases from the central (0-10°) to far peripheral (> 20°) vision representation (Condo and Casagrande, 1990). In macaque monkeys, Horton (1984) and Livingstone and Hubel (1984) reported that the size of the blobs decreases with eccentricity, and as in bush babies, the density increases. In contrast, however, Farias et al. (1997) recently reported that the spatial density of blobs is nearly constant in most V1. In addition, in New World primates such as cebus monkeys, squirrel monkeys and owl monkeys, V1 blob density does not increase from central toward the far peripheral representation (Cusick and Kaas, 1988; Tootell et al., 1985; Rosa et al., 1991).

In the present study, we examined the relationship between pinwheel centers and CO blobs at different eccentricities of V1 regions, and did not find a preferential alignment of pinwheel centers over CO blobs in either central or peripheral eccentricities. As reported before in bush babies and macaque monkeys (Bosking et al., 1996; Bartfeld and Grinvald, 1996) as well as in owl monkeys, our results suggest that CO blobs and orientation columnar systems are spatially independent, regardless of eccentricities. However, as we discuss in Chapter 3 that the number of pinwheels and the number of CO blobs is roughly 2:1 with a strong linear correlation, CO blobs and pinwheel systems may well co-exist in a complex way.

CHAPTER VI

THE ORGANIZATION OF SPATIAL FREQUENCY PREFERENCE IN BUSH BABY V1

Introduction

Most V1 neurons respond preferentially to stimuli with specific orientations and spatial frequencies. Although the organization of orientation selectivity has been thoroughly described (Chapter 3 and Bosking et al., 1996), the arrangement of spatial frequency (SF) preference in V1 is much less clear. Preferred spatial frequency has been suggested to have an orderly representation, although the details of its organization remain controversial (Maffei and Fiorentini, 1977; Tootell et al., 1981; Berardi et al., 1982; Tolhurst and Thompson, 1982; Bonhoeffer et al., 1995; Shoham et al., 1997). Recently, two sets of experiments used intrinsic signal imaging to characterize the tangential organization of SF preference in cat V1. Results support two contrasting models. In the first model, spatial frequency is represented in a binary fashion with high spatial frequencies clustered together and low spatial frequencies clustered together (Shoham et al., 1997; Huebner et al., 1997). In the second model spatial frequency is represented continuously across cortex, with independent multiple processing domains (Everson et al., 1998; Issa et al., 2000). Disagreement also exists over how spatial frequency organization relates to CO blobs and interblobs. In primates, previous single unit recordings in bush babies showed that CO blobs contain cells with higher SF preference than cells in interblobs, while in macaque monkeys it was shown that cells in CO blobs prefer lower spatial frequencies than cells in interblobs (Tootell et al, 1981;

Born and Tootell, 1991; DeBruyn et al., 1993; Edwards et al., 1995). Thus far optical imaging has not been used to examine the functional organization of spatial frequency preference in V1.

In this study, we used optical imaging of intrinsic signals to investigate the organization of spatial frequency in V1 of bush babies. We addressed three specific questions: 1) How is spatial frequency represented in V1? 2) What are the relationships between the cortical maps of spatial frequency preference and orientation preference? 3) What is the relationship between CO blob compartments and spatial frequency preference?

Methods and Materials

General preparation

The four bush babies used in this study were handled according to an approved protocol from the Vanderbilt University Animal Care and Use Committee. Animals were prepared for surgery, paralyzed and anesthetized as described earlier (Rosa et al., 1997, Xu et al., 2001; and see previous chapters). Paralysis and anesthesia were maintained by intravenous infusion of vecuronium bromide ($0.1-0.3 \text{ mg kg}^{-1} \text{ hr}^{-1}$) mixed in 5% dextrose lactated Ringer's, and propofol (2,6-di-isopropylphenol: $10 \text{ mg kg}^{-1} \text{ hr}^{-1}$), respectively, in two separate lines, respectively. In order to ensure that adequate levels of anesthesia were maintained throughout the experiment, heart rate, peak end tidal CO_2 and temperature were monitored continuously after paralysis and the level of anesthetic increased if necessary. Pupils were dilated with 1% atropine eye-drops, and clear gas

permeable contact lenses with 3mm artificial pupils were used to render the retina conjugate with the viewing screen 28.5 or 57 cm distant. An opening was made in the skull over V1 and was sealed with 1% agarose under a cover glass.

Optical imaging and visual stimuli

Intrinsic optical imaging signals were acquired with the Imager 2001 differential video-enhancement imaging system and VDAQ/NT data acquisition software (Optical Imaging Inc.). Reference images of cortical vasculature were acquired with a 540 nm green light. The cortex was illuminated with a 611 nm light during data acquisition.

For mapping spatial frequency preference, sine-wave gratings with a range of different SFs were used. In most instances 50% contrast was used with a temporal frequency of 2 Hz. Drifting gratings were presented at 4 orientations. At each orientation, 4 -7 SFs ranging from 0.1 - 2.4 c/deg were presented to the animal binocularly. Each grating was moved back and forth along an axis that was orthogonal to the orientation of the grating. A set of stimuli consisted of 16-28 different combinations of SFs and orientations plus 2 blank control conditions. Video images were acquired at a rate of 30 frames/sec, and all frames acquired for each condition during the 8-sec period of stimulation were summed together for 8 data frames for further analysis. These data acquisition periods were preceded by 10 sec interstimulus intervals. Stimulus sets were repeated 20 - 30 times.

In the same imaged area, orientation preference was mapped by using square wave gratings at 4 orientations (See Chapter 3); the visual field was also mapped and the representation of different eccentricities in the same cortical area determined (See Chapter 2).

Image analysis

All images associated with the same orientation and spatial frequency were normalized by blank controls to create single condition maps of a combination of orientation and SF. In addition, all the summed images acquired under the same SF condition across all the different orientations were divided by images from blank controls to create single condition SF maps. The method of simple averaging is not ideal for constructing SF maps since it does not take into consideration the fact that SF tuning is dependent on stimulus orientation (most cortical cells have a preferred orientation and respond best to this orientation and less well to other orientations). However, this is easy and a more direct way to reveal possible SF columns. These images were low pass filtered using a 7 x 7 pixel filter kernel, and high pass filtered with an 80 x 80 pixel filter kernel (Bosking et al., 1997). Then the images were “clipped” at 1- 2 standard deviations around the mean of the image pixel distribution and scaled in the range of 0–255 gray levels.

We did not use single condition SF maps to construct composite color-coded SF maps for the reason mentioned above. Color-coded SF preference maps were constructed based upon single condition maps of a combination of orientation and SF. This method takes into account the fact at each cortical location, cells have a preferred orientation and will respond best to this orientation and less well to other orientations (Issa et al., 2000). Basically, the preferred SF of a pixel is defined as the SF of the single stimulus condition that produced the strongest response at that pixel among all of the unique combinations of orientation and SF. In color-coded maps, the ranges of SF were assigned particular colors.

To construct maps of orientation preference, we summed together all images associated with the same orientation; the summed images acquired during the presentation of one orientation were divided by the summed images acquired during the presentation of the orthogonal orientation to create orientation difference maps. Vector summation of the difference images was done on a pixel by pixel basis to create a color coded orientation preference (angle) map. Orientation rate of change maps were also constructed for the same regions of cortex with the highest rate of change represented as white and the lowest as black. Locations of pinwheel centers were determined by thresholding the rate of change map to pinpoint those areas where the rate of change was greatest. These were defined as pinwheel centers, assuming that all orientations presented were represented around these points (Blasdel, 1992b).

Comparison of CO maps and SF preference maps

At the termination of each experiment, the animal was deeply anaesthetized with an overdose of sodium pentobarbital and perfused transcardially with a saline rinse followed by 2 % paraformaldehyde in 0.1 M phosphate buffer. The brain was removed and the imaged area of cortex was separated and flattened. The imaged piece of cortex was then frozen and cut with the surface vascular pattern preserved in the first 100 - 150 μ m section. Subsequent sections were cut at 50 μ m. CO staining was performed using methods described previously (Boyd and Matsubara, 1996).

Surface and radial blood vessels were the primary landmarks used to align histological sections to optical images. In the region of interest, the CO image was high-pass filtered at slightly larger than the average blob size (at a radius of \sim 1 mm) and low pass filtered at slightly smaller than the smallest blobs (at a radius of \sim 200 μ m). This

image was then thresholded and posterized into 3 gray levels: dark (CO blob proper), white (CO interblob proper), and grey (border area) (see Boyd and Casagrande, 1999) and aligned with the SF map. One-way ANOVA tests were used to compare the pixel distributions of peak SFs over CO blobs and interblobs. The p value ≤ 0.05 was considered statistically significant.

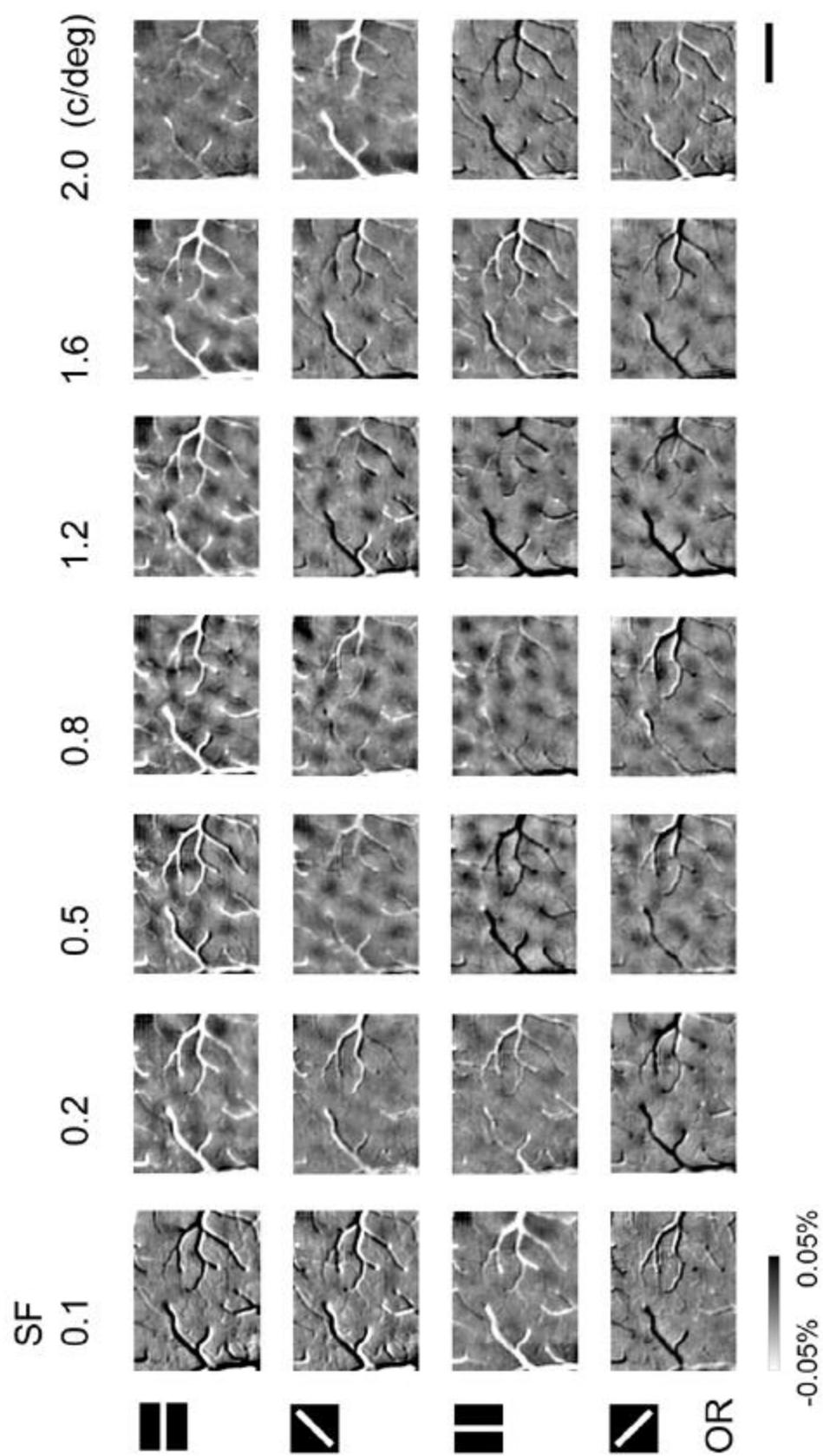
Results

General structure of SF maps

Figure 23 shows single condition maps of combinations of orientation and SF. Each image is a single condition orientation map at a single SF. The dark patches are the regions where cells responded best to particular orientations and SFs. The mid-range of SFs (0.5, 0.8, and 1.2 c/deg) showed the strongest activation; while the maps produced by either the lowest (0.1 c/deg) or highest (2.4 c/deg) SF did not exhibit as strong activation. At each orientation the maps at different SFs had a rather similar layout, but differed in domain size, shape, and position. Single condition SF maps from the same case (shown in Figure 23) are shown in Figure 24. In these maps, different SFs activated different regions of cortex and revealed clusters of activation within neighboring territories, suggesting a columnar arrangement of SF in cortex.

The color-coded map of SF preference (Figure 25) reveals the detailed features of SF organization. As can be seen, there are multiple SF processing domains and the full range of SFs is mapped across cortex. Within eccentricities of 0- 10^{B} , the average iso-SF domain size for the mid-range SFs was $0.095 \pm 0.05\text{mm}^2$ (mean \pm SD). We found that

Figure 23. Single condition maps of combinations of orientation and spatial frequency (SF). Rows represent different SFs and columns represent different orientation. Each image is a single condition orientation map at a single SF. Scale = 1 mm.



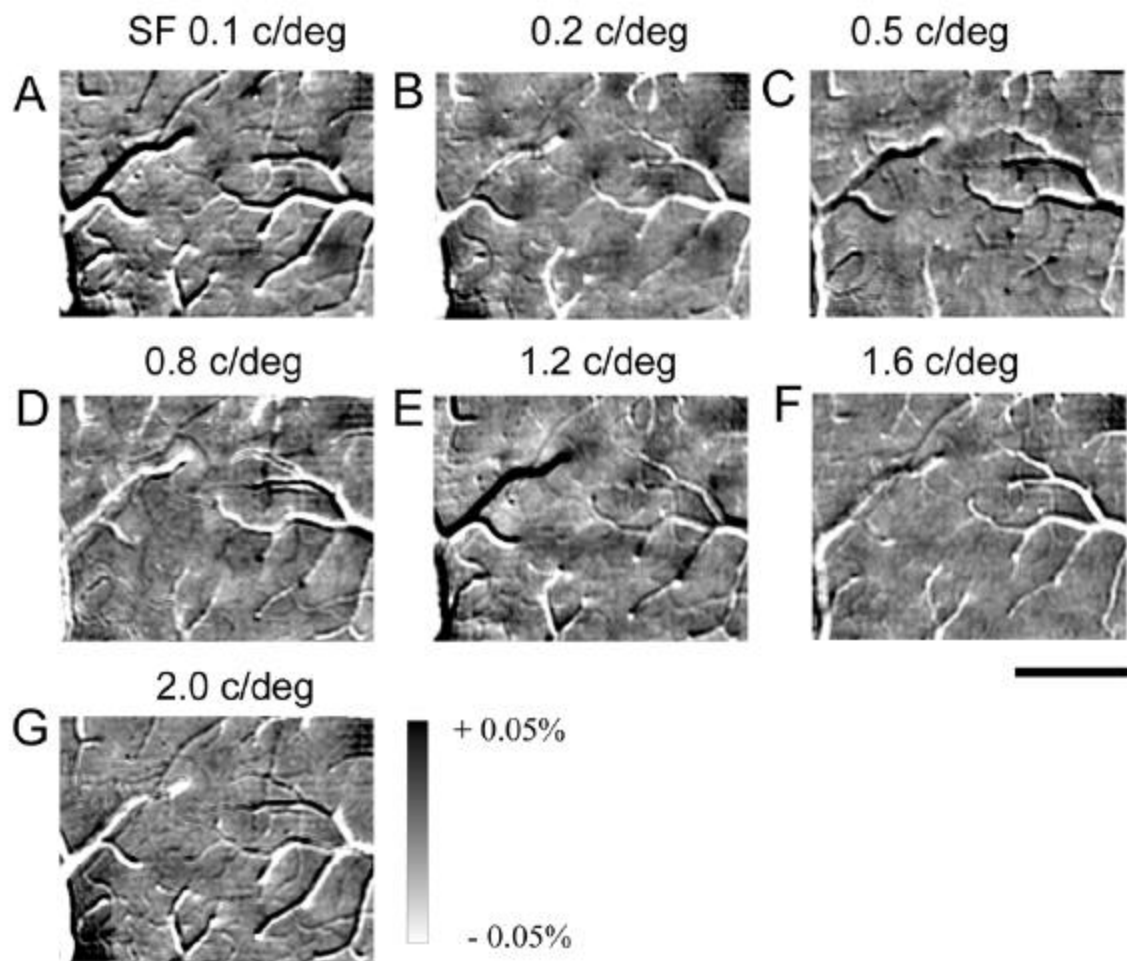


Figure 24. Single condition maps of SFs. These maps indicate that different SFs activate different regions of cortex suggesting a columnar arrangement. Scale = 1 mm

in SF maps there were locations where several SF domains met, but did not form pinwheels, because only a few SFs were represented around the junction point. The middle range of SFs occupied more territory (~75% of the map area) in the SF map (see Figure 25), consistent with the observation that mid-range of SFs provided the best activation in the single condition maps that combine orientation and SF (Figure 23). The lowest and highest SFs accounted for much less cortical area (only ~25% of the mapped area). We also noted that the highest and lowest SFs were usually separated by domains of intermediate SF preference.

Eccentricity dependent variation

We superimposed SF maps on visual field maps from the same imaged area and examined SF preference in relation to different eccentricities. As can be seen in Figure 26, the full range of SF is represented at each eccentricity. There is, however, the expected trend for the range of spatial frequencies to shift such that proportionally more cortex is devoted to higher SFs in central than in peripheral vision. As can be seen in Figure 26, the region close to the central vision representation shows a higher proportion of higher SFs (green and blue colors) and proportionally less of the lower SF range (red and yellow colors) than does the peripheral vision representation.

Relationship between maps of spatial frequency and orientation maps

Qualitatively, SF domains appeared to be organized differently from orientation domains. Orientation maps typically had pinwheels and linear zones; each orientation was more or less uniformly represented in cortex (Chapters II and III). As mentioned, SF maps did not have pinwheels, and the middle range of SFs were over-represented. Note, however, that SF preference, like orientation preference, was mapped continuously

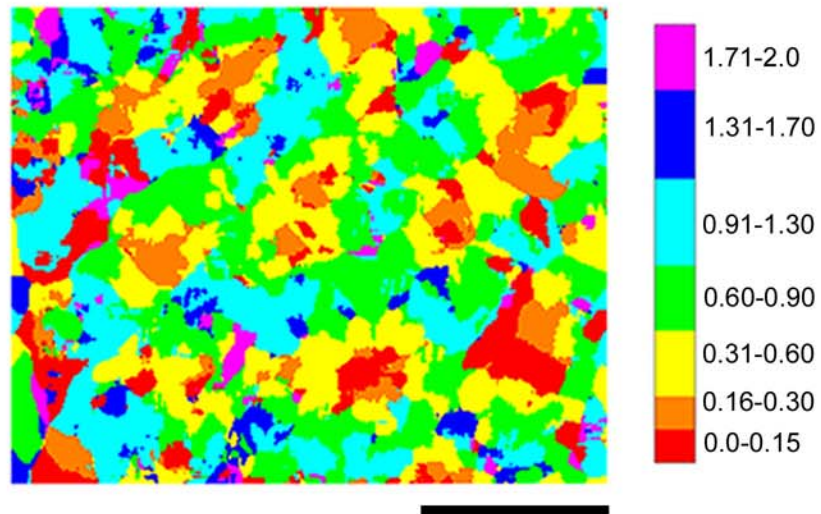


Figure 25. A color-coded SF preference map. The color key beside the map indicates SF preference. Red represents the lower SF range; yellow, green and light blue are mid-range SFs; and dark blue and purple are higher SF ranges. As can be seen SFs are mapped continuously across cortex in multiple SF processing domains. Scale = 1 mm.

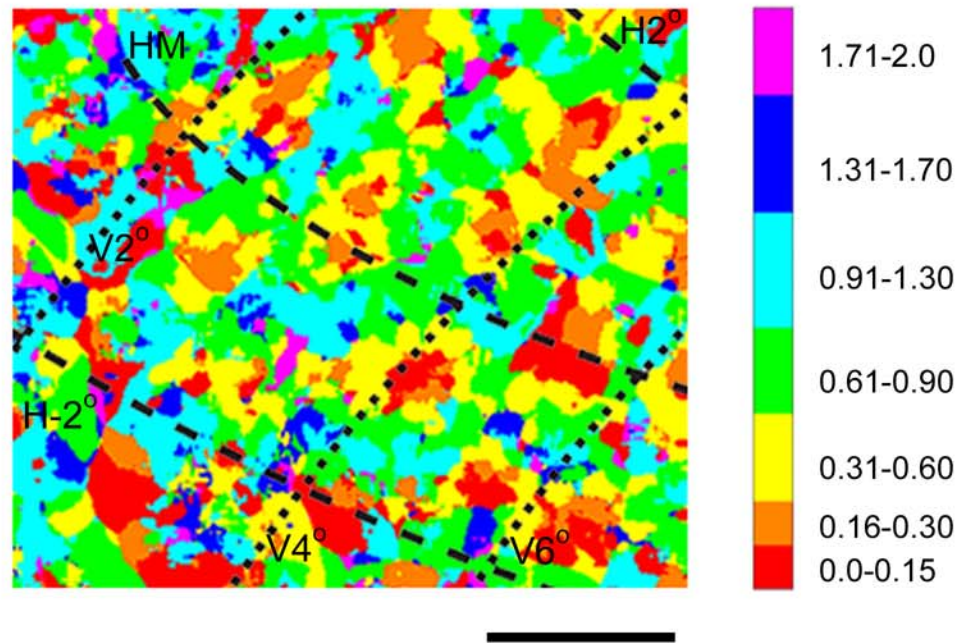


Figure 26. Eccentricity-dependent variation in spatial frequency representation.

A color-coded SF preference map, superimposed on a visual field map constructed from topographical mapping. For the visual field map, H -2° and H 2° are 2 degrees below and above the horizontal meridian (HM) representation, respectively; V 2° , V 4° and V 6° are 2, 4 and 6 degrees away from the vertical meridian representation, respectively.

Proportionally more cortex is devoted to higher SFs in central than in peripheral vision. Scale = 1 mm.

across V1, and that SF preference changed slowly in some regions of the SF map, while in other regions SF preference changed rapidly.

It appeared that orientation preference and SF preference showed a regular relationship such that pinwheels tended to be located at the borders between or in the centers of iso-SF domains (Figure 27 A and C). Since pinwheels contain the full range of orientations, this means that at each iso-SF domain, a range of orientations is represented. Figure 27B shows iso-orientation contours from the orientation preference map (Figure 27A). The iso-orientation contours (grey scale) were transferred to the SF map (Figure 27D). Each iso-orientation domain appears to cover several different SFs (Figure 27 B and D). These relationships are significant, because nearly all combinations of orientation and SF preference would be required in visual cortex to subserve visual perception.

Relationship between spatial frequency preference and CO modules

Figure 28 compares SF maps with CO maps in the eccentricity range $\leq 10^\circ$. A CO section is shown in Figure 28A with the contour plot transferred from the CO thresholded image in (Figure 28B). Green contours encircle CO blobs, blue contours encompass CO interblobs. Figure 28 D-I is a series of single condition SF maps for 0.1, 0.2, 0.5, 0.8, 1.2, 1.6 c/deg, respectively, superimposed on the CO contour map. In the single condition maps of SF, the dark regions indicate cells responding best to particular SFs; while the light regions suggest locations where cells did not respond well to particular SFs. Qualitative examination suggested that lower SFs are associated more with CO blobs than interblobs. For example, the arrow heads in Figure 28D-I point to the same CO blob, which was well activated by lower SFs (0.1, 0.2 and 0.5 c/deg in Figure

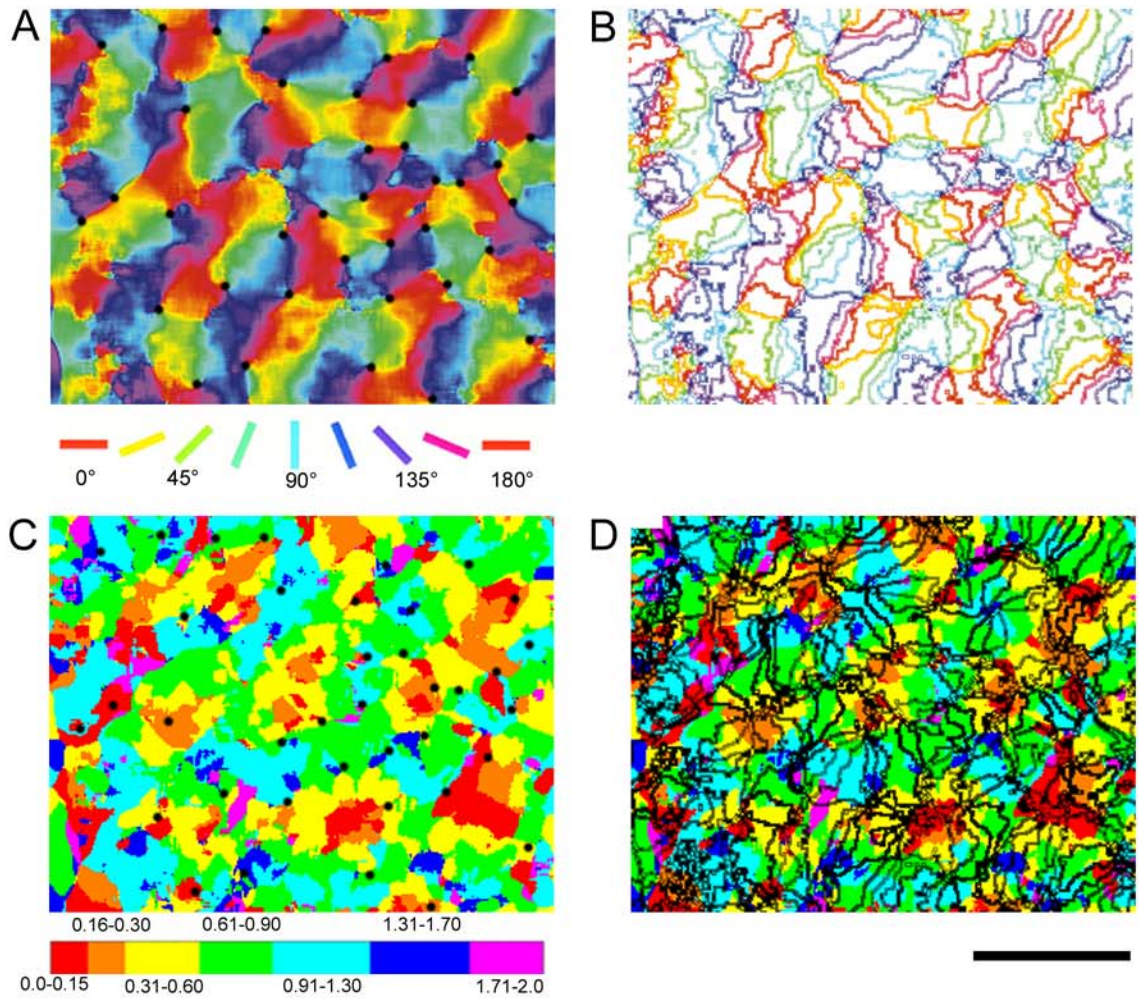
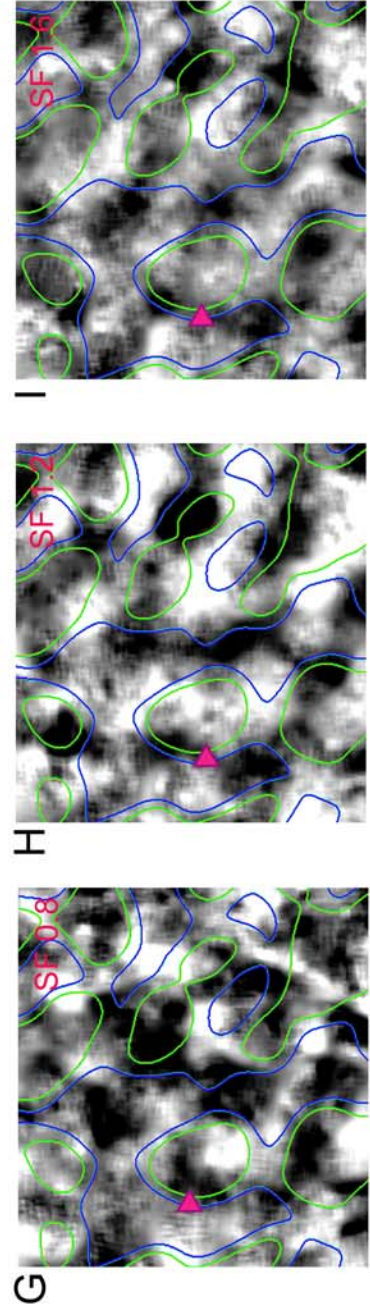
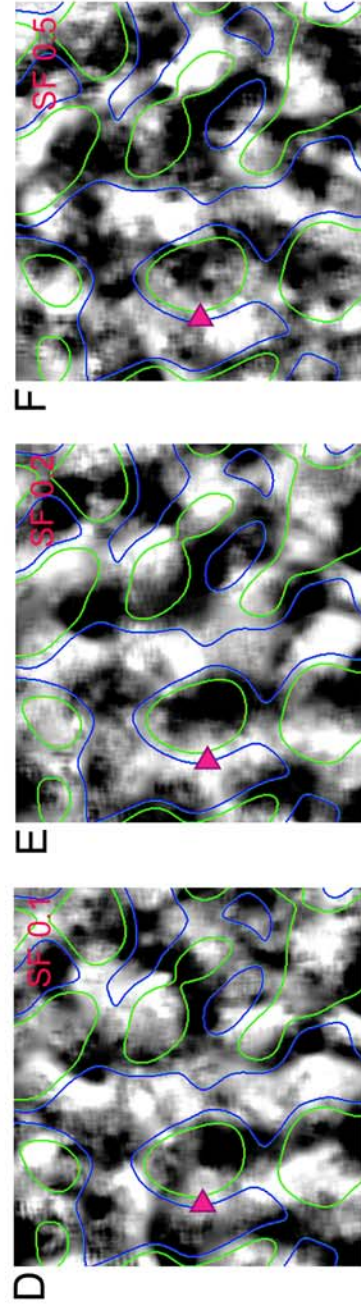
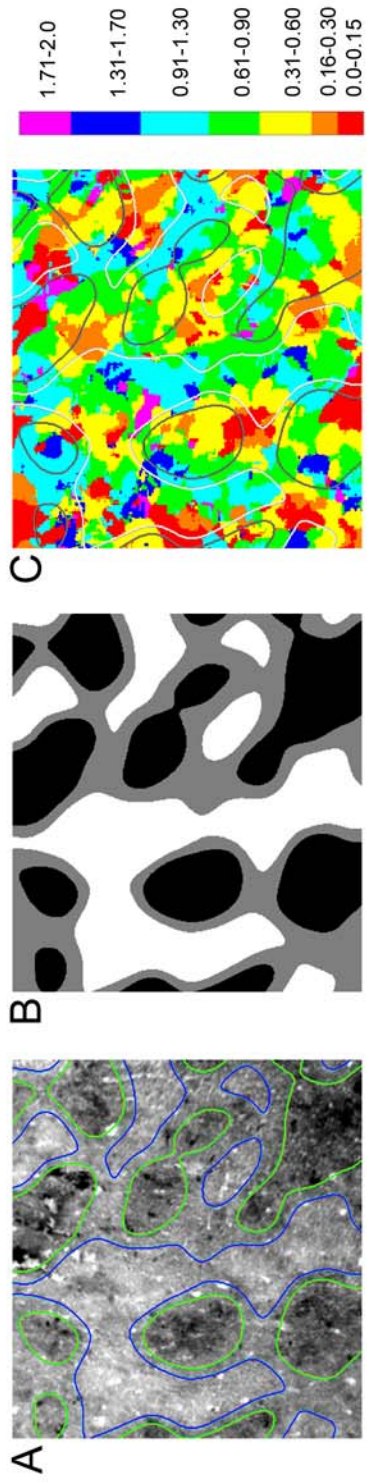


Figure 27. The relationship between orientation preference and SF preference maps. **A.** An orientation preference map with pinwheel centers marked as black dots. **B.** Iso-orientation contours made from **A**. Orientation preference is coded as indicated in the key below **A**. **C.** The distribution of pinwheel centers superimposed to the SF map. **D.** The SF preference map superimposed on a map of iso-orientation contours (gray instead of color) modified from **B**. Scale = 1mm.

Figure 28. Comparison between the spatial frequency map and the CO map. A. A CO section with the contour plot transferred from the CO thresholded image in **(B)**. Green contours encircle CO blobs, blue contours encompass CO interblobs. **C.** A color-coded SF preference map with the contour plot transferred from the CO thresholded image (Grey contours encircle CO blobs, white contours encompass CO interblobs). **D-I.** Single condition SF maps for 0.1, 0.2, 0.5, 0.8, 1.2, 1.6 c/deg, respectively, with green contours encircling CO blobs and blue contours encircling CO interblobs. Qualitative examination suggested that lower SFs are associated more with CO blobs than interblobs. For example, the arrow heads in **D-I** indicate the same CO blob, which was well activated by lower SFs (0.1, 0.2 and 0.5 c/deg), but not well activated by higher SFs (0.8, 1.2 and 1.6 c/deg). Scale = 1mm.



28D-F), but not well activated by higher SFs (0.8, 1.2 and 1.6 c/deg in Figure 28G-I). Figure 28C is a color-coded SF preference map superimposed on the CO contour plot. We quantitatively examined the distribution of pixels associated with different peak SFs in the color-coded SF map, relative to CO blobs and interblobs. Histograms in Figure 29 show the two distributions of peak SFs over CO blobs and interblobs for this case. The two distributions overlapped to a large degree, but the average peak SF in CO blobs (0.7 ± 0.4 (mean \pm std)) was significantly lower than the average peak SF in interblobs (0.78 ± 0.5 ($P < 0.05$, t-test)). More cases will be necessary to confirm this result. Together with the qualitative results from two other cases, this result suggests that lower SF domains are aligned preferentially with CO blob compartments.

Discussion

Cortical organization of SF preference

As mentioned in the introduction, there are two major contrasting views of the representation of spatial frequency in the primary visual cortex (V1). One holds that there are two complementary cortical regions, one selective for low and the other for high spatial frequency (Shoham et al., 1997; Huebener et al., 1997). The other view suggests that all spatial frequencies are continuously represented across the cortex (Everson et al., 1998; Issa et al., 2000). Our results support the second view. We found that spatial frequency is mapped continuously across bush baby V1, and that there are multiple SF processing domains in cortex. There is also converging evidence from previous studies suggesting that SF is mapped continuously in cortex. For example, the range of preferred

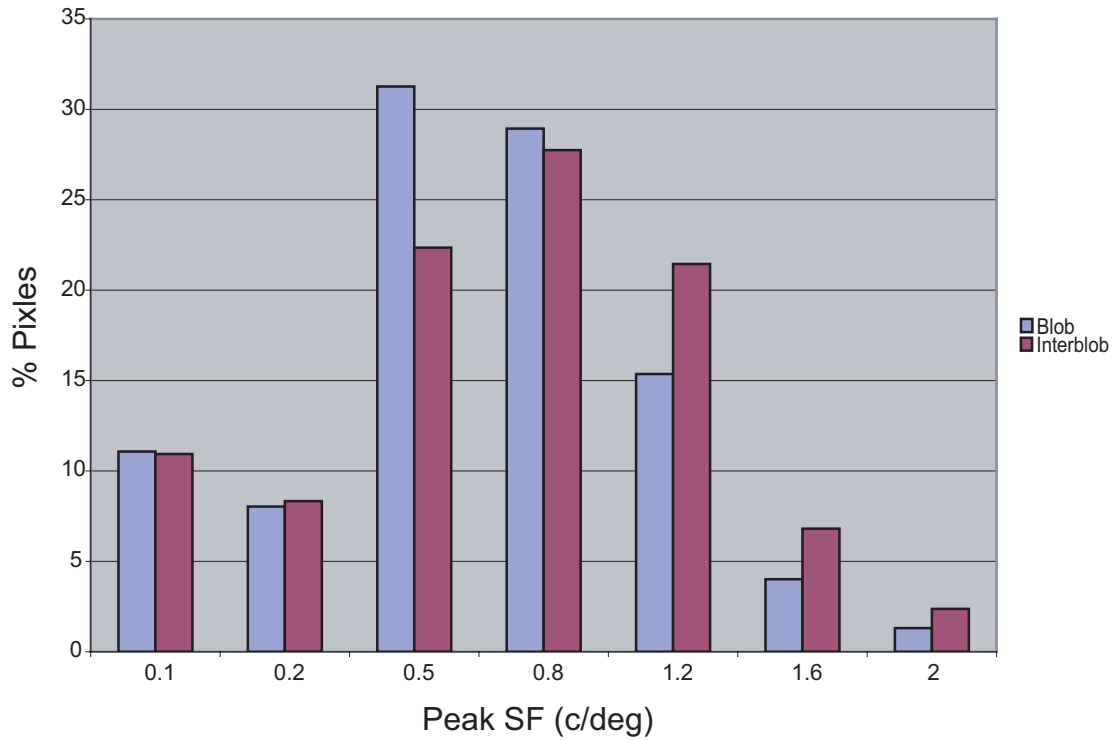


Figure 29. Histogram distributions of peak SFs over CO blobs and interblobs. The distribution of SF over CO blobs is indicated in red, and the distribution over interblobs is indicated in blue. The average peak SF in CO blobs was 0.7 ± 0.4 (mean \pm std) and was significantly lower than the average peak SF in interblobs was 0.78 ± 0.5 ($P < 0.05$, t-test).

SFs among neurons in V1 is wide as measured by single unit recordings, and cortical neurons with similar SF preference have been found to be clustered (see De Valois and De Valois, 1988). Importantly, as with orientation tuning, orderly changes in SF preference have been reported, when an electrode in macaque V1 moves tangentially (Born and Tootell, 1991). In addition, studies using 2-deoxyglucose functional labeling have suggested that spatial frequency is organized continuously across cortex (cat, macaque, Tootell et al., 1981; 1988a).

We found an eccentricity dependent variation in SF organization in bush baby V1, as reported for macaque monkeys using 2-DG labeling (Tootell et al., 1988a). The presence of proportionally higher SFs in central vision is consistent with the smaller receptive-field size and higher SF selectivity in central V1 (e.g., Movshon et al., 1978; De Valois et al., 1982; Rosa et al., 1997).

Comparison between maps of spatial frequency and orientation suggest that these two maps are organized to efficiently cover visual space, in such a way that multiple spatial frequencies are represented at each orientation, and multiple orientations are represented within each area of visual space.

Relationship between CO blobs and SF preference

The relationship between SF preference and CO blobs has not been clear. In macaque V1, it was proposed that there is a polar architecture of spatial frequency selectivity tied to the cytochrome oxidase blobs, and that CO blobs prefer lower spatial frequencies (De Valois and De Valois, 1988; Born and Tootell, 1991; Edwards et al., 1995). In bush baby V1, a previous electrophysiological study suggested the opposite, i.e., V1 cells in CO blobs have statistically higher peak SFs than cells in interblobs

(results were pooled from cells across an estimated 0-25° eccentricity) (DeBruyn et al., 1993). It also was reported that in macaque V1, the 2-DG patterns produced by various spatial frequencies vary with eccentricity, e.g., gratings of a "middle"-spatial-frequency range (4-5 cycles/deg) produce high uptake in the blobs near the foveal representation and high uptake in the interblobs at more peripheral eccentricities, including 5°. This result fits with physiological results since 4-5 c/deg would be low in the central vision representation and high in the peripheral vision representation in macaque monkeys.

In bush babies, comparison of SF maps with CO maps in central V1 ($\leq 10^\circ$ eccentricity) suggested that lower SFs are associated more with CO blobs than interblobs. This association, however, was weak (but significant), as the two distributions of peak SFs over CO blobs and interblobs overlapped to a large degree. The lack of consistency with the previous electrophysiological study could simply be due to the degree of averaging done across eccentricities and the low N reported in the recording study (DeBruyn et al., 1993).

The association between CO blobs and lower SF is supported by anatomical and physiological evidence of subcortical input pathways. Across primate species, K LGN cells are the only cells that project to CO blobs of layers III; in contrast, information from both M and P cells only get to CO blobs indirectly from layer IV (Lachica et al., 1992; 1993; Casagrande and Kaas, 1994). Since K LGN cells have average peak or cutoff SFs similar to M cells but significantly lower than P cells, the lower SF range in CO blobs might reflect the K input. It should be noted that interblobs in bush baby V1 receive indirect input via layer IV α from the LGN M cells, while in macaque monkeys interblob cells receive indirect input, via layers IV β and IIIB β , from the LGN P cells (macaque,

Lachica et al., 1992; bush baby, Lachica et al., 1993). Regardless, these results suggest that SF preference in CO blobs and interblobs cannot be predicted purely based upon anatomical connections and must reflect differences in the integrated signals that each of these compartments receives.

CHAPTER VII

CONCLUSIONS

This thesis used the recently developed method of optical imaging to examine the functional organization of visual cortical areas of two distantly related nocturnal primates, the prosimian bush baby and the New World owl monkey. The following general questions were addressed. First, can optical imaging be used to accurately map the organization of primary and higher order visual areas? Second, is the property of orientation preference organized differently in different primate species? Third, how is spatial frequency organized in relationship to other functional properties? Finally, does eccentricity affect the relationship between functional modules?

My colleagues and I were able to demonstrate in two visual cortical areas, V1 and MT that optical imaging can be used as a reliable and high-resolution tool. The visuotopic maps produced by the peak responses measured by optical imaging matched those produced by microelectrode mapping for both areas. In fact, optical imaging in V1 was able to resolve stimuli as small as 0.1 degree and shifts in stimulus position of as little as 0.25 degrees. Nevertheless, the activity revealed by this method appeared to reflect neural changes that are below the threshold for standard extracellular recording electrodes since the spread of activation consistently exceeded that predicted by extracellular recordings in each area by at least double. Using optical imaging with topographically limited stimuli, we also were able to demonstrate the locations of different visual areas including V1, V2 and V3 and verify that area MT has a global map

of the visual field. We also showed that visual areas surrounding MT also could be revealed using optical imaging. Additionally, our data demonstrated that the boundaries of MT measured with optical imaging matched boundaries identified anatomically using myelin and CO stains.

In answer to the second question, we showed that the organization of orientation selectivity in owl monkey V1 and bush baby MT are quite similar to that found in other primates. In both visual areas, orientation was organized in form of both pinwheels and linear zones suggesting that this geometric organization may be optimal for representing different orientation properties compactly. The domain sizes, within these areas however, differed significantly, being about 2 times as large in area MT as found in V1. In fact, orientation domain sizes in each visual area analyzed (V1, V2, V3 and MT) appeared to correlate with the increasing size of receptive fields of cells within each of these areas. Although in V1 CO dense compartments (blobs) and orientation pinwheels showed a 1:2 ratio suggesting that a relationship exists, this relationship did not result in a precise register between pinwheels and blobs since no statistically significant differences were found between the density of pinwheels in blobs, interblobs or border areas. In MT, however, each orientation preference domain did appear to be correlated with compartments representing directions such that each orientation compartment contained subcompartments that tended to respond to different directions of movement orthogonal to the preferred orientation at that location. Nevertheless, even maps of direction and orientation did appear to be precisely aligned.

In V2, the organization of orientation selectivity differs between owl monkeys and bush babies. In bush babies orientation is represented continuously in V2 while in

owl monkey V2 we found that this area could be divided into functional compartments with only two compartments showing evidence of orientation selectivity. Thus, in owl monkeys, as in other simians, V2 can be divided into either bands containing cells that show a high degree of orientation selectivity or bands that show low orientation selectivity. These two functional bands appear to relate to sets of CO dark and light bands in such a way as to suggest that four functional compartments exist in V2. Also, within the bands of high orientation selectivity, orientation is organized into pinwheels and linear zones just as in V1 but with domains that are significantly larger.

In owl monkey V3, we also identified zones of high and low orientation selectivity that correlated with zones of CO dark and light patches, respectively. Since this is the first study to investigate the compartmental organization of orientation in V3 we do not know if each of the compartments within V3 might be subdivided into other functional zones as might be predicted given the variety of cell types that have been identified in V3 in macaque monkeys (e.g., Adams and Zeki, 2001). Although we did not investigate the organization of V3 specifically in bush babies, we did not see any evidence of a band-like organization within the zone proposed to be V3 in bush babies during any experiments that imaged portions of this area of cortex. The existence of high and low orientation selectivity areas in owl monkey V2 (and V3) and macaque V2 but not in the V2 and V3 of bush babies, is intriguing and suggests that some segregated processing streams in extrastriate visual cortex may have appeared with the evolution of simian primates, but that color vision may not have been one of the driving forces.

For the third question we addressed the general issue of how spatial frequency is mapped in primate V1 using the bush baby as a model. In bush baby V1, investigations

of spatial frequency showed that this property is organized continuously across cortex without evidence of separate modules representing high and low spatial frequencies. This finding supports some recent data found for the organization of spatial frequency in cat area 17 (Issa et al., 2000). As in cats we found that all spatial frequencies were mapped to all locations within V1 but that much more territory was devoted to higher frequencies in the area of V1 representing central vision and conversely, much more territory was devoted to lower spatial frequencies in areas representing peripheral vision. Comparisons between maps of spatial frequency and orientation suggested that although all spatial frequencies could be found for any orientation in any broad visuotopic zone there was no strict relationship between the maps of orientation and spatial frequency. Nevertheless, statistical comparisons between spatial frequency maps and CO maps showed that lower spatial frequencies are associated significantly more often with CO blobs than interblobs.

Finally, we were able to show that no 1:1 relationships exist between functional modules regardless of eccentricity suggesting that, although each attribute appears to be represented at each visuotopic location, no common modular units exist in visual cortex.

Taken together, our findings do not support the “ice cube” modular organization of visual cortex proposed originally by Hubel and Wiesel (Hubel and Wiesel, 1977; Swindale, 1998; 2000), at least at the examined eccentricity range (i.e., = 15° in V1, and = 40° in MT). Instead our data suggest that even when functional maps show a loose relationship such as appears to be the case with CO blobs and orientation pinwheels in area V1 or more obviously between spatial frequency and orientation in V1 or between orientation and direction domains in area MT, these relationships are not precise. Each

map may appear to be related only because all the maps are constrained by the necessity to maintain coverage across visual space. It is certainly likely that multiple functional maps in primate visual cortex are superimposed to efficiently subserve visual perception without visual “holes”. Moreover, many aspects of the functional maps demonstrated in this thesis show cross species similarities and differences in the primates examined.

Some aspects such as the geometric organization of domains representing high orientation show great similarity across at least four areas. Such strong similarities found across distantly related primate species predicts that the same geometric arrangement will be found in homologous visual areas in humans.

REFERENCES

- Adams DL, Zeki S (2001) Functional organization of macaque V3 for stereoscopic depth. *J Neurophysiol* 86: 2195-2203.
- Albright TD, Desimone R, Gross CG (1984) Columnar organization of directionally selective cells in visual area MT of the macaque. *J Neurophysiol* 51: 16-31.
- Albright TD (1984) Direction and orientation selectivity of neurons in visual area MT of the macaque. *J Neurophysiol* 52: 1106-1130.
- Albright TD, Desimone R (1987) Local precision of visuotopic organization in the middle temporal area (MT) of the macaque. *Exp Brain Res* 65: 582-592.
- Allman J, Miezin F, McGuinness E (1985) Direction- and velocity-specific responses from beyond the classical receptive field in the middle temporal visual area (MT). *Perception* 14: 105-126.
- Allman J, Zucker S (1990) Cytochrome oxidase and functional coding in primate striate cortex: a hypothesis. *Cold Spring Harb Symp Quant Biol* 55: 979-982.
- Allman JM, Kaas JH (1971a) Representation of Visual Field in Caudal Third of Middle Temporal Gyrus of Owl Monkey (*Aotus trivirgatus*). *Brain Research* 31: 85-105.
- Allman JM, Kaas JH (1971b) Representation of Visual Field in Striate and Adjoining Cortex of Owl Monkey (*Aotus trivirgatus*). *Brain Research* 35: 89-&.
- Allman JM, Kaas JH, Lane RH (1973) The middle temporal visual area(MT)in the bush baby, *Galago senegalensis*. *Brain Res* 57: 197-202.
- Baizer JS (1982) Receptive field properties of V3 neurons in monkey. *Invest Ophthalmol Vis Sci* 23: 87-95.
- Baker JF, Petersen SE, Newsome WT, Allman JM (1981) Visual response properties of neurons in four extrastriate visual areas of the owl monkey (*Aotus trivirgatus*): a quantitative comparison of medial, dorsomedial, dorsolateral, and middle temporal areas. *J Neurophysiol* 45: 397-416.
- Bartfeld E, Grinvald A (1992) Relationships between orientation-preference pinwheels, cytochrome oxidase blobs, and ocular-dominance columns in primate striate cortex. *Proc Natl Acad Sci USA* 89: 11905-11909.
- Beck PD, Kaas JH (1998) Cortical connections of the dorsomedial visual area in prosimian primates. *J Comp Neurol* 398: 162-178.

- Berardi N, Bisti S, Cattaneo A, Fiorentini A, Maffei L (1982) Correlation between the preferred orientation and spatial frequency of neurones in visual areas 17 and 18 of the cat. *J Physiol* 323: 603-618.
- Blasdel G, Campbell D (2001) Functional retinotopy of monkey visual cortex. *J Neurosci* 21: 8286-8301.
- Blasdel GG, Salama G (1986) Voltage-sensitive dyes reveal a modular organization in monkey striate cortex. *Nature* 321: 579-585.
- Blasdel GG (1992a) Differential imaging of ocular dominance and orientation selectivity in monkey striate cortex. *J Neurosci* 12: 3115-3138.
- Blasdel GG (1992b) Orientation selectivity, preference, and continuity in monkey striate cortex. *J Neurosci* 12: 3139-3161.
- Bonhoeffer T, Grinvald A (1991) Iso-orientation domains in cat visual cortex are arranged in pinwheel-like patterns. *Nature* 353: 429-431.
- Bonhoeffer T, Kim DS, Malonek D, Shoham D, Grinvald A (1995) Optical imaging of the layout of functional domains in area 17 and across the area 17/18 border in cat visual cortex. *Eur J Neurosci* 7: 1973-1988.
- Bonhoeffer T, Grinvald A. (1996) Optical imaging based on intrinsic signals: the methodology. In: *Brain Mapping: The Methods* (Toga AW, Mazziotta JC, eds), pp 55-97. San Diego: Academic.
- Born RT, Tootell RB (1991) Single-unit and 2-deoxyglucose studies of side inhibition in macaque striate cortex. *Proc Natl Acad Sci USA* 88: 7071-7075.
- Born RT, Tootell RB (1992) Segregation of global and local motion processing in primate middle temporal visual area. *Nature* 357: 497-499.
- Born RT (2000) Center-surround interactions in the middle temporal visual area of the owl monkey. *J Neurophysiol* 84: 2658-2669.
- Bosking, W. H., White, L. E., Casagrande, V. A., and Fitzpatrick, D. (1996) Functional organization of areas V1 and V2 in the prosimian galago revealed by optical imaging. *Soc Neurosci Abstr* 22, 1610..
- Bosking WH, Zhang Y, Schofield B, Fitzpatrick D (1997) Orientation selectivity and the arrangement of horizontal connections in tree shrew striate cortex. *J Neurosci* 17: 2112-2127.
- Bosking WH, Kretz R, Pucak ML, Fitzpatrick D (2000) Functional specificity of callosal connections in tree shrew striate cortex. *J Neurosci* 20: 2346-2359.

- Bosking WH, Crowley JC, Fitzpatrick D (2002) Spatial coding of position and orientation in primary visual cortex. *Nature Neurosci* 5: 874-882.
- Boyd JD, Matsubara JA (1996) Laminar and columnar patterns of geniculocortical projections in the cat: relationship to cytochrome oxidase. *J Comp Neurol* 365: 659-682.
- Boyd JD, Casagrande VA (1999) Relationships between cytochrome oxidase (CO) blobs in primate primary visual cortex (V1) and the distribution of neurons projecting to the middle temporal area (MT). *J Comp Neurol* 409: 573-591.
- Casagrande VA, Kaas JH (1994) The afferent, intrinsic, and efferent connections of primary visual cortex in primates. In: *Cerebral Cortex* (Peters A, Rockland KS, eds), pp 201-259. New York: Plenum Press.
- Chapman B, Stryker MP, Bonhoeffer T (1996) Development of orientation preference maps in ferret primary visual cortex. *J Neurosci* 16: 6443-6453.
- Collins CE, Stepniewska I, Kaas JH (2001) Topographic patterns of V2 cortical connections in a prosimian primate (*Galago garnetti*). *J Comp Neurol* 431: 155-167.
- Condo GJ, Casagrande VA (1990) Organization of cytochrome oxidase staining in the visual cortex of nocturnal primates (*Galago crassicaudatus* and *Galago senegalensis*): I. Adult patterns. *J Comp Neurol* 293: 632-645.
- Curcio CA, Sloan KR, Jr., Packer O, Hendrickson AE, Kalina RE (1987) Distribution of cones in human and monkey retina: individual variability and radial asymmetry. *Science* 236: 579-582.
- Cusick CG, Kaas JH (1988) Surface view patterns of intrinsic and extrinsic cortical connections of area 17 in a prosimian primate. *Brain Res* 458: 383-388.
- Daniel PM, Whitteridge D (1961) The representation of the visual field on the cerebral cortex in monkeys. *J Physiol (Paris)* 159: 203-221.
- Das A, Gilbert CD (1995) Long-range horizontal connections and their role in cortical reorganization revealed by optical recording of cat primary visual cortex. *Nature* 375: 780-784.
- De Valois RL, Albrecht DG, Thorell LG (1982) Spatial frequency selectivity of cells in macaque visual cortex. *Vision Res* 22: 545-559.
- De Valois RL, De Valois KK (1988) *Spatial vision*. New York: Oxford University Press.
- DeBruyn EJ, Wise VL, Casagrande VA (1980) The size and topographic arrangement of retinal ganglion cells in the galago. *Vision Res* 20: 315-327.
- DeBruyn EJ, Casagrande VA, Beck PD, Bonds AB (1993) Visual resolution and sensitivity of single cells in the primary visual cortex (V1) of a nocturnal primate (bush

baby): correlations with cortical layers and cytochrome oxidase patterns. *J Neurophysiol* 69: 3-18.

Desimone R, Ungerleider LG (1989) Neural mechanisms of visual processing in monkeys. In: *Handbook of Neuropsychology* (Goodglass H, Damasio AR, eds), pp 267-300. Amsterdam: Elsevier.

DeYoe EA, Van Essen DC (1985) Segregation of efferent connections and receptive field properties in visual area V2 of the macaque. *Nature* 317: 58-61.

Diogo AC, Soares JG, Koulakov A, Albright TD, Gattass R (2003) Electrophysiological imaging of functional architecture in the cortical middle temporal visual area of *Cebus apella* monkey. *J Neurosci* 23: 3881-3898.

Dow BM, Snyder AZ, Vautin RG, Bauer R (1981) Magnification factor and receptive field size in foveal striate cortex of the monkey. *Exp Brain Res* 44: 213-228.

Edwards DP, Purpura KP, Kaplan E (1995) Contrast sensitivity and spatial frequency response of primate cortical neurons in and around the cytochrome oxidase blobs. *Vision Res* 35: 1501-1523.

Everson RM, Prashanth AK, Gabbay M, Knight BW, Sirovich L, Kaplan E (1998) Representation of spatial frequency and orientation in the visual cortex. *Proc Natl Acad Sci USA* 95: 8334-8338.

Farias MF, Gattass R, Pinon MC, Ungerleider LG (1997) Tangential distribution of cytochrome oxidase-rich blobs in the primary visual cortex of macaque monkeys. *J Comp Neurol* 386: 217-228.

Felleman DJ, Kaas JH (1984) Receptive-field properties of neurons in middle temporal visual area (MT) of owl monkeys. *J Neurophysiol* 52: 488-513.

Felleman DJ, Van Essen DC (1987) Receptive field properties of neurons in area V3 of macaque monkey extrastriate cortex. *J Neurophysiol* 57: 889-920.

Felleman DJ, Van Essen DC (1991) Distributed hierarchical processing in the primate cerebral cortex. *Cereb Cortex* 1: 1-47.

Fiorani M, Jr., Gattass R, Rosa MG, Sousa AP (1989) Visual area MT in the Cebus monkey: location, visuotopic organization, and variability. *J Comp Neurol* 287: 98-118.

Gallyas F (1970) Silver staining of micro- and oligodendroglia by means of physical development. *Acta Neuropathol (Berl)* 16: 35-38.

Gattass R, Gross CG (1981) Visual topography of striate projection zone (MT) in posterior superior temporal sulcus of the macaque. *J Neurophysiol* 46: 621-638.

Gegenfurtner KR, Kiper DC, Fenstemaker SB (1996) Processing of color, form, and motion in macaque area V2. *Vis Neurosci* 13: 161-172.

Gegenfurtner KR, Kiper DC, Levitt JB (1997) Functional properties of neurons in macaque area V3. *J Neurophysiol* 77: 1906-1923.

Granquist-Fraser, D., Polimen, J., and Schwartz, E. L. (2003) Physical limits to spatial resolution of optical recording: photon scatter and optical defocus. *Soc Neurosci Abstr Program* 125.3.

Horton JC, Hubel DH (1981) Regular patchy distribution of cytochrome oxidase staining in primary visual cortex of macaque monkey. *Nature* 292: 762-764.

Horton JC (1984) Cytochrome oxidase patches: a new cytoarchitectonic feature of monkey visual cortex. *Philos Trans R Soc Lond B Biol Sci* 304: 199-253.

Horton JC, Hocking DR (1996) Intrinsic variability of ocular dominance column periodicity in normal macaque monkeys. *J Neurosci* 16: 7228-7239.

Horton JC, Hocking DR (1996) Anatomical demonstration of ocular dominance columns in striate cortex of the squirrel monkey. *J Neurosci* 16: 5510-5522.

Hubel DH, Wiesel TN (1962) Receptive fields, binocular interaction and functional architecture in the cat's visual cortex. *J Physiol* 160: 106-154.

Hubel DH, Wiesel TN (1968) Receptive fields and functional architecture of monkey striate cortex. *J Physiol* 195: 215-243.

Hubel DH, Wiesel TN (1977) Ferrier lecture. Functional architecture of macaque monkey visual cortex. *Proc R Soc Lond B Biol Sci* 198: 1-59.

Hubener M, Shoham D, Grinvald A, Bonhoeffer T (1997) Spatial relationships among three columnar systems in cat area 17. *J Neurosci* 17: 9270-9284.

Huk AC, Dougherty RF, Heeger DJ (2002) Retinotopy and functional subdivision of human areas MT and MST. *J Neurosci* 22: 7195-7205.

Issa NP, Trepel C, Stryker MP (2000) Spatial frequency maps in cat visual cortex. *J Neurosci* 20: 8504-8514.

Jacobs GH, Deegan JF, Neitz J, Crognale MA, Neitz M (1993) Photopigments and color vision in the nocturnal monkey, *Aotus*. *Vision Res* 33: 1773-1783.

Jacobs GH, Neitz M, Neitz J (1996) Mutations in S-cone pigment genes and the absence of colour vision in two species of nocturnal primate. *Proc R Soc Lond B Biol Sci* 263: 705-710.

- Kaas JH, Lyon DC (2001) Visual cortex organization in primates: theories of V3 and adjoining visual areas. *Vision: from Neurons to Cognition* 134: 285-295.
- Kaas JH (2004) Early visual areas: V1, V2, V3, DM, DL, and MT. In: *The primate visual system* (Kaas JH, Collins CE, eds), pp 139-159. New York: CRC Press.
- Krubitzer L, Kaas J (1990a) Convergence of processing channels in the extrastriate cortex of monkeys. *Vis Neurosci* 5: 609-613.
- Krubitzer LA, Kaas JH (1990b) Cortical connections of MT in four species of primates: areal, modular, and retinotopic patterns. *Vis Neurosci* 5: 165-204.
- Lachica EA, Beck PD, Casagrande VA (1992) Parallel pathways in macaque monkey striate cortex: anatomically defined columns in layer III. *Proc Natl Acad Sci USA* 89: 3566-3570.
- Lachica EA, Beck PD, Casagrande VA (1993) Intrinsic connections of layer III of striate cortex in squirrel monkey and bush baby: correlations with patterns of cytochrome oxidase. *J Comp Neurol* 329: 163-187.
- Landisman CE, Ts'o DY (2002) Color processing in macaque striate cortex: relationships to ocular dominance, cytochrome oxidase, and orientation. *J Neurophysiol* 87: 3126-3137.
- Lennie P, Krauskopf J, Sclar G (1990) Chromatic mechanisms in striate cortex of macaque. *J Neurosci* 10: 649-669.
- LeVay S, Voigt T (1988) Ocular dominance and disparity coding in cat visual cortex. *Vis Neurosci* 1: 395-414.
- LeVay S, Nelson SB (2004) Columnar organization of the visual cortex. In: *The Neural Basis of Visual Function* (Leventhal AG, ed), pp 266-315. London: Macmillan Press.
- Leventhal AG, Thompson KG, Liu D, Zhou Y, Ault SJ (1995) Concomitant sensitivity to orientation, direction, and color of cells in layers 2, 3, and 4 of monkey striate cortex. *J Neurosci* 15: 1808-1818.
- Livingstone M, Hubel D (1988) Segregation of form, color, movement, and depth: anatomy, physiology, and perception. *Science* 240: 740-749.
- Livingstone MS, Hubel DH (1984) Anatomy and physiology of a color system in the primate visual cortex. *J Neurosci* 4: 309-356.
- Lyon DC, Kaas JH (2001) Connectional and architectonic evidence for dorsal and ventral V3, and dorsomedial area in marmoset monkeys. *J Neurosci* 21: 249-261.
- Lyon DC, Xu XM, Casagrande VA, Stefansic JD, Shima D, Kaas JH (2002) Optical imaging reveals retinotopic organization of dorsal V3 in New World owl monkeys. *Proc Natl Acad Sci USA* 99: 15735-15742.

- Lyon DC, Kaas JH (2002) Evidence from V1 connections for both dorsal and ventral subdivisions of V3 in three species of new world monkeys. *J Comp Neurol* 449: 281-297.
- Maffei L, Fiorentini A (1977) Spatial frequency rows in the striate visual cortex. *Vision Res* 17: 257-264.
- Malach R, Tootell RB, Malonek D (1994) Relationship between orientation domains, cytochrome oxidase stripes, and intrinsic horizontal connections in squirrel monkey area V2. *Cereb Cortex* 4: 151-165.
- Malonek D, Tootell RBH, Grinvald A (1994) Optical imaging reveals the functional architecture of neurons processing shape and motion in owl monkey area MT. *Proc R Soc Lond B Biol Sci* 258: 109-119.
- McIlwan JT (1986) Point images in the visual system: new interest in an old idea. *Trends Neurosci* 9: 354-358.
- Merigan WH, Maunsell JH (1993) How parallel are the primate visual pathways? *Annu Rev Neurosci* 16: 369-402.
- Movshon JA, Thompson ID, Tolhurst DJ (1978) Spatial and temporal contrast sensitivity of neurones in areas 17 and 18 of the cat's visual cortex. *J Physiol* 283: 101-120.
- Nascimento-Silva S, Gattass R, Fiorani M, Jr., Sousa AP (2003) Three streams of visual information processing in V2 of Cebus monkey. *J Comp Neurol* 466: 104-118.
- O'Keefe LP, Levitt JB, Kiper DC, Shapley RM, Movshon JA (1998) Functional organization of owl monkey lateral geniculate nucleus and visual cortex. *J Neurophysiol* 80: 594-609.
- Perry VH, Oehler R, Cowey A (1984) Retinal ganglion cells that project to the dorsal lateral geniculate nucleus in the macaque monkey. *Neuroscience* 12: 1101-1123.
- Poggio GF, Baker FH, Mansfield RJ, Sillito A, Grigg P (1975) Spatial and chromatic properties of neurons subserving foveal and parafoveal vision in rhesus monkey. *Brain Res* 100: 25-59.
- Preuss T (2004) Specializations of human visual system: The monkey model meets human reality. In: *The primate visual system* pp 231-260. Boca Raton, FL: CRC Press.
- Preuss TM, Beck PD, Kaas JH (1993) Areal, Modular, and Connectional Organization of Visual-Cortex in A Prosimian Primate, the Slow Loris (*Nycticebus coucang*). *Brain Behav Evol* 42: 321-335.
- Preuss TM, Kaas JH (1996) Cytochrome oxidase 'blobs' and other characteristics of primary visual cortex in a lemuroid primate, *Cheirogaleus medius*. *Brain Behav Evol* 47: 103-112.

- Purves D, Riddle DR, LaMantia AS (1992) Iterated patterns of brain circuitry (or how the cortex gets its spots). *Trends Neurosci* 15: 362-368.
- Purvis A (1995) A composite estimate of primate phylogeny. *Philos Trans R Soc Lond B Biol Sci* 348: 405-421.
- Roe AW, Ts'o DY (1995) Visual topography in primate V2: multiple representation across functional stripes. *J Neurosci* 15: 3689-3715.
- Roe A, Ts'o D (1997) The functional architecture of area V2 in the macaque monkey. In: *Extrastriate Cortex in Primates* (Rockland K, Kaas J, Peters A, eds), pp 295-333. New York: Plenum Press.
- Roe A (2004) Modular complexity of Area V2 in the Macaque Monkey. In: *The Primate Visual System* pp 109-139. Boca Raton, FL: CRC Press.
- Rosa MG, Gattass R, Soares JG (1991) A quantitative analysis of cytochrome oxidase-rich patches in the primary visual cortex of Cebus monkeys: topographic distribution and effects of late monocular enucleation. *Exp Brain Res* 84: 195-209.
- Rosa MG (1997) Visuotopic organization of primate extrastriate cortex. In: *Cerebral cortex* (Peters A, Jones EG, eds), pp 127-203. New York: Plenum Press.
- Rosa MGP, Casagrande VA, Preuss T, Kaas JH (1997) Visual field representation in striate and prestriate cortices of a prosimian primate (*Galago garnetti*). *J Neurophysiol* 77: 3193-3217.
- Ross C (1996) Adaptive explanation for the origins of the *Anthropidea* (Primates). *Am J Primatol* 40: 205-230.
- Roy JP, Wurtz RH (1990) The role of disparity-sensitive cortical neurons in signaling the direction of self-motion. *Nature* 348: 160-162.
- Roy JP, Komatsu H, Wurtz RH (1992) Disparity sensitivity of neurons in monkey extrastriate area MST. *J Neurosci* 12: 2478-2492.
- Schiessl I, McLoughlin N (2003) Optical imaging of the retinotopic organization of V1 in the common marmoset. *Neuroimage* 20: 1857-1864.
- Shmuel A, Grinvald A (1996) Functional organization for direction of motion and its relationship to orientation maps in cat area 18. *J Neurosci* 16: 6945-6964.
- Shmuel A, Grinvald A (2000) Coexistence of linear zones and pinwheels within orientation maps in cat visual cortex. *Proc Natl Acad Sci USA* 97: 5568-5573.
- Shoham D, Hubener M, Schulze S, Grinvald A, Bonhoeffer T (1997) Spatio-temporal frequency domains and their relation to cytochrome oxidase staining in cat visual cortex. *Nature* 385: 529-533.

- Silveria LC (2004) Comparative study of the primate retina. In: The primate visual system (Kaas JH, Collins CE, eds), pp 29-52. Boca Raton, FL: CRC Press.
- Sincich LC, Horton JC (2002) Divided by cytochrome oxidase: a map of the projections from V1 to V2 in macaques. *Science* 295: 1734-1737.
- Snowden RJ, Treue S, Andersen RA (1992) The response of neurons in areas V1 and MT of the alert rhesus monkey to moving random dot patterns. *Exp Brain Res* 88: 389-400.
- Spatz WB (1977) Topographically organized reciprocal connections between areas 17 and MT (visual area of superior temporal sulcus) in the marmoset *Callithrix jacchus*. *Exp Brain Res* 27: 559-572.
- Spitzer MW, Calford MB, Clarey JC, Pettigrew JD, Roe AW (2001) Spontaneous and stimulus-evoked intrinsic optical signals in primary auditory cortex of the cat. *J Neurophysiol* 85: 1283-1298.
- Swindale NV (1990) Is the cerebral cortex modular? *Trends Neurosci* 13: 487-492.
- Swindale NV (1998) Cortical organization: modules, polymaps and mosaics. *Curr Biol* 8: R270-R273.
- Swindale NV (2000) How many maps are there in visual cortex? *Cereb Cortex* 10: 633-643.
- Symonds LL, Kaas JH (1978) Connections of striate cortex in the prosimian, *Galago senegalensis*. *J Comp Neurol* 181: 477-512.
- Tigges J, Tigges M, Ansel S, Cross NA, Letbetter WD, McBride RL (1981) Areal and laminar distribution of neurons interconnecting the central visual cortical areas 17, 18, 19, and MT in squirrel monkey (*Saimiri*). *J Comp Neurol* 202: 539-560.
- Tolhurst DJ, Thompson ID (1982) Organization of neurones preferring similar spatial frequencies in cat striate cortex. *Exp Brain Res* 48: 217-227.
- Tootell RB, Silverman MS, De Valois RL (1981) Spatial frequency columns in primary visual cortex. *Science* 214: 813-815.
- Tootell RB, Hamilton SL, Silverman MS (1985) Topography of cytochrome oxidase activity in owl monkey cortex. *J Neurosci* 5: 2786-2800.
- Tootell RB, Silverman MS, Hamilton SL, Switkes E, De Valois RL (1988a) Functional anatomy of macaque striate cortex. V. Spatial frequency. *J Neurosci* 8: 1610-1624.
- Tootell RB, Hamilton SL, Silverman MS, Switkes E (1988b) Functional anatomy of macaque striate cortex. I. Ocular dominance, binocular interactions, and baseline conditions. *J Neurosci* 8: 1500-1530.

- Tootell RB, Switkes E, Silverman MS, Hamilton SL (1988c) Functional anatomy of macaque striate cortex. II. Retinotopic organization. *J Neurosci* 8: 1531-1568.
- Toth LJ, Rao SC, Kim DS, Somers D, Sur M (1996) Subthreshold facilitation and suppression in primary visual cortex revealed by intrinsic signal imaging. *Proc Natl Acad Sci USA* 93: 9869-9874.
- Ts'o DY, Gilbert CD (1988) The organization of chromatic and spatial interactions in the primate striate cortex. *J Neurosci* 8: 1712-1727.
- Ts'o DY, Frostig RD, Lieke EE, Grinvald A (1990) Functional organization of primate visual cortex revealed by high resolution optical imaging. *Science* 249: 417-420.
- Ungerleider LG, Mishkin M (1982) Two cortical visual systems. In: *Analysis of Visual Behavior* (Ingle DJ, Goodale MA, Mansfield RJW, eds), pp 549-586. Cambridge, Massachusetts: MIT Press.
- Ungerleider LG, Mishkin M (1979) The striate projection zone in the superior temporal sulcus of *Macaca mulatta*: location and topographic organization. *J Comp Neurol* 188: 347-366.
- Ungerleider LG, Haxby JV (1994) 'What' and 'where' in the human brain. *Curr Opin Neurobiol* 4: 157-165.
- Van Essen DC, Maunsell JH, Bixby JL (1981) The middle temporal visual area in the macaque: myeloarchitecture, connections, functional properties and topographic organization. *J Comp Neurol* 199: 293-326.
- Van Essen DC, Newsome WT, Maunsell JH (1984) The visual field representation in striate cortex of the macaque monkey: asymmetries, anisotropies, and individual variability. *Vision Res* 24: 429-448.
- Van Essen DC, Felleman DJ, DeYoe EA, Olavarria J, Knierim J (1990) Modular and hierarchical organization of extrastriate visual cortex in the macaque monkey. *Cold Spring Harb Symp Quant Biol* 55: 679-696.
- Vanduffel W, Tootell RB, Schoups AA, Orban GA (2002) The organization of orientation selectivity throughout macaque visual cortex. *Cereb Cortex* 12: 647-662.
- Walls GL (1967) *The vertebrate eye and its adaptive radiation*. New York: Hafner Publishing Company.
- Weliky M, Bosking WH, Fitzpatrick D (1996) A systematic map of direction preference in primary visual cortex. *Nature* 379: 725-728.
- Weller RE, Wall JT, Kaas JH (1984) Cortical connections of the middle temporal visual area (MT) and the superior temporal cortex in owl monkeys. *J Comp Neurol* 228: 81-104.

Wikler KC, Williams RW, Rakic P (1990) Photoreceptor mosaic: number and distribution of rods and cones in the rhesus monkey retina. *J Comp Neurol* 297: 499-508.

Wikler KC, Rakic P (1990) Distribution of photoreceptor subtypes in the retina of diurnal and nocturnal primates. *J Neurosci* 10: 3390-3401.

Wong-Riley M (1979) Changes in the visual system of monocularly sutured or enucleated cats demonstrable with cytochrome oxidase histochemistry. *Brain Res* 171: 11-28.

Xiao Y, Wang Y, Felleman DJ (2003) A spatially organized representation of colour in macaque cortical area V2. *Nature* 421: 535-539.

Xu X, Ichida JM, Allison JD, Boyd JD, Bonds AB (2001) A comparison of koniocellular, magnocellular and parvocellular receptive field properties in the lateral geniculate nucleus of the owl monkey (*Aotus trivirgatus*). *J Physiol* 531: 203-218.

Zeki SM (1983) The distribution of wavelength and orientation selective cells in different areas of monkey visual cortex. *Proc R Soc Lond B Biol Sci* 217: 449-470.

Zeki SM (1974) Functional organization of a visual area in the posterior bank of the superior temporal sulcus of the rhesus monkey. *J Physiol (Lond)* 236: 549-573.